Spatial Data Analysis and Integration for Regional-Scale Geothermal Prospectivity Mapping, West Java, Indonesia

Hendro Wibowo
March, 2006

Spatial Data Analysis and Integration for Regional-Scale Geothermal Prospectivity Mapping, West Java, Indonesia

by

Hendro Wibowo

Thesis submitted to the International Institute for Geo-information Science and Earth Observation in partial fulfilment of the requirements for the degree of Master of Science in Geo-information Science and Earth Observation, Specialisation: **Applied Geophysics**.

Supervisors:
Dr. E.J.M. Carranza
Dr. S. Barritt

Thesis Assessment Board
Prof.Dr. F.D. van der Meer (Chair)
Prof. Dr. S.B. Kroonenberg (External)
Dr. E.J.M. Carranza (1st Supervisor)
Dr. S. Barritt (2nd Supervisor)

Observer:
Dr. P.M. van Dijk (Programme Director)

INTERNATIONAL INSTITUTE FOR GEO-INFORMATION SCIENCE AND EARTH OBSERVATION
ENSCHEDE, THE NETHERLANDS

Disclaimer

This document describes work undertaken as part of a programme of study at the International Institute for Geo-information Science and Earth Observation. All views and opinions expressed therein remain the sole responsibility of the author, and do not necessarily represent those of the institute. Data used in the thesis will not be used for publishing without written permission of the thesis supervisor.

Abstract

An existing geothermal prospectivity map in West Java (Indonesia) has been created at least 30 years ago. Since then many geothermal fields have been discovered. Further exploration for unknown geothermal fields in West Java would require an improved regional-scale map showing variations in degrees of geothermal prospectivity based on discovered (known) geothermal occurrences. The present study is concerned with the analysis and integration of available geoscience datasets in order to construct an improved regional-scale geothermal prospectivity map.

Based on review of relevant literature, several geological features in the study area are considered indicative of geothermal prospectivity. These geological features are (a) faults/fractures, because they enhance rock permeability for circulation of geothermal fluids, (b) hot springs, because they are surface manifestations of geothermal activity, (c) hydrothermal alteration, because they manifest presence of geothermal activity, (d) volcanic rocks, because they act as cap rocks in known geothermal fields, (e) regional low Bouguer anomalies, because they could represent terranes where volcanoes (which betray heat sources in the subsurface) and sedimentary reservoir rocks are present; and (f) epicentres of shallow (say, <10 km) earthquakes, because they could reflect seismically active zones associated with regional structures. Based on these geological features of interest, geoscience datasets that are available in public-domain archives were collected, processed and analysed. From published and unpublished geological maps, separate map layers of faults/fractures, hot springs, volcanic centres, volcanic rocks, and shallow-earthquake epicentres were prepared. On shaded-relief images of SRTM (Shuttle Radar Topography Mission) DEMs (digital elevations models), interpretation of faults/fractures was made to augment mapped faults/fractures. Using Landsat TM multispectral data, hydrothermal alteration was detected. Using gravity data, a Bouguer anomaly map was created and analysed resulting in interpretation of a regional volcano-tectonic depression. In addition, a map of geothermal occurrences was compiled.

Maps of point features (i.e., geothermal occurrences, volcanic centres, hot springs, shallow-earthquake epicentres) were analysed using a Fry plot method, which revealed from the different datasets common directional patterns reflecting similar geological controls. Spatial associations of the known geothermal occurrences with the individual sets of geological features were quantified by distance distribution analysis, which revealed varying degrees of spatial associations between known geothermal occurrences and different sets of geological features. The results of the Fry plot analyses and the distance distribution analyses allowed definition of conceptual model of geothermal prospectivity, which was made the basis for GIS-based predictive mapping of areas prospective for geothermal fields. A data-driven method using evidential belief functions (EBFs) was applied to model geothermal prospectivity. Different predictive maps of geothermal prospectivity have been created by using different evidential layers to determine which evidential layers are efficient for geothermal prospectivity mapping and, finally, to select an optimum predictive model. The optimum predictive map of geothermal prospectivity was then compared with the existing geothermal prospectivity map. Most of the predicted prospective areas coincide with portions of previously mapped “reliable” and “questionable” prospective areas. However, there are still other predictive prospective areas not demarcated by the existing geothermal prospectivity map nor associated with known geothermal occurrences.

The results of this study demonstrate the ability and usefulness of (a) spatial data analysis in defining a conceptual model of regional-scale geothermal prospectivity and (b) spatial data integration in predictive mapping of regional-scale geothermal prospectivity. The procedures conducted in this study could also be applied elsewhere, particularly in regions along the Sunda trench, in which similar geological and tectonic settings could provide favourable conditions for occurrences of geothermal fields.

Acknowledgements

I would like to thank STUNED Scholarship Programme for allowing and awarding me to pursue further study in order to build-up my skill and knowledge.

My special thanks and appreciation go to my first supervisor Dr. Emmanuel John M. Carranza for his supervision, guidance, critical review of the manuscripts without which the quality of the study would not reached its present state. I appreciated those days I spent with him since those days are days of knowledge I gained. However, errors and limitation of this study are due to my stubbornness.

Great thanks and appreciation go to my second supervisor Dr. Sally D. Barritt for her constructive suggestions and critical comments in all aspects in order to improve my work.

Although I have not fully consulted the expertise of Dr. Mark van der Meijde, his willingness to assist my work is highly acknowledged. I also express my sincere gratitude to Dr. Prihadi Sumintadiredja for endorsing my STUNED grant application. I extend my special thanks to Dr. Dicky Muslim, for our discussions during his short stays in Netherlands. Staffs of ITC library (Marga Koelen, Petry Maas – Prijs and Carla Gerritsen) are also thanked for their remarkably supportive attitude in providing me information to complete this work.

Finally, I am most grateful to be given a very best friend, Niknok, who inspired this work since the beginning. Her immense supports and prays has always blessed me throughout this study.

Sunday, February 19, 2006
Enschede, The Netherlands

Table of contents

List of figures

List of tables

Chapter 1: Introduction

1.1. Background to research

The Indonesian archipelago has numerous volcanic centres representing magmatic activity associated with the 7000 km-long Sunda trench, which is the convergent plate boundary between the Indo-Australian plate and the Eurasian plate (Figure 1.1). This geodynamic setting of the Indonesian archipelago has given rise to several geothermal fields, along a trend parallel to the plate margin, in the islands of Sumatra, Java, Bali, and Flores (Figure 1.2). Consequently, many geological studies have been conducted to explore and exploit the energy resources from such geothermal fields.

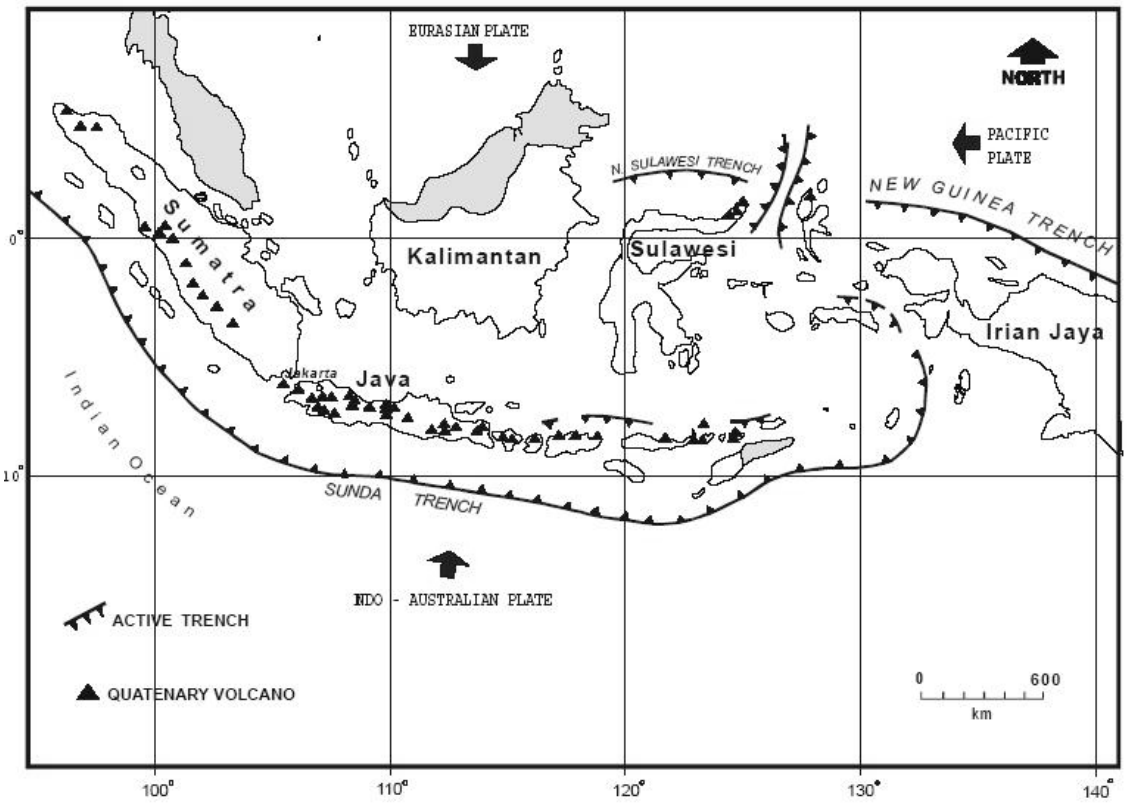

Figure 1.1: Active volcanic belts in Indonesia (from Fauzi et al., 2000)

Serious exploration of geothermal energy resources in Indonesia commenced in the early 1970s. Major development of these resources began in the late 1970s and has continued to the present. The Ministry of Energy and Mineral Resources (MEMR) of Indonesia has indicated that the total resource base for geothermal energy in the archipelago is about 20,000 MW (equivalent to about 9 billion barrels of oil). Of this estimated total geothermal energy resource base, the total proven reserve is 2,245 MW and the total probable and possible reserves are 7,165 MW (Sudarman et al., 2000). To meet future energy demands, there is a need for further exploration of the remaining geothermal energy resource base.

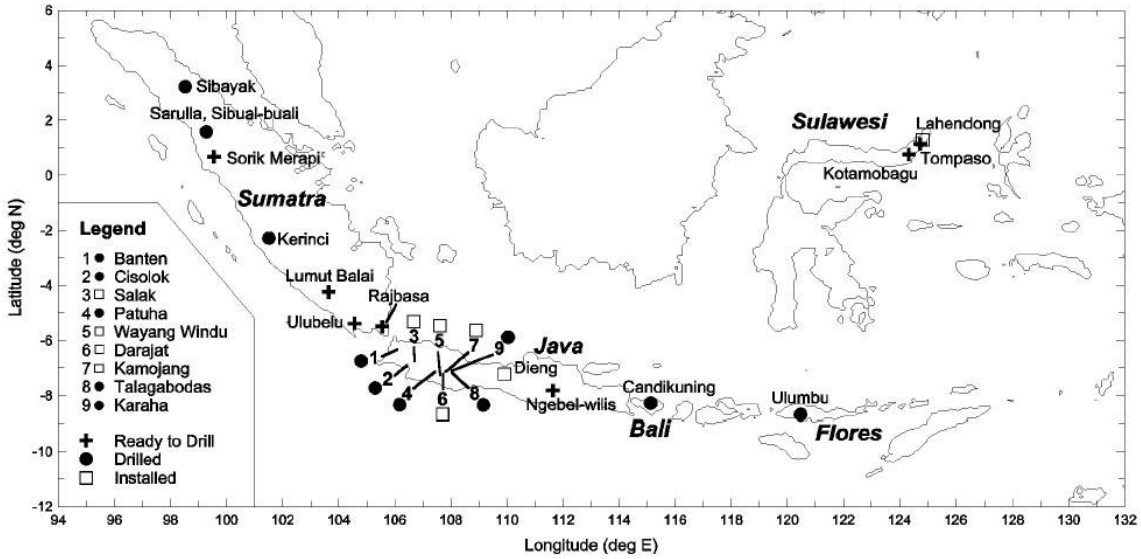

Figure 1.2: Some of the developed geothermal areas of Indonesia (Mahon et al., 2000)

1.2. Research problem

Further exploration for unknown geothermal energy resources would require a regional-scale map showing variations in degrees of prospectivity for geothermal occurrences. Prospectivity refers to combination of (or spatial intersections between) sets of indicative geological features for geothermal occurrences. If in one area there are more intersections between sets (or map layers) of indicative features than in another are, then the former has higher prospectivity.

Regional-scale (not larger than 1:1,000,000) exploration for geothermal energy resources in Indonesia has been based mostly on geological mapping. Many geophysical surveys, such as using gravity methods, have also been used to provide insights to subsurface physical variations (e.g., Hochstein, 1974) or basin boundaries (Widianto et al., 2004). However, geophysical surveys of geothermal exploration in Indonesia are mainly conducted at local scales (i.e., within prospective geothermal fields). In this research, a compilation of reconnaissance and local ground gravity datasets will be processed and analysed for regional-scale mapping of geothermal prospectivity.

There are many public domain geosciences data available that could be useful in regional-scale exploration of prospective terranes for geothermal energy resources. These data, such as Landsat TM (Thematic Mapper), SRTM (Shuttle Radar Topography Mission) DEMs (digital elevation models), locations of earthquake epicentres, and geological map could probably be integrated to construct a regional-scale geothermal prospectivity model. However, analysis and integration of multi-source geoscience datasets have not been demonstrated as a useful tool in regional-scale geothermal exploration in Indonesia. Therefore, this research aims to analyse spatial relationships between various public domain geoscience datasets and known geothermal occurrences in order to produce a regional-scale geothermal prospectivity model. This objective will be pursued using a GIS.

1.3. Research hypotheses

Some regions of intense geothermal activity are within a broad volcano-tectonic depression[1]. This type of depression is commonly associated with rifting on and behind island arcs generated by plate subduction, and is characterized by extensive pyroclastic flow deposits and structural features typically associated with calderas and/or grabens. This structural arrangement could result in a broad low gravity anomaly zone (Kusumoto et al., 1999; Arana et al., 2000), such as the ones in The Kuju-Beppu Graben in Kyushu Island, Japan and Taupo Volcanic caldera in North Island, New Zealand.

[1] a generic term first used by Van Bemmelen (1949) to describe a large-scale depression, usually linear, that is controlled by both tectonic and volcanic processes (Bates and Jackson, 1987).

Similar Quaternary volcano-tectonic depressions containing geothermal fields occur in the Philippines and Indonesia (Tamanyu and Wood, 2003).

Geothermal systems found in Indonesia are normally volcano-hosted and related to subduction zones (Hadi et al., 2000). Studies of seismic and geologic profiles across the Java arc-trench system reveal that Java is island of inner volcanic arc with silicic and intermediate volcanism, which were formed due to subduction of oceanic plate under a thick and old continental crust (Katili, 1975). Špicák et al. (2005) concluded that the presence of seismically active columns beneath some active volcanoes in western Java island support the concept that the subducted oceanic lithosphere is the source region for the primary magma associated with calc-alkaline volcanoes at convergent plate margins.

The nature of active hydrothermal processes in many geothermal fields is similar to the processes that generate hydrothermal mineral deposits. Therefore, mineral deposit concepts are applicable to exploration of geothermal energy resources by identifying hydrothermal alteration zones (Bogie and Lawless, 2000). Remote mapping of hydrothermal alteration zones has been made possible with the use of spectral satellite imagery. It is because certain alteration minerals associated with hydrothermal mineral deposits show diagnostic spectral characteristics that permit their remote identification (Gladwell et al., 1983; Whitney et al., 1983 Lee and Raines, 1984; Carranza and Hale, 2002a).

Fault/fracture zones (frequently kept open by seismic activity) provide paths and enhance rock permeability for circulating fluids in geothermal systems (Rybach and Muffler, 1981; Soengkono, 2000; Tezuka et al., 2000).

Therefore, it is hypothesized that analysis and integration of several layers of regional-scale geoscience information representing evidences of geothermal activity could result in mapping of prospective areas for further exploration of geothermal energy resources. Based on readily available public-domain regional-scale geosciences data, it is further hypothesized that, in the study area, West Java Province of Indonesia:

a) Negative gravity anomalies represent terranes associated with volcano-tectonic depressions, which are prospective for geothermal fields;
b) Zones proximal to shallow-earthquake epicentres are indicative of geothermal prospectivity;
c) Zones proximal to areas with hydrothermal alteration, remotely sensed from multi-spectral satellite imagery, are useful for regional-scale mapping of geothermal prospectivity;
d) Zones proximal to faults/fractures are indicative of geothermal prospectivity and represent structurally permeable zones where surface features (e.g., hot springs, mud pools) associated with geothermal fields could occur.

A combination of geological conditions mentioned above could result in integrated predictor maps that represent prospectivity for geothermal fields.

1.4. Research objectives

The main objective of this study is to demonstrate that an integrated spatial analysis of public domain geoscience datasets is a useful tool for regional-scale geothermal prospectivity mapping. Geothermal systems are usually characterized by indicative geological features that may be subtle or not easily enhanced by one analytical method. The combined applications of several different techniques/methods and study of spatial relationships between exploration datasets seem to be the most logical strategy. It is through this approach that the following research sub-objectives, whose successive order reflect the system of data analysis, may be realised:

1) To quantify spatial relationships between individual regional-scale indicators of geothermal prospectivity and known (explored/developed) geothermal fields.
2) To analyse geophysical (gravity and earthquake epicentre) data and multi-spectral satellite imagery for regional-scale geological indicators of geothermal prospectivity.
3) To generate predictor maps representing the different regional-scale indicators of geothermal prospectivity.
4) To integrate predictor maps for regional-scale delineation of terranes prospective for geothermal fields.

1.5. Overall research methodology

The methodologies in this research (Figure 1.3) involve extraction and analysis of geological information from several public domain geoscience datasets. Geological datasets representing conditions favourable for geothermal fields are divided into three categories, surface (geological map, Landsat and volcanoes), subsurface (gravity and earthquake epicentres), and structural control. Each map is analysed towards enhancing surface and subsurface features indicative of geothermal prospectivity. Spatial analysis is then directed toward quantifying spatial relationships between regional-scale indicators of geothermal prospectivity and known geothermal occurrences to determine relative weights of individual indicator. The analysis will result in several classified maps, which are buffered[2] according to their relative significance with respect to known geothermal occurrences. Finally, these different layers of weighted indicators are integrated to create a regional-scale geothermal prospectivity map.

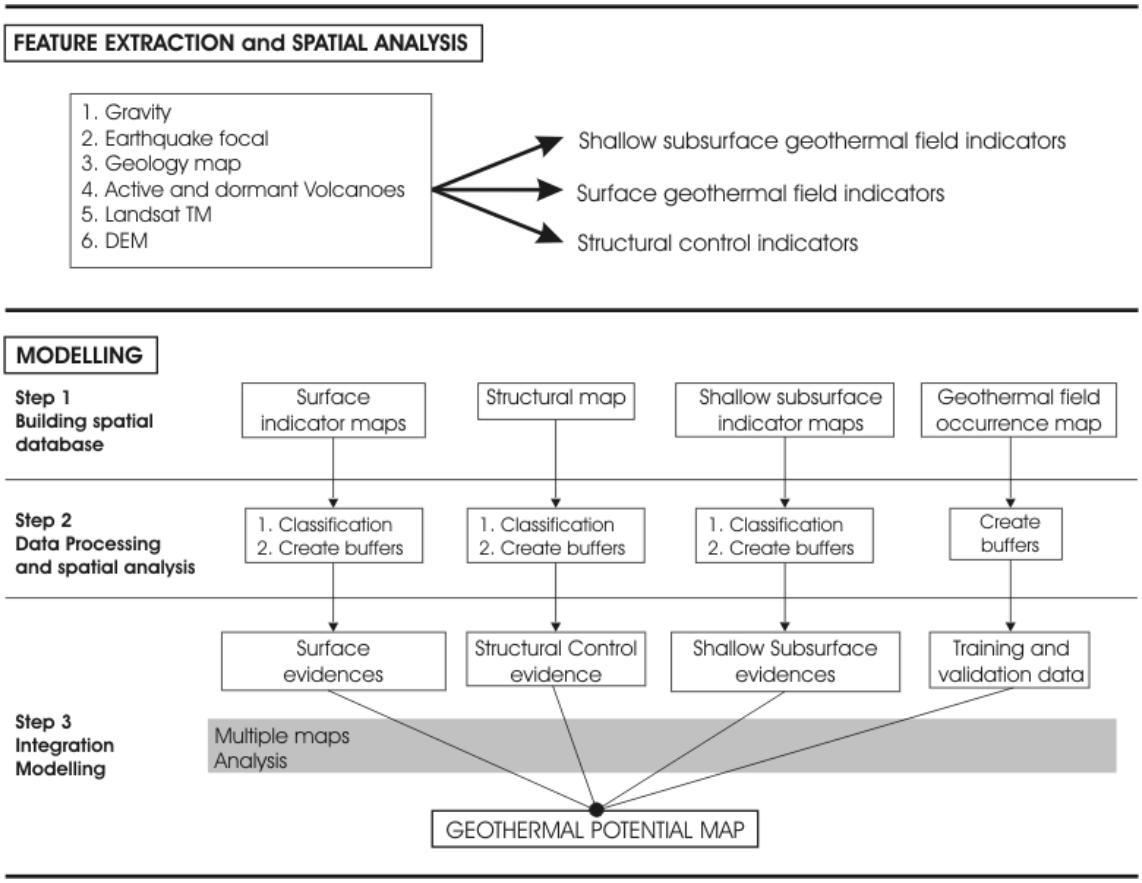

Figure 1.3: Workflow of research methodology

1.5.1. Geophysical data processing and interpretation

The main purpose of geophysics (i.e., gravity survey) in geological mapping is to determine the extent at depth of surface features and formations and to trace geological bodies that lie beneath areas of poor exposure. Bodies that are covered by unconsolidated sediments and bodies that terminate well below the surface are often detected. For the gravity survey to yield useful information, the density contrast between the rocks on each side of the contact must be large enough to generate a detectable gravity anomaly. In this study, density contrasts are enhanced through filtering techniques of Bouguer anomalies. The filtering technique has also been used as an objective way to separate anomalies into

[2] In spatial information systems, buffer is a polygon enclosing an area within specified distance (or proximity) from a point, line, or polygon. Accordingly, there are point buffers, line buffers, and polygon buffers (Bonham-Carter, 1994).

long and short-wavelength components (Sleep and Fujita, 1997). Long-wavelength components, in terms of geological significance, are usually correlated with deep massive features in the subsurface (assumed to be near-spherical, or nearly equidimensional, objects). Short-wavelength or high-frequency components relate with shallow bodies. Thus, enhanced Bouguer anomalies might give explanations or some evidences about subsurface geological conditions favourable for geothermal systems.

Another available dataset in this study is earthquake epicentres. Spatial patterns and distributions of earthquake epicentres will be analyzed to determine whether there is a relationship with geothermal occurrences. Spatial pattern is enhanced using a Fry plot, a method of point pattern analysis that uses separations between all objects of an object distribution (Fry, 1979; Vearncombe and Vearncombe, 1999). This method allows an easier visual interpretation of spatial distribution of point objects, since it enhances the point pattern many times revealing even subtle patterns not seen in the original spatial point distribution. Spatial association of earthquake epicentres with known geothermal occurrences is also evaluated quantitatively using distance distribution analysis. This method has been applied previously in mineral exploration. Bonham-Carter et al. (1985) statistically characterised spatial association between mineral occurrences and lineaments by measuring the distances from each mineral occurrence to the nearest lineament, and comparing the observed distance distribution to a predicted distance distribution that would be expected if a random process generated the occurrences.

1.5.2. Analysis and interpretation of satellite remote sensing data

Structural interpretation of shaded-relief images of SRTM DEMs is conducted to complement existing map of faults/fractures. A software defoliant technique (Fraser and Green, 1987), which involves processing of Landsat TM5, is applied to map hydrothermal alteration in areas of dense tropical vegetation (e.g., Carranza and Hale, 2002a).

1.5.3. Predictor map generation and integration

Predictor maps represent certain spatial criteria, which are based on conceptual models and on characteristics of target spatial objects (in this case, prospective zones for geothermal occurrence). Data-driven evidential belief functions (EBFs) are used to create and integrate predictor maps to delineate prospective terranes for geothermal fields. Data-driven EBF modelling is suitable for situations where a number of geothermal field occurrences are known (Carranza, 2002). This method has been used for mineral prospectivity mapping to manage uncertainty in certain predictor maps (Carranza and Hale, 2003; Carranza et al., 2005).

1.6. Thesis outline

This thesis is organized into four parts. First, a general review on existing methods for geothermal exploration is discussed (Chapter 2). This part is supported by a review of the previous works on geothermal exploration in the study area (Chapter 3). The second part consists of spatial data analysis and of individual datasets to define conceptual model of spatial indicators of geothermal prospectivity (Chapters 4, 5 and 6). The third part involves modelling of spatial indicators of geothermal prospectivity as EBFs, which are then integrated to model regional-scale geothermal prospectivity (Chapter 7). Finally, general discussions, conclusions, and recommendations based on significant results of the study are placed in Chapter 8.

Chapter 2: Geothermal Exploration – A Review

Although the earth is an immense source of heat, most of this heat is either buried too deeply or is too diffuse to be exploited economically. However, in some places the heat is concentrated as a result of certain geological and hydrological processes, and it is in these geothermal regions that conditions sometimes occur to allow the heat to be extracted through drill-holes sunk to modest depths in the earth's crust. The purpose of this chapter is to summarise the general characteristics of geothermal fields, to discuss geothermal resources and to describe components of exploration activities for geothermal energy.

2.1. What are geothermal systems?

The term 'geothermal' refers to the internal thermal energy of the earth; in general, it is employed to denote systems in which the earth's heat is sufficiently concentrated to form an energy resource (Rybach and Muffler, 1981). The concentration of thermal energy in geothermal systems, in one terrane relative to adjacent terrane, is characterized by the existence of *geothermal anomalies*. Geologic and hydrologic factors as well as heat transfer phenomena can be of importance in forming geothermal anomalies: young magmatic heat sources at high crustal levels, hydrothermal circulation of meteoric water in fault/fracture systems, and irregularities in conductive heat transfer (differences in regional heat flow from deep crustal levels, contrasts in thermal conductivity and/or radiogenic heat production of the rocks). The most significant geothermal anomalies are related to upward moving magma.

The degree of concentration of thermal energy in a geothermal reservoir can be appreciated from a comparison between the average heat content of crustal rocks in the upper 10 km, which is 85kJ/kg, and the average heat of saturated steam in a geothermal reservoir, which is 2970 kJ/kg (Rybach and Muffler, 1981). The factor of enrichment is thus in the order of 30 in the extractable fluid in a 'high-grade' geothermal resource. The concentration of geothermal energy requires, beside high porosity ('storage coefficient'), also high permeability ('hydraulic conductivity') of the reservoir rocks.

2.1.1. Thermal regimes

A major component of heat flow[3] at the earth's surface is the heat input at the base of the lithosphere, the outer spherical shell of the Earth. The lithosphere is defined as the strong, outer most layer of the earth that deforms in an essentially elastic manner. It is made up of the crust and upper-most mantle. The lithosphere is underlain by the asthenosphere, which is much weaker and reacts to stress in a fluid manner. The lithosphere is divided into plates, of which the crustal component can be oceanic and/or continental, and the relative movements of plates take place upon the asthenosphere. The thickness of the lithosphere is characterised by its thermal, seismic, elastic, and temporal properties, with thermal properties mainly controlling the strength of subsurface materials. The mean lithosphere thickness beneath ocean ranges from 60-70 km; beneath continents the lithosphere has a thickness of 110-150 km (Kearey and Vine, 1996).

The most pervasive process of heat transfer from the earth's interior to the surface is simple heat conduction. The difference in temperature between deep hotter zones and shallow colder zones generates a conductive flow of heat from the former towards the latter, with a tendency to create uniform conditions, although, as often happens with natural phenomena, this situation is never actually attained. The mean terrestrial heat flow of continents and oceans is 65 and 101 mW/m^2, respectively, which, when areally weighted, yield a global mean of 87 mW/m^2 (Pollack et al., 1993). These values are based on 24,774 measurements at 20,201 sites covering about 62% of the Earth's surface. However, where fluids, such as water, carbon dioxide, or even magma, move through the lithosphere, the pattern of conductive heat flow is strongly modified by convection. Consequently,

[3] Heat flow refers to the rate at which heat flows out of the solid earth (Khesin and Eppelbaum, 1994). The heat flow (**q**) is determined by measuring the thermal gradient (**dT/dz**) in near surface rocks and their thermal conductivity (k): **q = -k dT/dz** (Fourier's law of heat conduction). Heat flow unit is milliJoule/sec.m^2 or milliWatt/m^2.

there are numerous localised thermal areas where the net heat flow or heat flux averages two orders of magnitude higher and in which temperatures may reach several hundred degrees at depths of only a few kilometres. As a reference, the normal temperature gradient is about 20-25ºC/km (Kearey and Vine, 1996).

A second important process, which also modifies the conductive heat flow through the lithosphere, is heat production by decay of the radioactive isotopes U-238, U-235, Th-232, and K-40. These isotopes are relatively enriched in the upper continental crust, and it has been estimated that their decay contributes 18-38 mW/m^2 to the observed heat flow (Pollack and Chapman, 1977). The oceanic crust, however, is virtually barren of radioactive isotopes, and only about 4 mW/m^2 can be attributed to this source. Rybach (1981) has shown that heat production of rocks is governed by the amount of radioactive isotopes present, which vary greatly with rock type. However, the variation of heat generation with rock type exhibit certain regularities due to the similar geochemical behaviour of U, Th, and K during processes that determine the distribution of the natural radioelements (magmatic differentiation, sedimentation, metamorphism). In igneous rocks, heat production decreases from silicic (e.g., granites) through basic to ultrabasic rock types (e.g. peridotites). In metamorphic rocks, heat production depends on metamorphic grade. Sedimentary rocks, which make up only small portions of the earth's crust, have in general very low heat production (Rybach, 1976).

2.1.2. Geothermal systems and plate tectonics

The geological setting in which a geothermal reservoir is to be found can vary widely. The largest geothermal fields currently under exploitation occur in rocks that range from limestone to shale, volcanic rock, and granite. Volcanic rocks are probably the most common rock type in which geothermal reservoirs occur. Rather than being identified with a specific lithology, geothermal reservoirs are more closely associated with heat flow systems. As far as geology is concerned, therefore, the more important factors in identifying a geotherma1 reservoir are not rock units, but rather the existence of tectonic elements such as fracturing, and the presence of high heat flow (Manzella, 2000).

Study of regional heat flow allows inferences to be made on the relative significance of previous mentioned processes of heat transfer and production. Broad provinces with relatively uniform heat flow can be defined, whose distribution reflect differences in composition, evolution and present tectonics. In the more stable, older regions of the continents, for example, in the eastern and central parts of the USA, heat flow is low and can be accounted for by a simple conduction model. This model, with only a modest radioactive component, is sufficient to produce low temperature (<90ºC) geothermal reservoirs. However, moderate temperature (90-180ºC) and high temperature geothermal fields (>180ºC) occur only in regions exhibiting volcanic and/or earthquake activity during the last few million years, where large thermal anomalies occur on both regional and local scales, for example, in Indonesia.

Because high temperature geothermal fields are frequently associated with young volcanoes, it is evident that their heat sources are usually igneous intrusions derived commonly from the same magma chamber associated with the volcanoes or the magma chamber itself. The worldwide distribution of these volcanic zones and geothermal anomalies is far from random. Instead, it is a manifestation of the fact that the earth's mantle, part of the interior lying beneath the lithosphere, is convecting vigorously on a geologic time scale, i.e. with velocities of the order of 1 to 10 cm/year (Kearey and Vine, 1996). A major consequence of this mantle convection is its effects on the lithosphere, which is divided into 8 or 9 major, essentially rigid plates, and several minor ones (Figure 2.1).

The edges of lithospheric plates are the prime loci of crustal deformation, earthquakes, and high heat flow, with associated volcanoes and geothermal fields (Figure 2.1). Thus, there is a high occurrence of volcanism and high temperature geothermal fields around the margins of the Pacific Ocean, along which are a series of convergent plate margins. These are sites where the oceanic lithosphere may partially melt as it is subducted into the mantle. There is also a clear relationship between high heat flow and active volcanism in zones of active spreading along the mid Atlantic Ridge, the East Pacific Rise and in the Red Sea (Rybach, 1981). High temperature geothermal systems are also fairly abundant along complex continental plate boundaries, i.e., areas of recent thrust

faulting, volcanism and mountain building, especially in the great volcanic chains running through Central America and South America, the Cascade Range of the USA., the Aleutian Islands, Japan, the Philippines and Indonesia (Edwards et al., 1982).

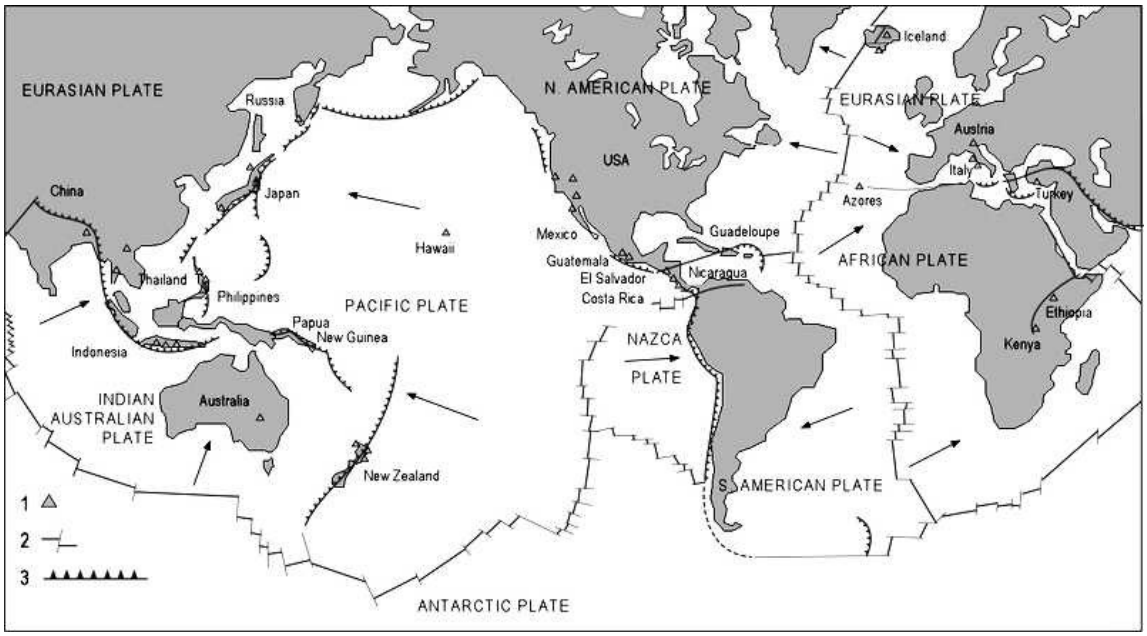

Figure 2.1: World pattern of tectonic plates. Arrows show direction of plate movements. 1 = geothermal fields producing electricity. 2 = mid-oceanic ridges crossed by transform faults. 3 = subduction zones (from Dickson and Fanelli, 2004).

In general, some sort of upward transfer of heat by moving masses (e.g., magma) leads to the development of geothermal anomalies. Geothermal anomalies related to magmatic activity originate from transient storage of heat at high crustal levels (<10 km, Muffler (1976)) by magmatic intrusions. In considering uprising magma in the crust, distinction must be made between basaltic and silicic magma.

Basaltic magmas originate from mantle material by partial melting (Wyllie, 1971). If they rise directly to the surface forming dykes and thin sheets, they dissipate their heat content rapidly and thus no large shallow intrusive bodies will be formed. On the other hand, if they solidify near the base of the crust in extensional regimes, like the Basin and Range Province U.S.A (Lachenbruch, 1978), they greatly enhance the regional heat flow, which in turn can trigger hydrothermal convection along steep fault systems created by the extensional regimes (Lachenbruch and Sass, 1977).

Silicic magmas can be generated by partial melting of mantle material as well as by differentiation of basaltic magma (Robinson et al., 1976), but usually some kind of remelting of crustal material is involved. Due to higher viscosity of silicic (relative to basaltic) melts, these magmas usually get trapped at several kilometres depth in the crust. This results in supply of heat to roof rocks by intrusions of 'batholitic' type, i.e., magmatic bodies with great thickness and lateral extension. On continents, geothermal resources are more likely to be associated with silicic volcanism than with basaltic volcanism (Smith and Shaw, 1973).

Since igneous intrusions have typical temperatures in the range of 700-1200ºC, they can significantly heat their neighbourhood upon emplacement. Corresponding surface heat flow can exceed several mW/m^2. Due to conductive and convective cooling of an intrusion, a considerable thermal influence can prevail after emplacement for a limited time only. As a general rule, only Quaternary intrusions (with ages in the range of 10^4 to 10^6 years) in the upper crust (<10 km) are still active thermally today (Healy, 1976). However, as an exception to general rule, older intrusions with very high, evenly distributed radioelement content, could still be thermally active, because of long half-lives decay.

The predominant process of a magma formation is partial melting of the asthenosphere above the subducted slab due to water release below it. The water can be supplied by the pore fluids of subducted sediments and/or by metamorphic (dehydration/breakdown) reactions (Rybach, 1981). The magmas will appear in a volcanic belt paralleling the zone of subduction at a certain distance, which depends on the dip of the downgoing slab. The extent of geothermal anomalies associated with this volcanism will depend on the chemical composition of magmas. The latter will vary according to whether the subduction zone is an oceanic-continental plate margin (this results in intermediate composition), oceanic-oceanic plate margin (this results in basic magmas) or continental-continental plate margin (this results in predominantly silicic magmas).

2.1.3. Types of geothermal systems

Geothermal systems can be subdivided, according to their geologic environments and heat transfer regimes, into two broad categories: *convective* and *conductive* geothermal systems (Figure 2.2) (Rybach, 1981).

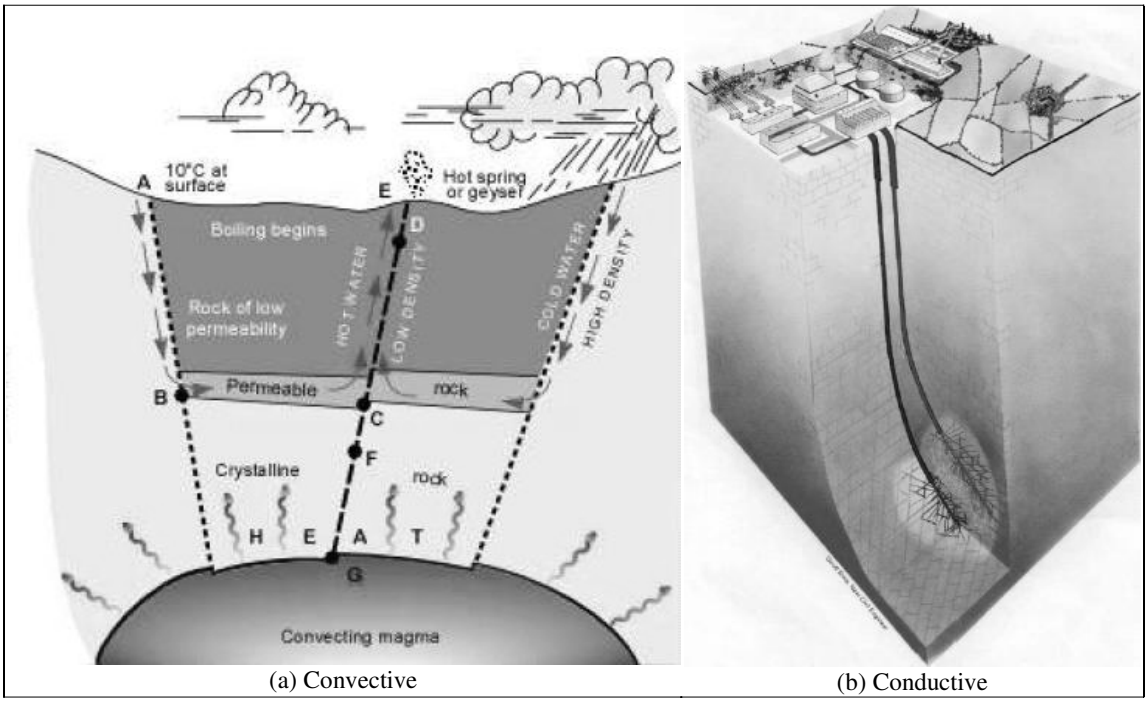

(a) Convective (b) Conductive

Figure 2.2: General types of geothermal systems.

2.1.3.1. Convective geothermal systems

Convective geothermal systems are characterised by natural circulation of the working fluid (Figure 2.2a). The driving force to move the working fluid is related to the density difference between cold, downward-moving recharge water and hot geothermal water, the latter rising towards the earth's surface by buoyancy. Convection tends to increase the temperature in the upper parts of the circulation system while temperatures in the lower parts decrease.

The most common convective geothermal system is *hydrothermal* systems in high porosity and high permeability environments. High regional heat flow can sustain hydrothermal convection systems, provided that the upper few kilometres of the earth's crust is sufficiently fractured to allow fluid circulation. Such systems have relatively short lifetimes. Much longer lasting hydrothermal systems can be supported by local crustal heat sources like shallow intrusions. Such intrusions occur primarily in specific geologic environments: spreading ridges, convergent plate margins, continental rifts, and intraplate collisions. The systems may persist for several million years (cooling by conduction alone). The age and solidification history of the intrusion are thus dominating factors.

Hydrothermal systems may be further divided into *liquid dominated* or *vapour dominated* systems, depending on the ratio of water to steam in the reservoir (White et al., 1971). Liquid dominated or hot water hydrothermal systems may be of low, moderate, or high temperature type. They are the most common kind of geothermal system being exploited commercially today, for example Salak in Indonesia (Mahon et al., 2000), Palinpinon field, Negros Island in Philippine (Rae et al., 2004). Vapour dominated reservoirs are much rarer but include such large developed resources as Darajat in Indonesia (Moore, 2002), Larderello in Italy, and The Geysers in the USA (Rybach and Muffler, 1981). It is a misnomer to call them "dry steam reservoirs", because liquid water and vapour co-exist with them; however, vapour is the continuous, pressure controlling phase.

The category of hydrothermal systems includes practically all geothermal systems which, to date, have been actually been developed for commercial electric power production. The high porosity/permeability reservoir must be at depths shallow enough (<3 km) to be tapped by drill holes. The high permeability of the reservoir rocks enables inflow and production of geothermal fluids in substantial quantities.

Another variation of convective geothermal system is *circulation* systems, which is characterised by low porosity, fracture permeability environments. This system can develop in regions devoid of young igneous intrusions and may result from deep circulation of meteoric water in the thermal regime of conductive regional heat flow. The prerequisite for such systems is the presence of fault/fracture zones with sufficient permeability for water circulation. The temperature attained by the water is dependent primarily upon the magnitude of the regional heat flow and the depth to which the water circulates. All other things being equal, higher temperatures will occur at shallower depth in regions of higher conductive heat flow. Examples of circulation systems of this kind are given by the numerous thermal springs spread all over the world. They occur in widely differing geologic setting and various rock types, the latter generally characterised by low primary porosity and permeability. Example of circulation system is Boise field, Idaho (IDWR, 1987) where principal flow of production wells is derived from fractures in rhyolite within the fault zone. While discharge areas are mostly of limited extent (usually at or near intersections of fault/fracture systems), recharge areas are larger by orders of magnitude.

2.1.3.2. Conductive geothermal systems

Conductive geothermal systems are characterised by a thermal regime due to conduction alone. The working fluid is either present (e.g., in deep aquifers in sedimentary basins) or must be supplied (hot dry rock systems) (Figure 2.2b). Convective circulation is prohibited by low temperature contrast or by low permeability.

Low temperature contrast reservoir is found in sedimentary aquifers in which the pore fluids are under pressure exceeding that of the water column (hydrostatic pressure). In fact, the pore fluids bear a large fraction of the total overburden or lithostatic pressure (i.e., the pressure due to the weight of overlying rocks), hence the name *geopressurised reservoir*. It has typical temperatures in the range of 150-230ºC because these geopressured zones have high heat capacity and low thermal conductivity. An example is the huge Tertiary basin along the Gulf Coast of Louisiana and Texas, USA (Edwards et al., 1982).

Low permeability reservoir could transfer heat in a purely conductive flow. Low permeability rocks, such as granites, have very low porosity and thermal storability. Its temperatures exceed 300ºC at 2-3 km depth. Because of the low thermal conductivity of the rock matrix, the surface areas required for rock fluid heat transfer are large, yet pressure and fluid losses must be minimized. Both characteristics of high temperature and the non-existence of circulating fluids lead to the name of *hot dry rock reservoir* type. Examples can be found Los Alamos, New Mexico, USA, Northern France and on the island of Honshu in Japan (Dickson and Fanelli, 2004), where high-pressure water is pumped through a specially drilled well into a deep body of hot, compact crystalline rock, causing its hydraulic fracturing. The water permeates these artificial fractures, extracting heat from the surrounding rock, which acts as a natural reservoir.

2.1.4. Geothermal energy resources

Geothermal resources has been defined by several authors (e.g., Rybach and Muffler, 1981; Muffler and Cataldi, 1978; Dickson and Fanelli, 2004) as all the thermal energy in the earth's crust under a given area or the heat contained within the earth that generates geological phenomena, which could be recovered and exploited by man. Geothermal resources that are shallow enough to be tapped by production drilling in the foreseeable future are termed the *accessible geothermal resource base.* Given that recovery factors are much less than unity, the geothermal resource is defined as "those fractions of the accessible resource base that might be extracted economically now (i.e., the *economic geothermal resource*) and at some reasonable time (the *sub-economic geothermal resource*)".

Rowley (1982) has defined the following terms and definitions for geothermal reserve and resource (Table 2.2). *Geothermal resource base* includes all the stored heat, in both rock and fluids, above 150ºC, within a portion of the earth's crust. Depth is restricted to 10 km into the crust. This resource base is better defined as an *accessible resource base*. All geothermal resource and reserve estimates are subsets of the accessible resource base. *Geothermal resource* is a term used to define that quantity of geothermal heat that is likely to become available if certain technology and economic conditions are met at some future (specified) time. *Geothermal reserves* consist of identified economic resources that are recoverable at a cost that is competitive now with other commercially developed energy sources. *Demonstrated reserve* is defined as a geothermal area or field that has at least one borehole or well drilled into it and for which estimates of the areal size of the deposit of heat are available.

Table 2.1: Resource-reserve terminology and basic aspects of energy sources (from Rowley, 1982)

Aspects and factors	**Occurrence**: geologic knowledge	**Economic**: production costs and energy prices	**Technology**: extrapolations and extensions of present and new concepts
Terms			
Reserves	Known	Present cost	Currently feasible
Resources	Known	Any cost level	Currently feasible and later feasibility indicated
Resources base	Known + unknown	Irrelevant	Feasible + infeasible

Recently, a group of experts has estimated the geothermal potential of each continent in terms of high and low temperature resources (Table 2.3).

The data reported by Friedleifsson (2003) give some idea of the role played by geothermal energy with respect to other renewable energy sources. Of the total electricity (i.e., 2826 TWh) produced from renewable energy sources in 1998, 92% came from hydro-power, 5.5% from biomass, 1.6% from geothermal, 0.6% from wind, 0.05% from solar, and 0.02% from tidal. If exploited correctly, geothermal energy could certainly assume an important role in the energy balance of some countries. In certain circumstances even small-scale geothermal resources are capable of solving numerous local problems and of raising the living standards of small isolated communities.

Table 2.2: Geothermal potential world-wide (from IGA, 2001)

	High-temperature resources suitable for electricity generation		Low-temperature resources suitable for direct use in million TWh/yr of heat (lower limit)
	Conventional technology in TWh/yr of electricity*	Conventional and binary technology in TWh/yr of electricity	
Europe	1830	3700	> 370
Asia	2970	5900	> 320
Africa	1220	2400	> 240
North America	1330	2700	> 120
Latin America	2800	5600	> 240
Oceania	1050	2100	> 110
World potential	11 200	22 400	> 1400

*Energy unit: 1 terraWatt-hour (TWh) =10^{12} Wh = 3,600 terraJoule (TJ) = 3.41 terra-BTU

2.2. State-of-art methodologies in geothermal exploration

This section discusses geophysical methods related with the convective type geothermal resources, such as those found mostly in Indonesia. Apart from the fact that hydrothermal systems are by far the most economic for a commercial power production, this type of geothermal systems is very dominant in the geological setting of the study area (see Chapter 3). It can be concluded from sections 1.1 and 2.1.2 that Indonesia's geothermal fields are associated with active volcanic belts, resulted from magmatic activity along the convergent plate margin (Figures 1.1 and 2.1). Thus, hydrothermal systems supported by shallow intrusions are more likely to occur in this area than the other geothermal system types.

A geothermal exploration programme for hydrothermal systems is based on a number of phenomena associated with the intrusive model for a geothermal system. The intrusive model for a geothermal system needs a source, in the form of intrusions that have been emplaced no more than half a million to one million years ago, so that excess heat still exists. The region above the source of the geothermal system must have high porosity/permeability or be fractured by tectonic activity, fluids must be available for circulation in a convection cell, and the precipitation of a cap rock must have taken place. All these elements represent targets for the application of geological, geophysical, and geochemical prospecting techniques. Because of the high temperatures involved, both in the geothermal reservoir and in the source of the geothermal system, major changes have taken place in the physical, chemical, and geological characteristics of the rock, all of which can be studied in an exploration project. Heat is not easily confined in small volumes of rock. Rather, heat diffuses readily, and a large volume of a rock around a geothermal system will have its properties altered. The rock volume in which anomalies in properties are to be expected will, therefore, generally be large. Exploration techniques need not offer a high level of resolution (Manzella, 2000); instead, an approach that is capable of providing a high level of confidence that geothermal fluids will be recovered on drilling.

2.2.1. Geophysical methods in geothermal exploration

The discussion in this section covers the application of geophysical methods in hydrothermal exploration. Table 2.2 is a classification of geophysical methods which is also shows the common geothermal targets for each method. Gravity and earthquake epicentres are the data available in this study. Other important geophysical methods are briefly mentioned to complete the discussion.

Table 2.3: Geophysical targets in geothermal exploration (slightly modified from Wright et al., 1985)

METHOD	TARGETS
Thermal gradient / heat flow	Thermally anomalous rocks or fluids
Electrical	
Resistivity	Hot brines, alteration, faults
Induced Polarisation	Alteration, mineralization
CSEM & Scalar AMT	Hot brines, alteration, faults
MT/AMT	Hot brines, magma chambers, partial melt, structure
Self Potential	Flow of fluid and heat
Tellurics	Hot brines, alteration, faults
Gravity	Structure, alteration, densification, intrusion
Magnetics	Structure, alteration, rock type
Seismic	
Microseismics	Active hydrothermal processes
Microearthquakes	Active faulting and fracturing, distribution of velocity and attenuation
Teleseismics	Deep magma chamber
Refraction	Structure, distribution of velocity and attenuation
Reflection	Structure, distribution of velocity and attenuation
Radiometric	Alteration, Rn^{226}, Ra^{222}
Well logging	Anomalous temperature, porosity, permeability, rock type
Borehole Geophysics	
VSP	Velocity distribution, fractures
Electrical	Hot brines, alteration, faults

2.2.1.1. Gravity

Density contrast among rock units permit use of the gravity method to map intrusions, faulting and geologic structure in general. In Karaha geothermal field, Indonesia, positive gravity anomaly is associated with quartz diorite intrusion that provides the heat source (Tripp et al., 2002). Gravity anomaly maps of the geothermal fields in Vulcano Island (Italy) were used to identify gravity features caused by near-surface geological structures which probably controlled the geothermal activity (Sugihara et al., 2002). Smith et al. (2001) were able to delineate steeply dipping fault at the western side of Dixie Valley geothermal field in Nevada, USA. At prospect scales, high-precision gravity surveys have been used to monitor the gravity changes believed to result from the migration of geothermal fluid (Berrino, 2000; Nishijima et al., 2000). Regional gravity studies and their interpretation could play a major role in understanding the tectonic framework of geothermal systems (e.g., Pakiser, 1964; Malengreau et al., 1999; Götze and Krause, 2002; Woldetinsae and Götze, 2005).

2.2.1.2. Seismic

These methods can be divided into two main subclasses: passive seismic methods, which deal with the effects of natural earthquakes, and active seismic methods, which cover all seismic prospecting having an artificial wave source. In passive seismic method, it has been observed by many researchers that geothermal systems occur mainly in areas characterised by a relatively high level of microseismic activity (Hanus and Vanek, 1989; Doi et al., 2000; Zhao, 2001). In active method, both seismic reflection and seismic refraction surveys have been used to give information about the geological structures (Manzella, 2000).

2.2.1.3. Other methods

Magnetic surveys can be used for structural or lithologic mapping or for mapping decrease in the magnetisation of rocks, caused by hydrothermal alteration (e.g., Soengkono, 2001).

Thermal survey responds directly to high rock of fluid temperature, hence it is the most direct indication of a geothermal resources. A comprehensive discussion on heat flow measurement and interpretation, together with the effects of high temperature gradients on the rheology of geothermal areas can found in Ranalli and Rybach (2005).

When rocks become conductive because of thermal excitation in thermal areas, the distribution can be determined by electrical and electromagnetic methods (e.g., Lugão et al., 2002; Caglar and Isseven, 2004; Oskooi et al., 2005).

Radiometric methods exploit the natural radioactivity of many minerals (CSUI, 2006). The spectral signatures of the radiation emitted by rocks are compared to the characteristic spectral signatures of certain rock types or alteration to identify the source of the radiation. Radiometric methods can also be used to measure the proportions of different radioisotopes in a rock sample. The known half-lives of the isotopes are then used to calculate the age of rock.

2.2.2. RS/GIS in geothermal exploration

The nature of active hydrothermal processes in many geothermal fields is similar to the processes that generate hydrothermal mineral deposits. Therefore, mineral deposit exploration concepts are applicable to exploration of geothermal energy resources, for example, by identifying hydrothermal alteration zones (Bogie and Lawless, 2000).

Imaging systems for geologic investigations went through advances in the last decade with the new sensor technologies to record the earth's physical properties as well as chemical properties through spectral information. Gupta (2003) elaborates the role of remote sensing for geological, stratigraphical-lithological, geomorphological, structural, rock alteration, and geobotanical guides. Sabine (1999) discusses the remote sensing strategies for mineral exploration.

Many authors have applied remote sensing technique in geothermal exploration. Yang et al. (2001) separate three major clay alteration zones in Broadlands-Ohaaki geothermal system in New Zealand using Short-Wave Infrared (SWIR) spectroscopy. Nash and Hernandez (2001) demonstrate application of remote sensing to map vegetation anomalies for geothermal exploration. Carranza and

Hale (2002a) also demonstrate a mineral imaging technique for hydrothermal alteration mapping in heavily vegetated terranes. They apply spectral unmixing of hydrothermally altered rock (clay and iron oxide) using software-defoliant technique (Fraser and Green, 1987). This method enhanced the spectral component of interest (e.g., hydrothermal alteration) in one band over another band that has spectrally interfering component (e.g., vegetation).

Fault/fracture zones provide paths for circulating fluids in geothermal systems. Thus, fault/fracture zones represent attractive targets for exploration. In this respect, geologic mapping along with remote sensing techniques can be used. For example, Soengkono (2000) generated a map of fault and fracture density (FFD) from digital topography data to reveal spatial relationship between geological structures and the high temperature geothermal system at Mokai geothermal field in New Zealand.

It should be appreciated that there is one important limitation of remote sensing data in exploration - the depth aspect. Most mineral deposits occur at a certain depth and are not localised on the surface. However, remote sensing data has a depth penetration of about a few microns in the visible to near-infrared region of the electromagnetic spectrum, to a few cm in the thermal infrared and some metres in the microwave region (Drury, 1993). Therefore in most cases, remote sensing data interpretation must rely on indirect clues, like general geological setting, alteration zones, associated rocks, structure, lineaments, oxidation products, morphology, drainage, vegetation anomaly, etc., since only rarely is it possible to directly pinpoint location of mineral deposits or geothermal fields based solely on remote sensing data.

Recently, applications of GIS recently also went through rapid advances in many fields of studies related with spatial information. Geosciences database such as geology and geophysics, including satellite imagery data can be analysed and integrated in a GIS environment. Many spatial datasets are now being generated by government agencies, private companies, and university researchers. They would be ineffectively used and result in wasted resources without good systems of data management. GIS allows the manipulation and analysis of individual layers of spatial data, and it provides tools for analysing and modeling interrelationships between data layers. A GIS enables a unified approach to organize, visualize, query, analyse spatial data. It also enables development of predictive model based on certain algorithms (Bonham-Carter, 1994).

Examples of spatial analysis done in GIS for mineral exploration can be found in Bonham-Carter et al. (1985), and Carranza and Hale (2002b). Those authors dealt with quantitative analysis of spatial associations between point and curvilinear geological features (e.g., gold occurrences and faults, respectively). Several techniques of integrated mineral prospectivity mapping using GIS modelling have also been investigated by Carranza (2002).

Several authors, such as Prol-Ledesma (2000), Faulds et al. (2002), Coolbaugh et al. (2004) and Coles et al. (2004), have demonstrated relative success of GIS applications to geothermal resource exploration at various scales. GIS have been used in geothermal studies as an aid for geologic structure interpretation (Nielson and Nash, 1997) and to create knowledge based exploration models (Nash and Wright, 1996; Prol-Ledesma, 2000). However, GIS has not been widely adapted by the geothermal industry, unlike in the petroleum industry, where it has proven itself to be an invaluable tool for data visualization, correlation, analysis, sharing, and archiving, even in smaller companies (Nash and Adams, 2001).

2.3. Concluding remarks

Almost all of geothermal energy, which to date has actually been tapped for commercial power production, is of the hydrothermal variety. The heat energy in hydrothermal systems is supported by shallow intrusions and transported upwards by the convection process of circulating fluids.

Gravity method of exploration is mostly used to extract geological structure information in the subsurface. In geothermal applications, indications of locations of convective hydrothermal systems are given by its association to shallow intrusions or to areas where enhanced permeability by faults/fractures occurred. Regionally, gravity method is also applied to investigate the tectonic framework favourable for geothermal systems.

Remote sensing techniques in geothermal exploration have been pioneered in several works with relative success. Many applications of the remote sensing and GIS techniques in mineral deposit can also be applied to geothermal exploration. Furthermore, a GIS could provide useful tools to analyse and integrate spatial relationships in and between different datasets, which are relevant to geothermal exploration.

Chapter 3: The Study Area

3.1. General

The study area is located in the western part of Java Island in Indonesia, within about 105º-109ºE longitude and 6º-8ºS latitude, and measures approximately 400 km by 200 km (Figure 3.1). Indonesia lies astride the equator and has a tropical climate characterised by heavy precipitation (annual rainfall of 875-1000 mm), steady temperature (20-35ºC), and high humidity (80%) throughout the year.

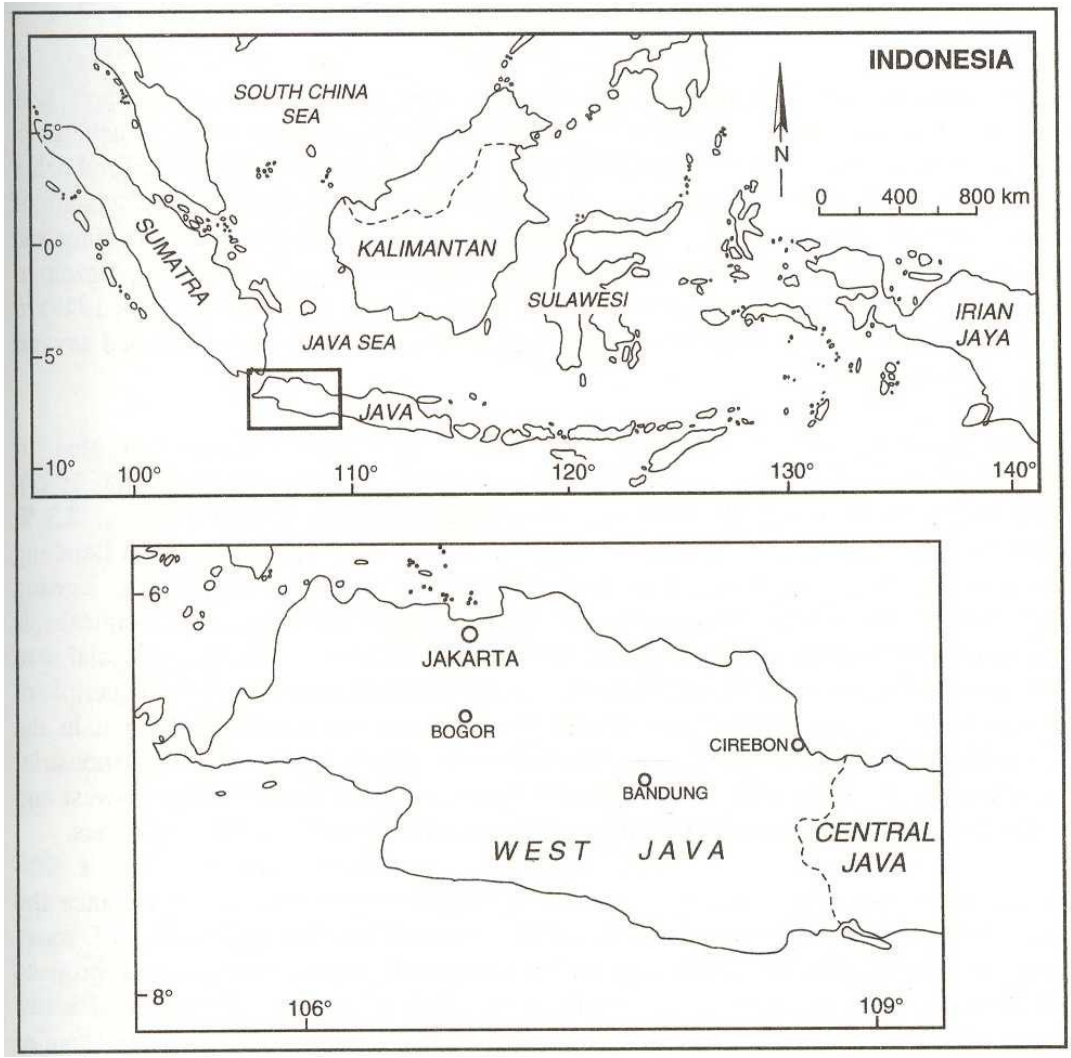

Figure 3.1: Map of Indonesia and study area

Indonesia lies within the botanical region of Melanesia, covering the Malay Peninsula south of the isthmus of Kra, the Indonesian archipelago, the Philippines and the whole of Papua New Guinea and Papua, except the Solomon Islands. For the most part, the Melanesian region is covered by luxuriant growth of tropical rainforest vegetation.

3.2. Regional geological setting

Van Bemmelen (1949), in his extensive discussion of the geology of Java, introduced a physiographic classification and proposed the zonation as illustrated in Figure 3.2. It is still widely applied today. He divided West Java into four units, from South to North:

1. The *Southern Mountains* composed of volcanic arc products associated with interstratified volcano-sedimentary series of Late Eocene and Early Oligocene (Soeria-Atmadja et al., 1990) and are gently tilted southwards;
2. A West-East *central depression zone* with more or less isolated active stratovolcano complexes and sediments derived from these complexes;
3. The *Bogor Anticlinorium zone*, which is a second range of lifted sedimentary deposits or folded mountain belt of Miocene to Pliocene shelf edge and deep basinal turbidites (Bauman et al., 1972; Martodjojo (1984) in Dardji et al. (1994));
4. An *alluvial plain*, made up of Miocene to Pleistocene shelf sediments (Martodjojo (1984) in Dardji et al. (1994)) eroded from the more mountainous areas to the south.

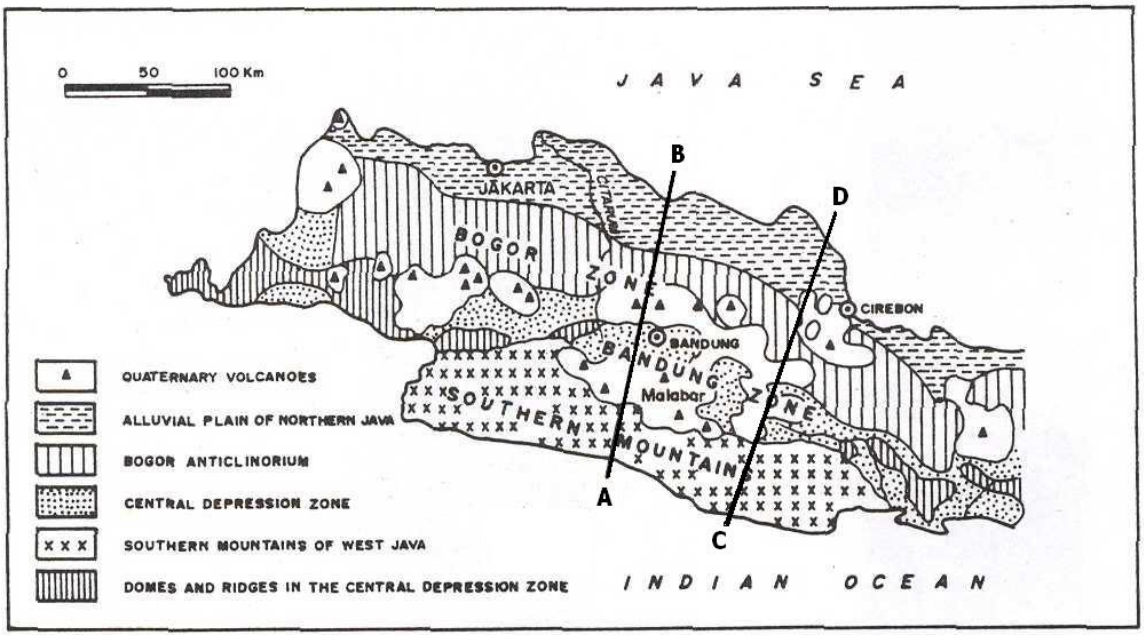

Figure 3.2: Main physiographic elements of West Java (from Van Bemmelen, 1949). Interpretations of cross-sections A-B and C-D are shown in Figure 3.5.

The main physiographic units of West Java are associated with the active Sunda-arc subduction system, which is located south of Java Island (Figures 1.1 and 3.3). The regional tectonic context of this part of the arc-trench system has been discussed by, among others, by Katili (1975) and Hamilton (1979). The oceanic segment of the Indian-Australian plate is thrust under the semi-continental margin of the Eurasian plate with velocities of up to 6-10 cm/year during the Quaternary. The subduction process is accompanied by intensive seismic activity. Moderate to strong earthquakes are therefore common phenomena, especially in the southern part of West Java (Dam, 1994).

The Cenozoic paleogeographical evolution of West Java has been described by Martodjojo (1984) in Dam (1994). From Late Cretaceous to Eocene, a NE-SW trending subduction zone was active (Figure 3.3). In that time, the northern parts of West Java acted as a magmatic arc, while the Cimandiri Fault Zone (CFZ) (Figure 3.4) and the Southern Mountains formed, respectively, a forearc and a trench region. Three small melange terranes (Figure 3.3) mark the approximate position of the subduction complex at the beginning of the Tertiary (Hamilton, 1979; Katili, 1989). The boundary of the Cretaceous continental crust runs approximately from Sumatra to the western part of Java, along the northern coast, crossing the Java Sea and trending to the eastern part of Kalimantan (Figure 3.3). The remnant structure in this NE direction can still be observed on CFZ and the Central Java Fault (CJF) (Figure 3.4) follows what is known as Meratus trend. Evidence for the continuation of the Cimandiri Fault Zone (CFZ) has been identified by Hamilton (1979) in the Java Sea by a structural zone that connects the CFZ to the Meratus Mountains south-east of Kalimantan.

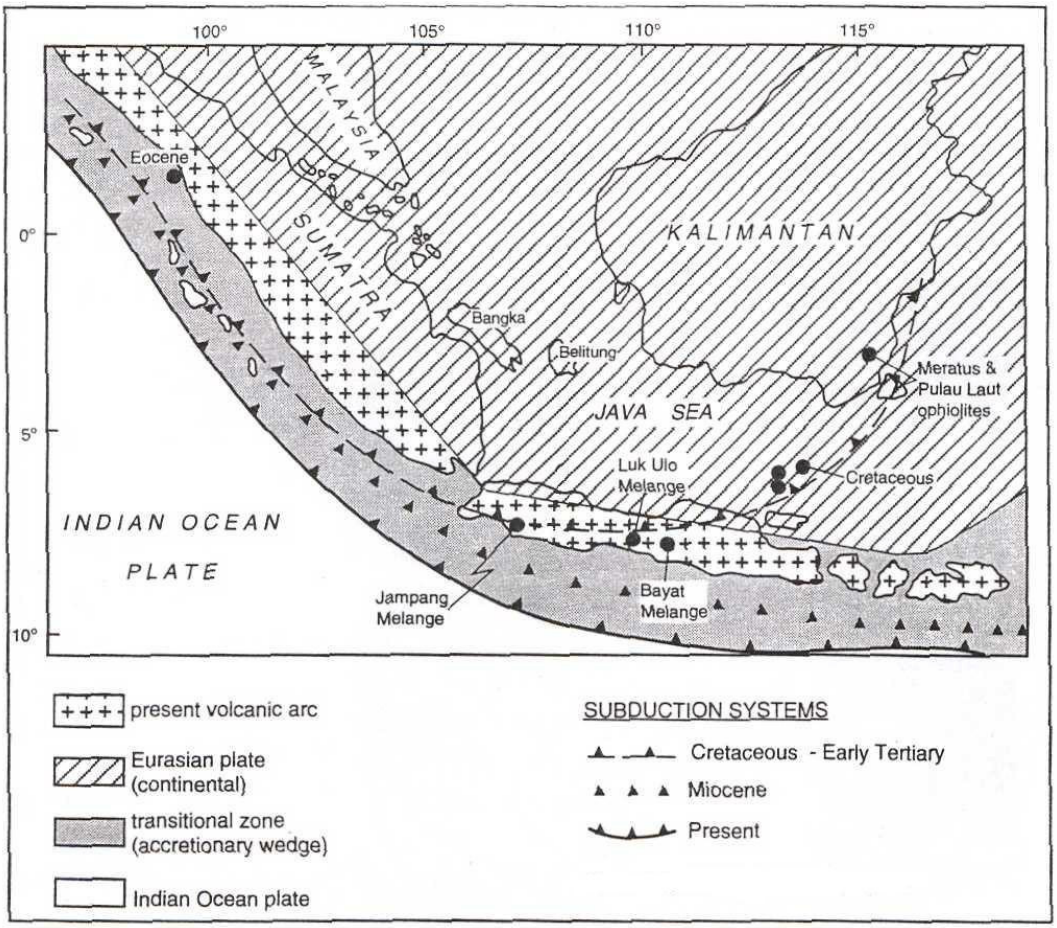

Figure 3.3: Regional tectonic setting of West Java, within the framework of shifting Cenozoic subduction systems in Western Indonesia. After Katili (1989) in Dam (1994).

During Eocene to Oligocene, which was a period of overall tectonic quiescence, the melange wedges and island-arc ridges became base-levelled, started to subside, and were overlain by fringing reef limestones. The Oligocene sediments were developed by reefal limestones, marls, and marly clays, interfingering with quartz sandstones. Pyroclastic sediments were also poured into basins and formed thin tuff and volcanic sandstone intercalated and interbedded with other kinds of sediments. Large proportions of sediments were deposited intermittently in transgressive-regressive series (Thamrin, 1985). It is considered likely [Hamilton (1989) in Dam (1994)] that complete termination of subduction in the Oligocene caused extension and faulting in the overriding semi-continental crustal wedge and the overlying marine sediments. Because of this, sedimentary rocks have different thicknesses and magmatic intrusions occur in different areas (Thamrin, 1985).

A reorganisation of oceanic spreading centres in the Indian Ocean, beginning in Early Oligocene, led to the establishment of a new subduction system along the present Java trench (Figure 3.3) (Soeria-Atmadja et al., 1990). Northward directed thrusting occurred [Martodjojo (1989) in Dam (1994)]. Magmatism and generation of voluminous volcanic rocks as a result of and following this renewed subduction took place during Late Oligocene to Lower Miocene (Soeria-Atmadja et al., 1994). The main magmatic arc was located approximately along the present-day southern coastline of Java, as a row of emerging volcanoes and volcanic islands. Throughout the Southern Mountains region, the Lower Miocene is uniformly characterised by massive andesite breccias, tuffs, and lava series. The climax of volcanic activity was supposedly reached during Lower Miocene. Older melange terrane is intruded by Lower Miocene gabbro/diorite dykes and plutons. North of the volcanic arc, in the present Bandung-Bogor zones (Figure 3.2), the volcaniclastics were deposited as turbidites. Towards the transition with the old continental mass to the north, more shallow marine sedimentation

(marls and limestones) predominates. Towards the end of Middle Miocene, marine sedimentation became dominant again, suggesting decreased volcanic activity.

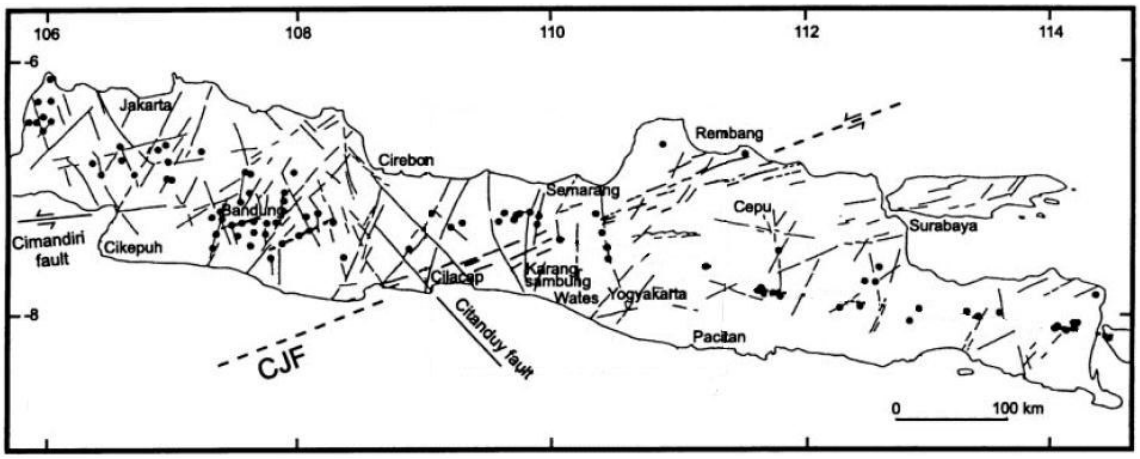

Figure 3.4: Tectonic lineament of Java as inferred from satellite image. Dots denote volcano summits, CJF = Central Java Fault Zone. After Hoffmann-Rothe et al. (2001).

Towards the end of Middle Miocene, the reactivation of arc volcanism in the southern area led to the arching up of the Southern Mountains (Simandjuntak and Barber, 1996). Uplift was most pronounced at the site of earlier volcanism, as a result of strong magmatic inflation of the volcanic arc. This caused strong erosion and base-levelling of the exposed parts (Dam, 1994). Van Bemmelen (1949) assumed that, as a result of the pronounced uplift, several parts of the anticlinal volcanic arc broke off along a west-east trending fault system (Gn. Kancana fault, Figure 3.5a) and slipped towards the North-Java basin. As a result, compressional folding and thrusting is observed in older sediments in the Bandung and Bogor zones to the north. Simultaneously, as a result of the strong deformations originating from the south and the fracturing of the underlying basement, the fold belt in the Bandung and Bogor zones was intruded by andesitic and dacitic magmas. These volcanoes were partly submarine. During the culmination of Upper Miocene to Pliocene events in the basins of the Bandung and Bogor zones, the Southern Mountains already underwent subsidence and base levelling. Large parts of the western and eastern extensions of the volcanic arc were submerged and covered with shallow marine volcaniclastic sediments.

Tectonically, Late Pliocene and Quaternary times are characterised by an extensional regime in the overriding semi-continental crustal wedge, induced by strong subsidence (and a roll-back effect of the subsiding oceanic plate [(Hamilton, 1989) in (Dam, 1994)]). Simultaneously, renewed magmatic uplift took place, which centred in the Bandung zone (Van Bemmelen, 1949), and caused upcoming of the volcanic arc. Uplift resulted from magmatic inflation of the pre-existing crust. Ascending magma chambers and their associated stratovolcano edifices were consequently affected by gravitational spreading which is a major cause for structural deformation. As a result, significant structural features as half-graben and subsidence basins developed within the volcanic arc [(Cas and Wright, 1987; Hamilton, 1989) in (Dam, 1994)].

The tensional regime across the volcanic arc, in combination with magmatic uplift and activity, culminated in the development of a major, deep-seated E-W trending ruptures through the central part of volcanic arc, with the northern part subsiding down and northward. As a result of faulting and dislocation of the anticlinal central arc, the Tertiary strata in the northern Bogor zone became compressed and folded. Shortly after the initiation of the major east-west trending fault zone along the southern boundary of the Bandung zone, volcanic activity led to the built up of the main volcanoes south of Bandung. To the north, a high volcanic range was formed, when magmatic intrusions settled between the deformed strata in the Bogor Anticlinorium zone.

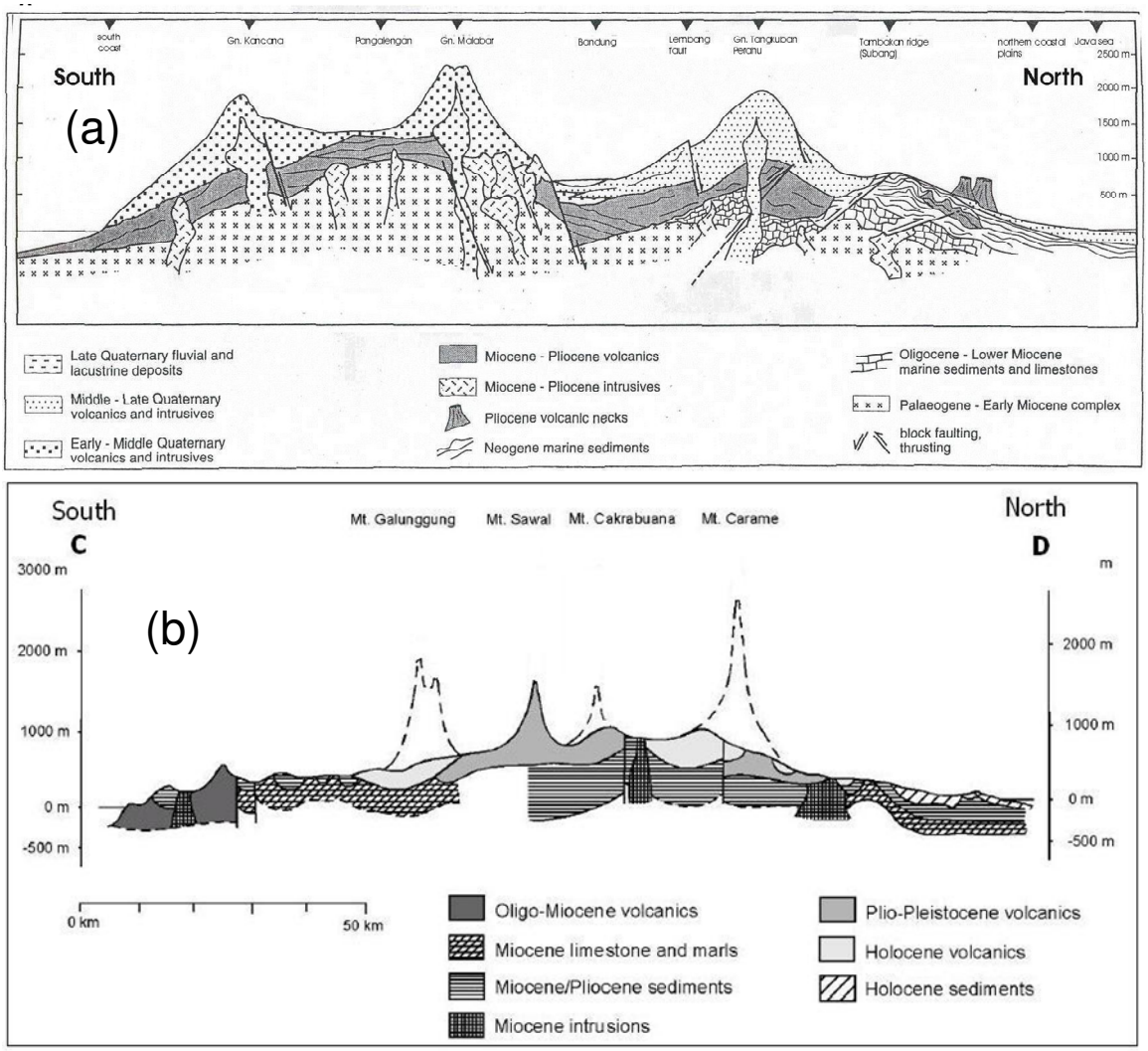

Figure 3.5: Schematic cross-sections through West Java. (a) Section AB (Dam, 1994) and (b) Section CD (Dijk, 2002). See Figure 3.3 for locations of these sections.

In summary, general geology of study area consists of (Figure 3.5):

a) Volcanics and intrusives – Early to Middle Quaternary in age in the south and Middle to Late Quaternary in age in the north;
b) deformed strata (Middle Miocene to Pliocene) of Bogor Anticlinorium zone;
c) Tertiary (Miocene–Pliocene) volcanics and intrusives;
d) Oligocene–Pliocene marine and volcaniclastic sediments; and
e) Paleogene basement complex, consists of various igneous (diorite, monzonite) and metamorphic rocks (argillite) (Patmosukismo and Yahya, 1974).

Generally, structural patterns in West Java and its surroundings can be divided into three major groups (Widianto et al., 2004):

1. The NE–SW trend can be traced NE to Kalimantan at Meratus mountains; hence its name *Meratus Structural Domain*;
2. The N-S trend is very dominant in northern off-shore West Java. The best example is the Sunda basin in northern West Java; hence the name *Sunda Structural Domain*; and
3. The NW–SE to E–W trend is the most developed structure in Java Island; hence the name *Java Structural Domain*. This structural domain cuts the Meratus and the Sunda domains, so it is younger.

The NW-SE trend is commonly found in the western part of Java Island following the NW-SE trend of Sumatra Island, which is associated with the NW-SE trending portion of the Sunda Trench where the Indo-Australian plate subducts beneath the Eurasian plate (Figure 1.1). The dominant NE-SW and NW-SE trends of lineaments and faults found in the study area are also attributable to the N-S compression due to the collision between the Indo-Australian and Eurasian plates along E-W trending portion of Sunda Trench to the south of Java Island (Figure 1.1). This is based on analogy to many observations of uplifted crustal material, where conjugate faults were formed, as a result of deformation in a "brittle" upper crust (Mandl, 1988). Furthermore, subduction zones tend to initiate on pre-existing weakness zones (Windley, 1995).

3.3. Known geothermal resources

A large part of the Indonesian archipelago is occupied by volcanic product, with some young volcanoes that form active volcanic belts (Figure 1.1). Tectonic movements in the past were usually followed by inner and intense external volcanism, causing the ascent of magma to shallow depths. The presence of shallow magma, abundant precipitation (about 3000-4000 mm/year in the western region) and volcanic rocks that could act as cap and reservoir rocks, have created ideal conditions for the development of geothermal systems (Alzwar, 1986).

The volcanoes of geothermal interest in Indonesia are dominantly andesitic and the characteristic cones of stratavolcanoes can be recognised throughout the landscape of the country. Many of the countries geothermal areas occur on or adjacent to these volcanic edifices and complexes (See Figures 1.1 and 1.2). Frequently, more than one geothermal field is associated with a volcanic complex, although only part of a complex is still volcanically active, e.g., Guntur and Kamojang geothermal fields. Calcareous sediments of Tertiary age frequently underlie much of the Quaternary andesitic volcanics (Mahon et al., 2000), which can provide a possible environment of geothermal reservoir.

The present day volcanic arc in Java is a superposition of Tertiary and Quaternary volcanoes and is prospective for geothermal energy development. Within this volcanic arc, volcanoes can be classified as Type A, Type B and Type C according to their activity stages. Type A volcanoes are those that erupted at least once after A.D. 1600. Type B volcanoes never erupted after A.D. 1600; however, the activities are still indicated by solfatara[4]. Type C volcanoes are those whose eruptions are unknown, but past activities are shown by fumarole fields. Several geothermal prospects had already been investigated by Pertamina Geothermal division, Directorate of Mineral Inventory (DIM), and private companies. Four geothermal power plants generating electricity lie within this volcanic arc. Awibengkok Gunung Salak power plant, operated by UNOCAL, occurs in type B volcano, while the other three [i.e., Kamojang (Pertamina), Wayang Windu (MNL), and Darajat (Amoseas)] coincide with type C volcanoes.

To this date, West Java Province has geothermal potential of 5311 MWe, but so far only 805 Mwe is exploited for electricity. The producing geothermal areas are Kamojang (140 MWe), Salak (345 MWe), Darajat (135 MWe), and Wayang Windu (185 MWe) (Huttrer, 2001; Bertani, 2005). Fauzi et al. (2000) reported the reservoir characteristics of these geothermal areas. Kamojang is a vapor-dominated system with an average reservoir temperature and pressure of about 245ºC and 35 bars. The Salak field hosts a liquid-dominated reservoir with temperatures ranging from 240ºC to 310ºC. The Darajat reservoir is vapor-dominated with a temperature of about 245ºC. Wayang Windu reservoir is liquid-dominated, and temperatures range from 250ºC to 270ºC. Another geothermal area which has been confirmed and ready to be developed is the Karaha field with liquid-dominated reservoir overlain by a steam cap and temperatures range from 230ºC to 245ºC. Table 3.1 shows other high temperature geothermal potential.

[4] Solfatara: A type of fumarole, the gases of which are characteristically sulphurous. Fumarole: A vent or opening through which issue steam, hydrogen sulphide, or other gases. The craters of many dormant volcanoes contain active fumaroles.

3.4. Previous exploration works

Geothermal energy exploration started in Indonesia in the early 1900's. In the 1920's, the Dutch drilled successful shallow test wells at Kamojang, West Java, which triggered a country-wide inventory of geothermal features. In 1926-1928, studies on the exploitation of geothermal energy for electrical power generation were carried out by Van Dijk and Taverne, and later by Van Bemmelen (Zen and Radja, 1970).

Table 3.1: Energy resources (in MWe unit) geothermal fields in West Java (from INAGA, 2005).

Prospect	Exploited (out of Total)	Reserves		Resources	Total
		Proven	Possible		
Kamojang	140	230	70	-	300
Salak	330	485	115	-	600
Darajat	125	280	70	-	350
Cisolok	-	-	50	50	100
Patuha	-	170	247	65	482
Wayang-Windu	110	250	135	75	460
Karaha	-	30	170	50	250
Telaga-Bodas	-	-	200	75	275
Cibuni	-	120	-	-	120
Tangkuban-Perahu	-	-	90	100	190
Batukuwung	-	-	55	50	105
Citaman	-	-	25	50	75
G. Endut	-	-	30	20	50
G. Gede-Pangrango	-	-	130	130	260

In 1966, UNESCO wrote a favourable report on the possibilities of utilizing geothermal energy for commercial purposes, and this encouraged the Institute of Power Research of Indonesia to sponsor a preliminary survey to map several geothermal areas in Java. Zen and Radja (1970) reported that several areas have been found to be prospective for further exploration. The areas considered potential in West Java are G. Tampomas (Mount Tampomas) and surroundings, the solfataric field of Kawah Kamojang, and the hot spring area of Cisolok. The geological conditions of the different geothermal fields (except Kawah Kamojang) are similar, consisting of Tertiary sedimentary series – which act as reservoir and cap rocks; intruded by magmatic stocks during the last phases of volcanism, which act as heat sources. Structurally, these areas are dissected by faults.

In 1972, the Indonesian government conducted a more complete inventory with technical assistance from Italy, Japan, New Zealand, and USA. The earliest map of regional prospective geothermal areas of West Java was published by Geological Survey of Indonesia (Figure 3.6). In 1986, Alzwar studied 128 young Quaternary volcanoes in Indonesia described as eruption centres related to several tectonic systems, of which 27.3% (35) of those volcanoes are located in Java Island. These volcanoes are evidence of the relationship between geothermal system and active volcanism in Indonesia.

Extensive geological and geochemical surveys had been conducted in this area, organised by Pertamina (Geothermal Division) – a government agency for geothermal development in Indonesia. Since 1991, several joint-operations and contracts between Pertamina and authorised private companies have resulted in many studies exploring this area for geothermal energy. While geological studies has been the main method in regional geothermal surveys, geophysical surveys is more focused on a detailed survey within proven fields to delineate possible field extensions and to increase the accuracy of drilling targets.

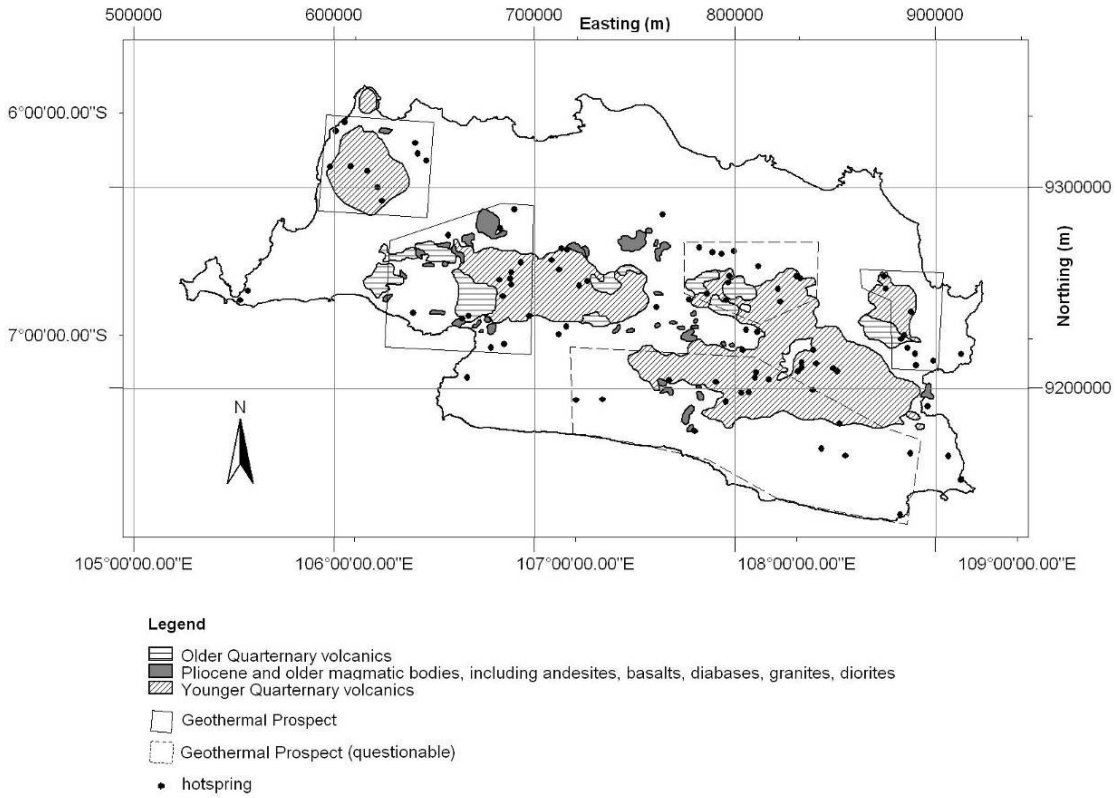

Figure 3.6: Map of prospective geothermal areas in West Java (modified from Purbo-Hadiwidjojo, 1970)

3.5. Research datasets

The datasets used in this research are in public domain, which means they can be obtained easily from public archives, such as government agencies and internet. The datasets used here are derived from published maps and papers.

3.5.1. Gravimetric

The gravity datasets have been compiled by the Geological Research and Development Centre (GRDC) of Indonesia. The compilation consists of ground gravity datasets from different survey campaigns of different purposes and time of acquisition. There are 7550 data points of Bouguer values and location (Figure 3.7).

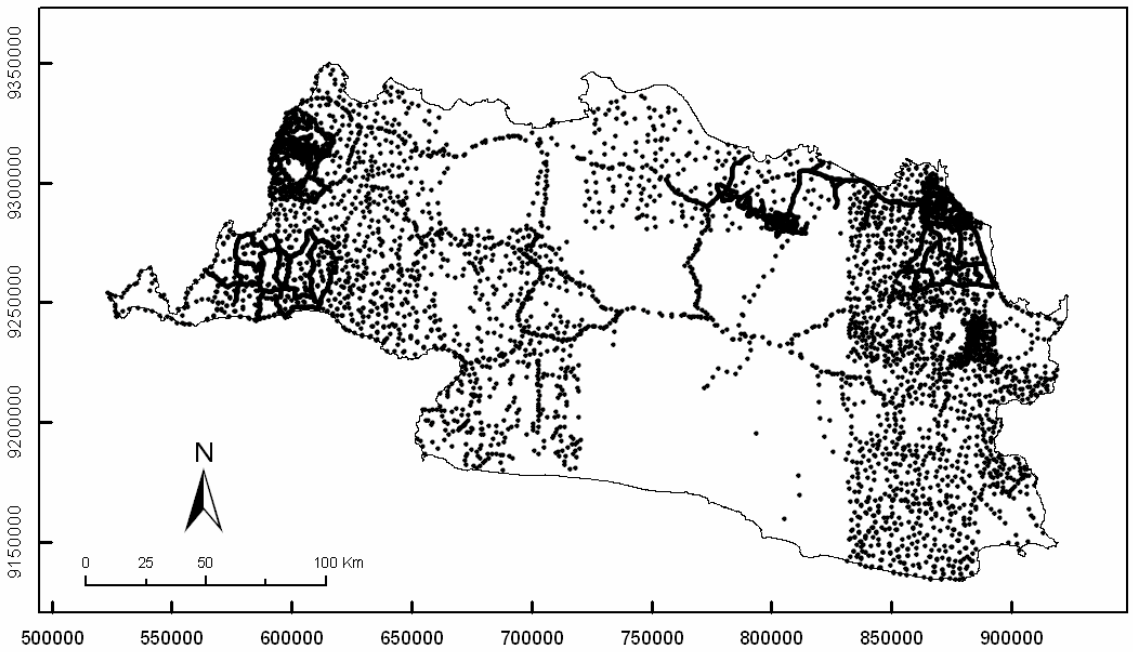

Figure 3.7: Map of locations of gravity data observation points.

3.5.2. Earthquake focal data

Earthquake epicentre data were obtained from the Meteorological and Geophysical Agency (National Seismological Centre) of Indonesia and Geological Research and Development Centre of Indonesia. In the study area, the data contain total 127 earthquake epicentre locations with magnitudes of 2.7-6.2 on the Richter scale and with approximate depths of less than 10 km (Figure 3.8).

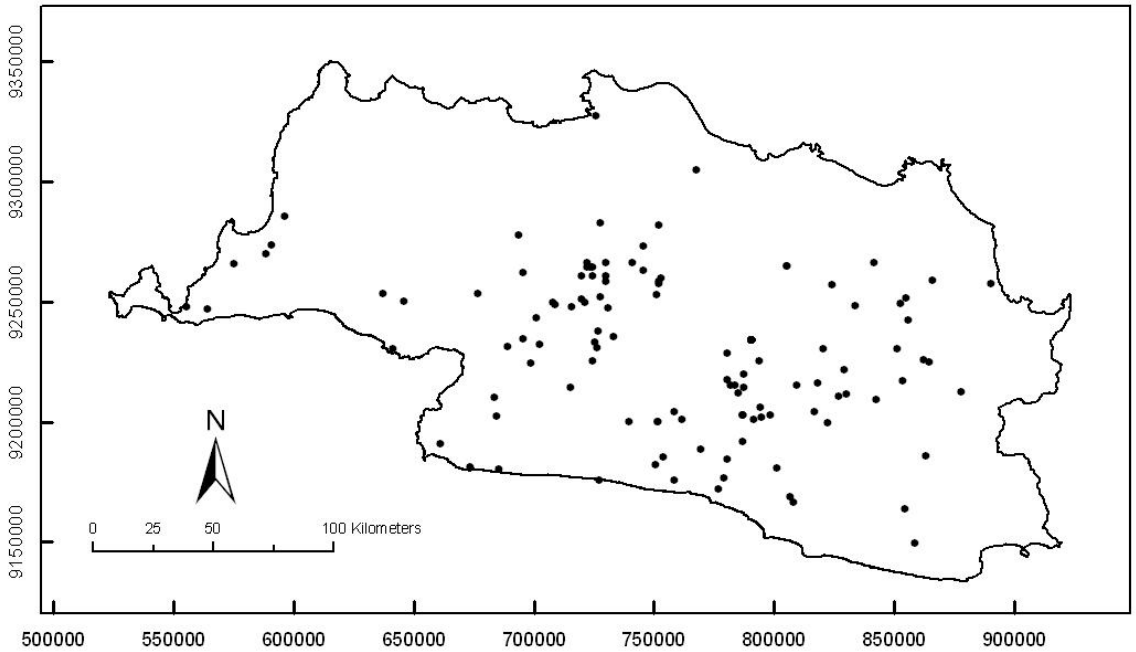

Figure 3.8: Earthquake epicentres (depth less than 10 km).

3.5.3. Geological map

The data were digitised from an existing 1:100,000 scale geological map sheet published by the Geological Research and Development Centre of Indonesia (Figure 3.9). The geological information, which is of higher detail for regional-scale purposes, was generalised (i.e., regionalised) to give general comparison with the regional gravity map used in this research.

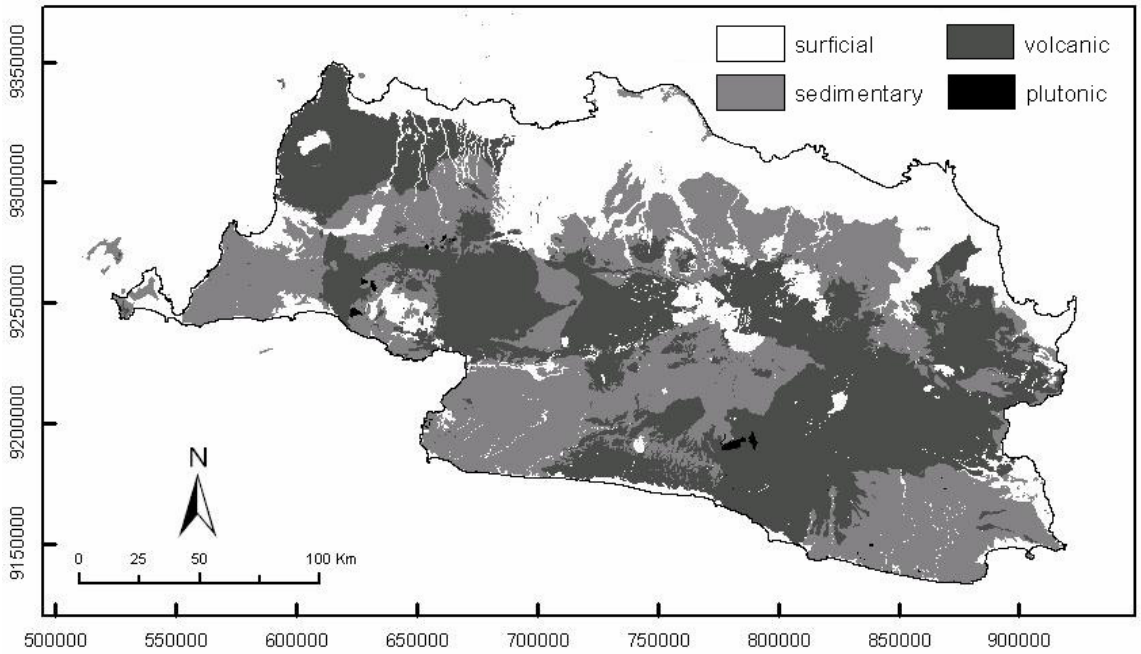

Figure 3.9: Generalised lithologic map.

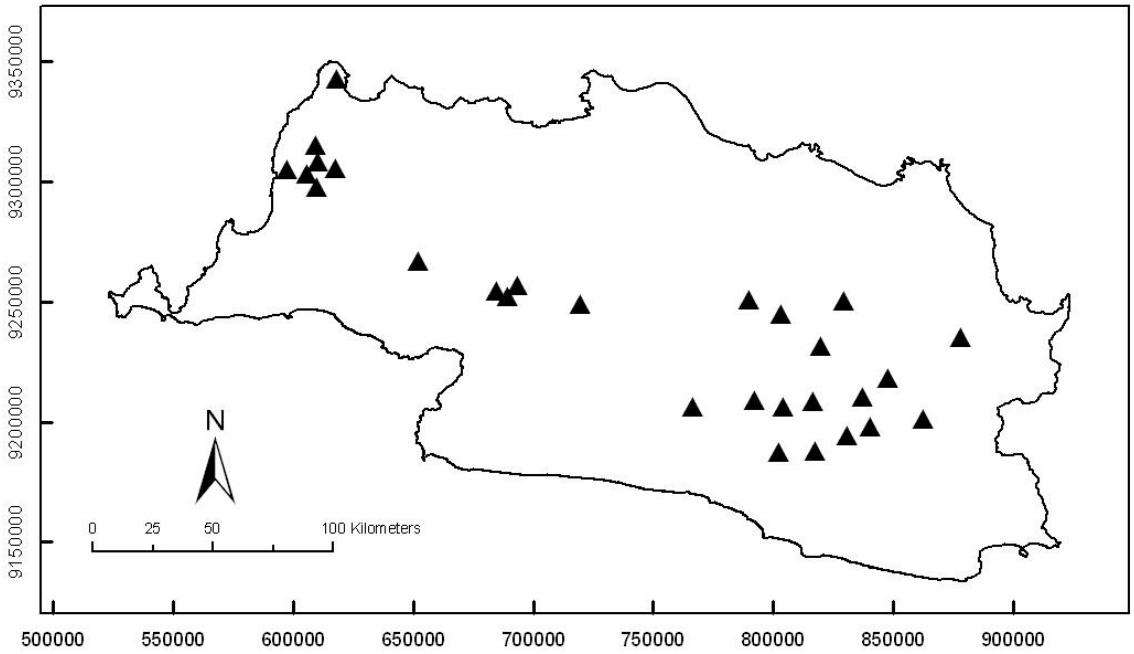

Figure 3.10: Map of location of volcano summits.

3.5.4. Volcanoes

The data of locations of volcanoes (Figures 3.10) were compiled from the Indonesian Directorate of Volcanology and Geological Hazard Mitigation, the literature (Van Bemmelen, 1949), digitised shaded-relief images of SRTM DEMs, and obtained from the internet (http://www.volcano.si.edu/world/).

3.5.5. Fault map

This was digitised from an existing 1:100,000 scale geological map sheet published by the Geological Research and Development Centre of Indonesia (Figure 3.11). The fault map was augmented by additional structural information from geoscience literatures (Hoffmann-Rothe et al., 2001; Susilohadi et al., 2005) and by interpretations of SRTM data.

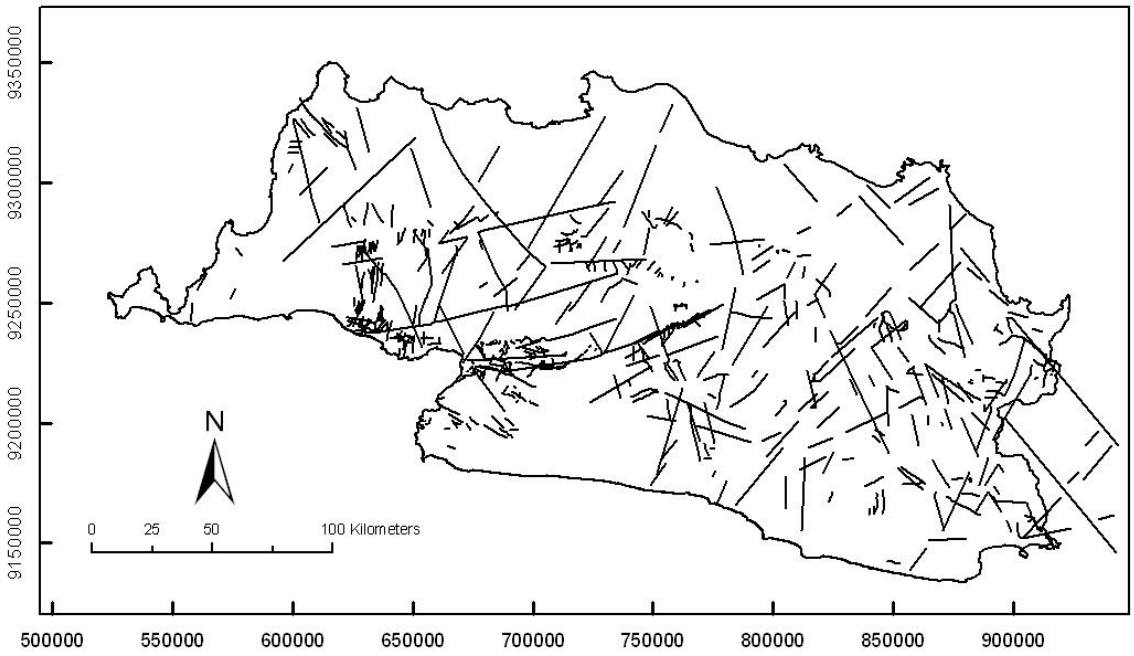

Figure 3.11: Map of faults digitised from various published maps.

3.5.6. Landsat TM and SRTM data

The study area is covered by six scenes (path 121-123 / row 64-65) of Landsat TM5 data, acquired in years 1989, 1991, and 1992 (Figure 3.12). It also covered by six scenes of SRTM DEMs acquired in year 2000 (Figure 3.14). The scenes are of the same path/row as Landsat TM5 data. These data were all downloaded freely from the website of Global Land Cover Facility (http://glcf.umiacs.umd.edu/data).

3.5.7. Geothermal occurrences

Data of geothermal occurrences were obtained from the Indonesian Directorate of Volcanology and Geological Hazard Mitigation (http://www.vsi.esdm.go.id/pbumi/index.html). The data contain information about 53 geothermal occurrences (Figure 3.14).

3.6. Concluding remarks

The geological and tectonic settings in West Java provide favourable conditions for occurrences of geothermal resources that can be utilised as energy source. These favourable conditions are mostly caused by volcanism associated with the subduction history in this area. Volcanism due to ascending magma chambers resulted in several stratovolcano edifices, providing potential heat sources for

geothermal fields. The resulting structural features, in the form of half-grabens and subsidence basins developed within the volcanic arc, provide structural control and potential reservoirs for geothermal fields.

The study area has been extensively explored for many years. Existing exploration and geothermal occurrence data are considered representative for this area, although details on each geothermal field are fragmentary, sometimes confidential and mostly extracted from public domain source. Analyses of the various available data sets presented in the succeeding chapters are performed to deduce further knowledge of geothermal prospectivity, which could be applied for regional-scale mapping of geothermal prospectivity in the study area.

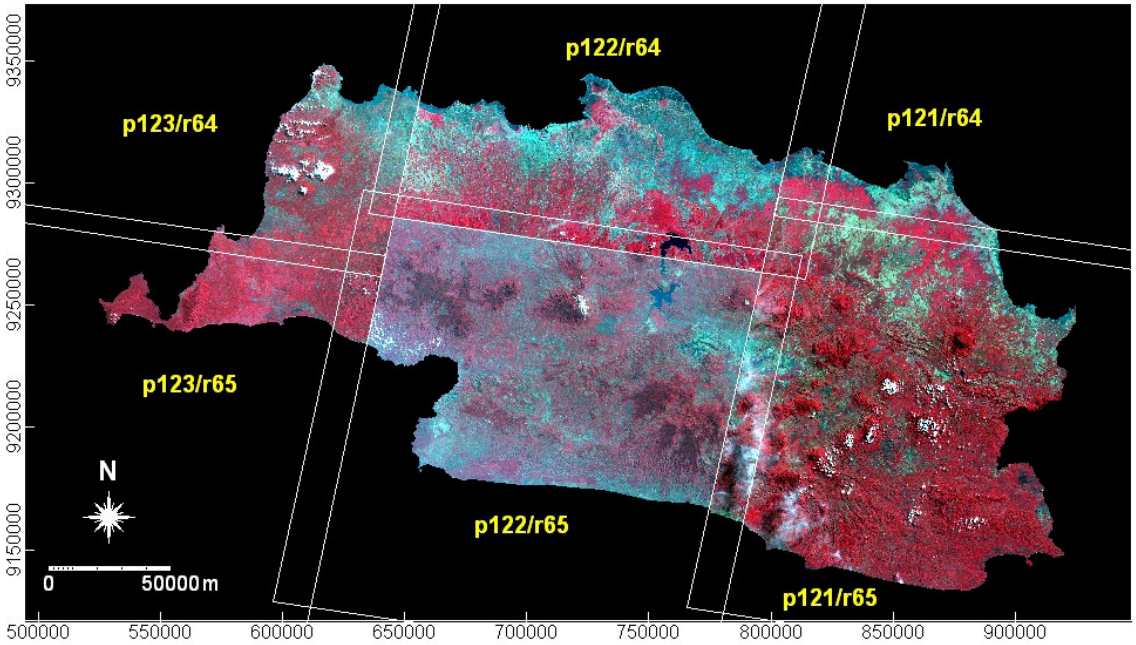

Figure 3.12: Mosaic of Landsat TM false colour composite (red = band4, green = band3, blue = band2).

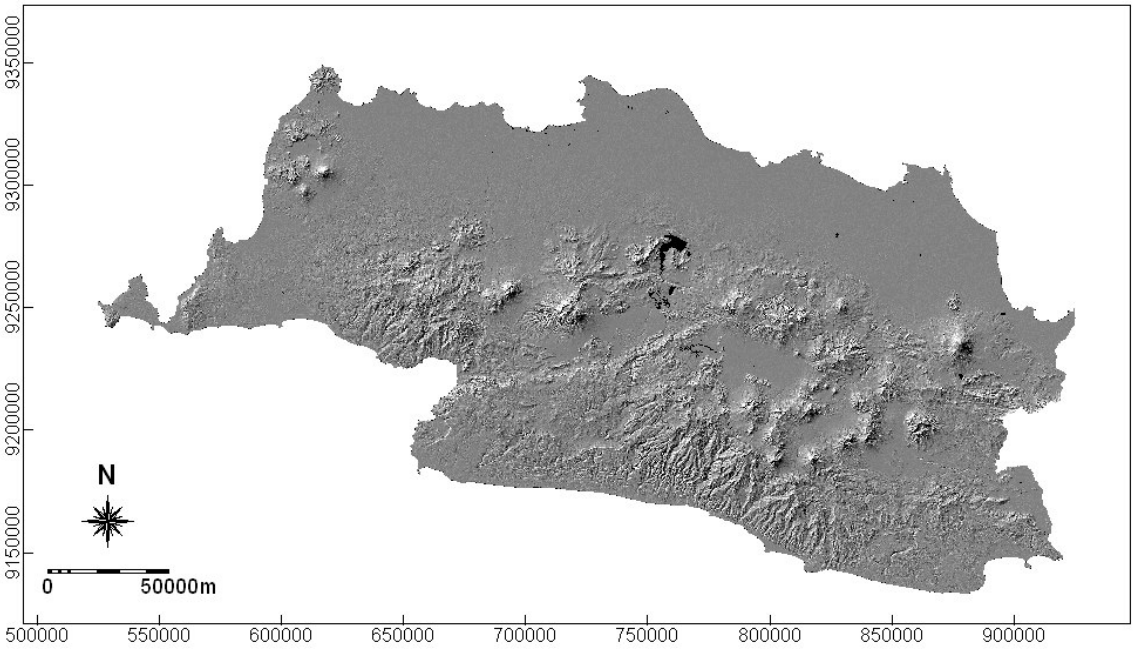

Figure 3.13: Shaded relief (NW-illuminated) SRTM DEM.

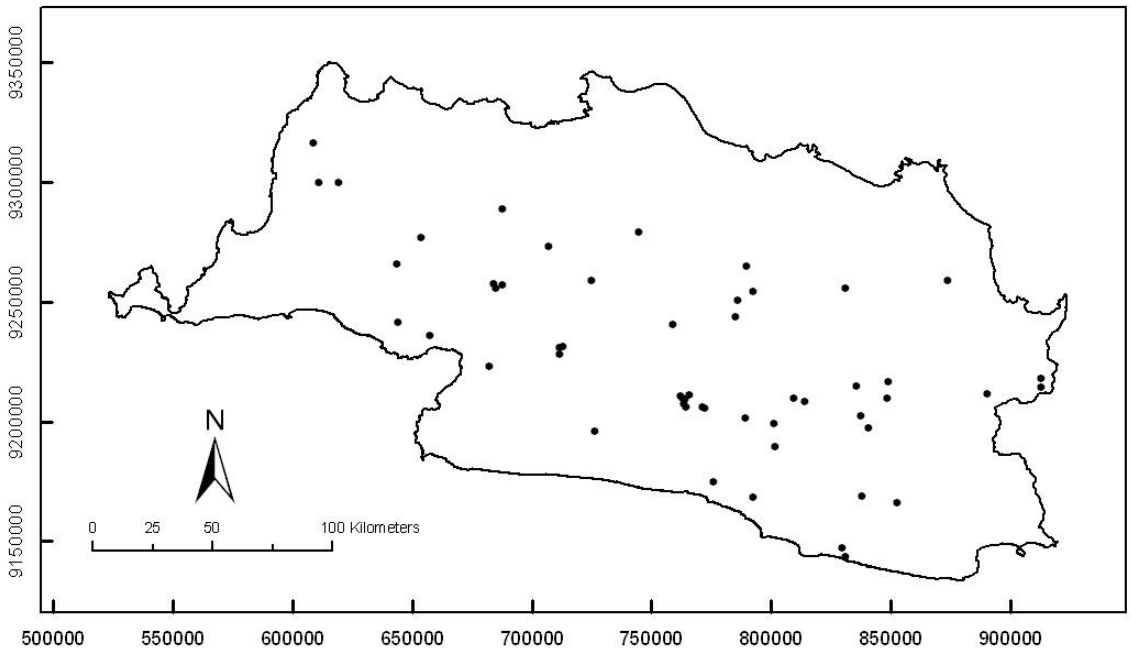

Figure 3.14: Geothermal occurrences location map

Chapter 4: Conceptual Model of Geothermal Prospectivity

The objective of this chapter is to formulate a conceptual model of regional-scale prospectivity for geothermal resources. As defined in Chapter 1, prospectivity refers to combinations of (or spatial intersections between) sets of indicative geological features for geothermal occurrences. So, if in one area there are more intersections between sets (or map layers) of indicative features than in another are, then the former has higher prospectivity.

The conceptual model of regional-scale prospectivity for geothermal resources is based on (a) review of literature for geological characteristics of known geothermal occurrences in the study area and supported by (b) analysis of spatial distributions of known geothermal occurrences and mapped geological features and (c) analysis of spatial associations between known geothermal occurrences and mapped geologic features. The spatial analyses were carried out to explore subtle, but nevertheless important, patterns in the data that are suggestive of geological controls on geothermal occurrence.

4.1. Literature review of geothermal occurrences

4.1.1. Global characteristics of geothermal occurrences

A summary of compilation of geological characteristics of known geothermal occurrences in the world is given in Table 4.1. Based on the summary and other information from the geological literature, important criteria to be considered in regional-scale exploration of prospective geothermal areas should include (a) heat sources, (b) reservoir rocks, (c) structural controls, and (d) surface manifestations.

Table 4.1: Summary of geothermal environments (from Muffler, 1976; Heiken, 1982).

CRITERIA	GEOLOGICAL ENVIRONMENTS					
	Regions with young volcanic rocks		Regions with basaltic volcanism	Tectonically active regions	Geo-pressurized geothermal	Regions of normal heat flow
	Large silicic magma bodies	Magma bodies of intermediate composition				
Description of source	Large (up to 1,000 x 50 km batholiths) bodies with smaller cupolas rising to the surface. May be thin (<10 km thick). Intrude to within 5 km of surface. Long cooling times (>10^6 years).	Thin frameworks of dikes and sills within cones and small (<1 km^3) "plugs" within central conduits. Slightly larger bodies present below volcanoes at depths of 5-15 km. Variable cooling times (days to 10^6 years).	Thin networks of dikes. Some sills, a few very small shallow bodies such as laccoliths. Unless rate of intrusion is high, the bodies cool very rapidly. Elongate dike systems.	High heat flow. Circulation of meteoric water down fault planes.	Hot water held in "sealed". Well-insulated thick sedimentary sections.	Old silicic terrane with high radiogenic heat production, overlain by blanket of insulating sediments.
Surface manifestations	Associated with large-volume deposits of silicic ash calderas, ring-dikes. Large depressions surrounding regions of volcanic activity. Large areas of hot spring, geyser activity.	Stratovolcanoes, domes, small calderas, some cinder cones. Short-term fumaroles activity, hot springs.	Fissures, shield volcanoes, cinder cones, associated with extension at faulting. Some fumaroles or hot spring activity.	Hot springs, normal faults. Active, recent tectonic activity.	None.	None: heat flow anomalies.
Tectonic setting	Subduction zones, "plumes". Offsets in major extensional faults.	Subduction zones. Some "plumes" and fault intersection.	Spreading centres. Continental rifts. Areas with extensional faults.	Crustal uplift, faulting on continents.	Continental margins with fast sedimentation rates.	Stable continent.
Possible geothermal reservoirs and extraction techniques that might be used.	Heat transfer by convection and conduction. Hot-water and steam reservoirs overlie cooling bodies. All techniques may be used, depending upon age, nature of hydrology within rocks over the source.	Heat transfer from larger bodies by convection and conduction. Smaller bodies –conduction. Small hot-water or steam systems. Might use HDR or "magma top" techniques.	Hot-water-steam systems maintained in regions with high rate of intrusion.	Hot water for "low-grade" geothermal use.	Top hot water steam, methane from permeable sediments.	Hot-dry rock, geothermal.

It can be concluded from sections 1.1 and 2.1.2 that Indonesia's geothermal fields are associated with active volcanic belts, which resulted from magmatic activity along the convergent plate margin along the Sunda Trench (Figures 1.1 and 2.1). Thus, geothermal systems supported by shallow intrusions are more likely to occur in this area than other types of geothermal systems. Based on previous discussions in the previous chapter, geological characteristics of known geothermal occurrences found in West Java indicate that the geothermal environments conform to that of regions of young volcanic rocks, particularly those with magmatic bodies of intermediate composition (Table 4.1; Katili, 1975).

4.1.2. Volcano-tectonic depressions and geothermal occurrences

Some regions of intense geothermal activity are within a broad volcano-tectonic depression. Similar Quaternary volcano-tectonic depressions containing geothermal fields occur on Philippines and Indonesia (Tamanyu and Wood, 2003). Structural features such as half-grabens and subsidence basins, might lead to the formation of geothermal reservoir system. For example, within the Taupo Volcanic Zone (TVZ) depression, New Zealand, rifting and tilting occurred, which resulted in the formation of a graben and horst structure in the modern TVZ (Wilson et al., 1995). The structural associations of TVZ geothermal fields were examined by Wood (1995) (in Tamanyu and Wood, 2003), who concluded that the majority of geothermal fields are located at the margins of major calderas. These calderas are believed to provide deep-rooted fracture systems, which allow circulation of both cold and hot water into heat-source regions that may not be directly beneath the shallow parts of the geothermal fields but are more centrally located within the calderas. Thus, structural control in the depression provides conduit paths for rising hot fluids, particularly in TVZ, where there are localised horst structures (Tamanyu and Wood, 2003).

In the study area, Bandung zone is located in central depression of West Java (Van Bemmelen, 1949). There are several geothermal fields in this zone. The Wayang Windu geothermal field is located approximately 40 km south of the provincial capital city, Bandung (Figure 4.1, right inset box). This field is associated with Mt Malabar, a large, extinct andesitic stratovolcano consisting of lavas, breccias, lahars, and tuffs of basaltic andesite to dacitic composition. Separate and distinct high enthalpy geothermal fields occur in the Bandung area, e.g., the developed Kamojang and Darajat geothermal fields, which are both associated with volcanic crater settings. Each of these fields is associated with a separate andesitic stratovolcano.

Danau Rawa (Lake Rawa) is also a volcanic depression (Figure 4.1, left inset box) and forms the focal point for the geothermal activities in this field (VSI, 2005). In the early Pleistocene, basaltic andesite and andesite lavas and pyroclastics were erupted to form a large volcanic complex with several flank eruptions forming cones in the northern part of the mountain. Explosive eruptions followed this mountain building phase resulting in a very large area surrounding the volcano being covered by pumice pyroclastic flow deposits and eventual collapse of the volcanic structure "along a system of pre-existing faults" to form the caldera. Pliocene-Quaternary volcanic sequence unconformably overlies a Tertiary volcanic sedimentary sequence which includes pyroclastic volcanics and terrestrial and marine sediments including limestones.

4.1.3. General characteristics of geothermal occurrences in study area

This section provides a summary of the geological characteristics of known geothermal fields in West Java. Table 4.2 contains the descriptions geothermal fields and serves as a reference for the discussion.

4.1.3.1. Plausible heat sources

Most of the known 53 geothermal occurrences in the study area are located within or near Quaternary volcanic areas (Figure 4.2). Frequently, more than one geothermal occurrence is associated with a volcano complex, although only a part of a volcano complex is still active (e.g. Guntur and Kamojang geothermal field). Špicák et al. (2005) has established that primary magma is parent material of the calc-alkaline volcanic rocks in the volcanoes in western Java Island. Alzwar

(1986) reviewed the geothermal energy potential in relation with volcanism in Indonesia and showed that geothermal occurrences are strongly associated with active volcanism from the nearby volcanoes (see also Table 4.2). Therefore, Quaternary volcanoes represent plausible heat sources of known geothermal occurrences in West Java.

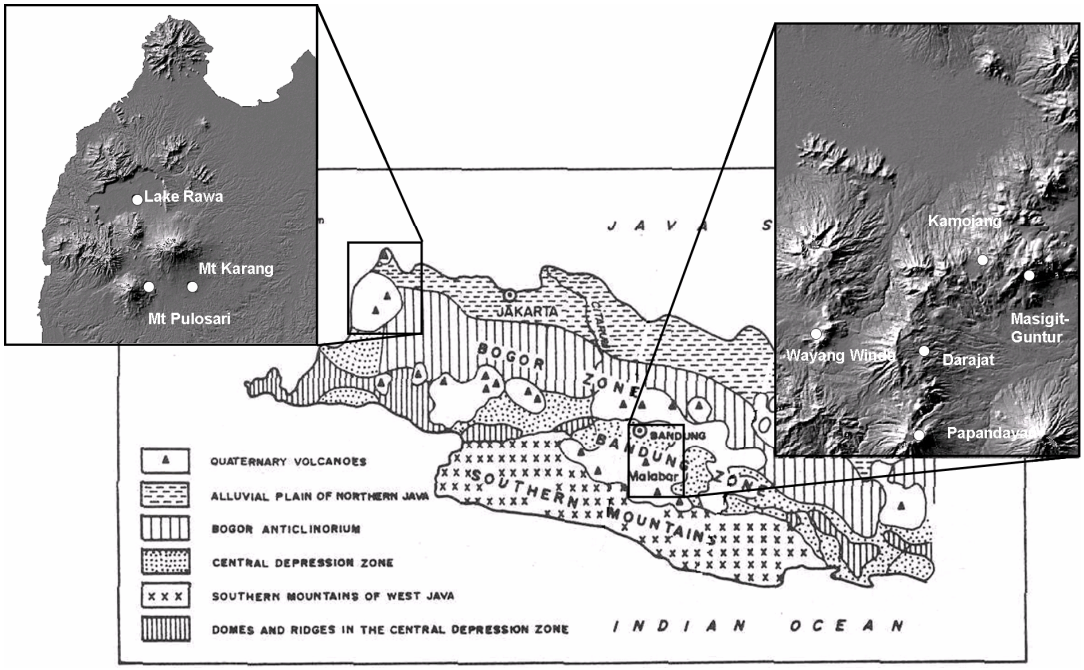

Figure 4.1: Lake Rawa geothermal system (left inset box) and Bandung zone geothermal complex (right inset box). Inset boxes shows geothermal occurrences (white dots) overlaid on a shaded-relief image of a SRTM-DEM.

4.1.3.2. Reservoir and cap rocks

The data in Table 4.2 indicate that sub-surface lithology in many geothermal prospects are sedimentary rocks, which serve as permeable mediums for fluids to circulate convectively. Most importantly, as can be examined from the table, geothermal prospects in areas with sub-surface lithology of sedimentary rocks are overlain by volcanic rocks. Therefore, reservoir rocks in the study area are either volcanic or sedimentary rocks, and cap rocks are mostly volcanic rocks. The spatial distributions of Quaternary volcanic rocks and geothermal occurrences are shown in Figure 4.2.

The occurrence of sedimentary rocks (which could act as reservoir rocks) in Java is due the decrease in the subduction convergence rate, which occurred in Middle Eocene when the Indian continent started to collide with Eurasia. This event led to the development of many extensional basins in Southeast Asia, including West Java [Karig et al. (1979) and Hall (1997, 1998) in Susilohadi et al. (2005)]. These basins were later filled for the most part by sediments derived from erosion starting mostly in the Eocene and Oligocene (Thamrin, 1985). Carbonate rocks were locally formed as reef growth, reefal beds, and fossiliferous limestone. Pyroclastic sediments were also poured into the basins and formed thin tuff and volcanic sandstone intercalated and interbedded with other kinds of sediments. These sedimentary and volcano-clastic formations could potentially serve as geothermal reservoirs, as can be found in Tampomas and Cisolok areas, where thick sediments ranging from sandstones and marls were intruded by magmatic intrusions (Zen and Radja, 1970). Other sources of sediment materials are strong erosion and base levelling of the exposed parts (Van Bemmelen, 1949; Dam, 1994) during uplift towards the end of Middle Miocene, when the anticlinal volcanic arc broke off. Finally, during the extensional regime of Late Pliocene to Quaternary, sediments filled the half-graben and its related subsidence basins within the volcanic arc [Cas (1987) and Hamilton (1989) in Dam (1994)].

Table 4.2: Summary of geothermal occurrences in West Java (from Suryantini et al., 2005)

Regency/ Kabupaten	Geothermal prospect	Surface manifestation	Geology	Structure	Geother-mometry
Bandung	Tangkuban Parahu	volcanic crater, solfatara, hot springs, steaming ground, rock alteration, mud pools, active silica sinter	stratovolcanic andesitic in Quaternary, collapse become caldera as center for recent volcanism	caldera (recent crater) Quaternary volcanism occur within graben complex Plio-Pleistocene but still active now, bounded by Tembakan fault at the S crossed by NE-SW younger fault	200°C
	Maribaya	hot springs	outflow of G. Tangkuban Parahu	Lembang fault	120°C
	Patuha	volcanic crater, hot springs, fumaroles, solfatara, cool mud pool, surface alteration, silica sinter	Tertiary volcanic rock related to Patuha volcano activities, overlies by Quaternary volcanic rock from the same volcanism	stratovolcanic complex, regional structure is NE and NW	> 240°C (up to 270°C)
	Cimanggu	outflow of Patuha to the west, sulphur, iron oxide and travertine at Cimanggu springs	similar to Patuha	stratovolcanic complex, regional structure is NE and NW	
	Rancawalini	outflow of Patuha to the NW, ebullient hot springs (CO2) with sulphur deposit, iron oxide, and carbonate sinter	related to Patuha volcanism	stratovolcanic complex, regional structure is NE and NW	
	Barutunggul	NE of Patuha, hot springs with iron oxide and travertine	related to Patuha volcanism	stratovolcanic complex, regional structure is NE and NW	270°C
	Kawah Putih	SE of Patuha, acid warm, springs, mud pools, solfatara, steaming ground	related to Patuha volcanism	stratovolcanic complex, regional structure is NE and NW	
	Cibuni crater	Steaming ground, fumaroles, solfatara, mud pools, and hot springs, extensive surface alteration rock. Predicted as upflow different from Patuha system	related to Patuha volcanism	NE-SW trending normal fault Cibuni controlled the crater and W-E faults	240°C
	Ciwidey	interpreted as upflow, fumaroles, solfatara, mud pools and hot springs, surface alteration rock	Related to old Patuha volcanism. Andesitic lava flow and lava dome overlies Tertiary volcanic rock	two NW-SE trending normal fault forming graben in this system	240°C
	Saguling Rajamandala	hot springs	Thermal manifestations occur within the calcareous sedimentary rock of Rajamandala Fm. The stratigraphy consist of sedimentary rock of Citarum and Rajamandala Fm.	fracture dominantly trending W-E and NE-SW, thrust fault trending W-E, strike slip fault trending N-S	120-135°C
	Wayang Windu	two volcanic craters (Wayang and Windu craters), hot and nearly boiling springs, steaming ground, fossil hydrothermal system (Burung crater) with Sulfur deposit, silica sinter, surface alteration, fumaroles, solfataras, and geyser	Located within old volcanic complex known as Pangalengan High. Stratigraphycally Wayang Windu is volcanic cone occupied by volcanic rocks of Quaternary age.	NW-SE, N-S, and NE-SW lineament from aerial photo and Landsat	250-270°C
	Kamojang	hot springs, fumaroles, mud pools, volcanic crater, surface alteration	stratigraphically the area occupied by younger augite-hypersthene andesite of Gandapura unit on the west and older pyroxene andesite of Pangkalan unit on the east	Prominent NW-SE and NE-SW lineament. Local normal fault trending NW-SE forming graben and cross-cutting by NE-SW faults	steam dominated 245°C
Bogor	Ciseeng	warm springs with travertine deposit, flow rate 2-5 l/sec, occur in alluvial unit	the system probably caused by thermal water pass trough fault and occur as warm springs	strongly control the system	
	G. Pancar Sanggabuana	hot springs, weak ebullient, travertine, low Sulfur content	The system is located within Bogor Zone Anticlinorium. The heat source probably from cooling intrusion of andesite porphyry	N-S trending faults, NNE-SSW fractures	mod-high T

Continued on the next page

Table 4.2. Continued

Regency/ Kabupaten	Geothermal prospect	Surface manifestation	Geology	Structure	Geother-mometry
	Awibengkok; G. Salak	hot springs, fumaroles, solfatara	located within stratovolcanic complex of andesite-andesitic basaltic volcanism in Late Pliocene-recent	NE-SW trending strike slip fault, NW-SE normal fault. N-S regional stress causing N-S open fracture in the reservoir	245-325^{o}C
	Kawah Ratu; G. Salak	hot springs, fumaroles, solfatara, mud pools, volcanic crater, surface alteration	located within stratovolcanic complex of andesite-andesitic basaltic volcanism in Late Pliocene-recent	NE-SW trending strike slip fault, NW-SE normal fault. N-S regional stress causing N-S open fracture in the reservoir	225-325^{o}C
Ciamis	Panulisan	warm springs with travertine and iron oxide, flow rate 1-2 l/sec, altered ground, fossil of solfatara	covered by Quaternary and recent volcanic and alluvial rock respectively	normal and strike slip fault both trending NW-SE	
	G. Sawal	altered ground	dominated by Quaternary volcanic rock, product of old volcanism	normal fault trending W-E, NE-SW, and NW-SE	
Cianjur	Tanggeung-Cibungur-Cibuni	hot springs occurred in several places	Intrusion of andesite porphyry is probably the heat source of geothermal system. It intruded Miocene sedimentary rock of Jampang and Beser Fm.	inferred normal faults and strike slip faults trending W-E, NE-SW, and NW-SE	103-197^{o}C (low temperature)
	Cipanas-Pacet	hot springs	covered by Tertiary sedimentary rock - Cantayan Fm overlies by volcanic rock	inferred normal faults and strike slip faults trending W-E, NE-SW, and NW-SE	103-197^{o}C (low temperature)
Cirebon	G. Kromong	mud pools, hot pools, hot springs, travertine, silica sinter, altered ground	Sedimentary rock of Tertiary age overlies by volcanic rock of Quaternary age. Andesite intrusion of Quaternary age	Regional structure is fold and fault. Radial normal faults are part of this structure due to the formation of lava dome. Two normal faults trending SSW-NNE and NNW-SSE are not related to radial faults and controlled the occurrence of surface manifestation	interpreted as low enthalpy
Garut	Talaga Bodas	hot springs, fumaroles, solfatara, Sulfur deposit around vent, weak ebullient, hydrothermal alteration	covered by Quaternary volcanic rock	NW-SE structures controlling distribution surface manifestations	
	Papandayan	volcanic crater, solfatara, hot ground, altered ground, hot springs and mud pools	Papandayan is recently active volcano. The rock found in this area includes volcanic rock of Quaternary age.	Two major strike faults trending NE-SW (Walirang fault and Papandayan fault parallel to each other) occur in this area. The direction coincides with regional trend	
	Cipanas-Tarogong (G. Masigit-Guntur)	hot springs	covered by Quaternary volcanic rock	normal faults controlled the system	
	Cilayu	hot springs and hydrothermal alteration along fault zone, travertine and iron oxide around the springs	Diorite-micro diorite intrusion crossing sedimentary rock of Bentang Fm and volcanic rock	NE-SW fault controlled the geothermal system and intrusion	168^{o}C
	Ciarinem	hot springs, hydrothermal alteration	Miocene sedimentary rock overlain by Quaternary volcanic rock and andesite intrusion	Normal fault trending W-E controlling springs distribution. Strike slip fault trending NNE-SSW and ENE-WSW	low enthalpy 120^{o}C
	Kawah Darajat	volcanic crater, fumaroles, hot ground, altered ground, hot springs, boiling pool and mud pools	covered by Quaternary andesitic-basaltic rock	NE-SW Kendang fault and Gagak fault	245^{o}C
Kuningan	Subang	hot springs with Sulfur deposits around it	the area dominated by sedimentary rock of Tertiary age, overlain by Quaternary volcanic rock product of Ciremai volcano	Fold with W-E trending axis, normal fault trending W-E and strike slip fault trending N-S	
	Cibingbin	hot springs	Tertiary sedimentary rocks overlain by Quaternary volcanic rock	normal faults controlling springs distribution	

Continued on the next page

Table 4.2. Continued

Regency/ Kabupaten	Geothermal prospect	Surface manifestation	Geology	Structure	Geother-mometry
	G. Ciremai-Sankanhurip	hot springs	the area covered by Quaternary volcanic rock produced by Ciremai volcanism	inferred normal faults trending WNW-ESE and N-S	
Subang	Ciater	hot springs with silica deposits, iron and aluminum oxide and phosphate deposits	occupy by Tertiary volcanic rocks of Sunda volcanism and overlain by Quaternary volcanic rock from Tangkuban Parahu	inferred normal faults trending WNW-ESE and N-S	
	Sagala Herang	hot springs, travertine, iron oxide around the springs and H2S smells	occupy by Tertiary volcanic rocks of Sunda volcanism and overlain by Quaternary volcanic rock from Tangkuban Parahu		
Sukabumi	Cisolok	hot springs, geysers, solfatara, altered ground	The system probably outflow from mountain range at the north. The reservoir is limestone, and volcanic material occur in the fault complex	Intersection of structure trending N20E and N110E controlled the occurrence of geyser. Regional structure forming graben extending N from Pelabuhan Ratu to G. Salak	140^{o}C and 220^{o}C
	Cisukarame	hot springs	The system probably outflow from mountain range at the north. The reservoir is limestone, and volcanic material occur in the fault complex	Regional structure forming graben extending N from Pelabuhan Ratu to G. Salak. The same graben as it is in Cisolok area	200^{o}C
	Santa	hot springs with iron oxide deposited around the springs	Oligocene rock of Walat Fm, Batuasih Fm and Rajamandala Fm overlain by Miocene rock of Jampang Fm, Bojang Lopang Fm and Nyalindung and overlain unconformably by Quaternary volcanic rock	fold with W-E trending axis, normal fault trending N-S and NE-SW	low enthalpy 130^{o}C
	Cikundul-Cimandiri	hot springs with Sulfur deposits around it	Quaternary volcanic rock	faults are dominant	100-140^{o}C
Sumedang	Congeang-Cileungsing, G. Tampomas	hot springs with salt, silica sinter and iron oxide	The rock is sedimentary rock. This unit is overlain by lava andesitic and the youngest is alluvial deposits. Intrusion occur in several places	fault trending NW-SE controlled the distribution of springs	low enthalpy
Tasikmalaya	Kawah Karaha	volcanic crater, fumaroles, hot ground, altered ground, hot springs	The area is located in the volcanic complex. Quaternary volcanic rock overlain by Holocene volcanic rock	NW-SE faults are the regional trend. The NE-SW faults are the younger one that bound the Hg anomaly in this area	
	Cipacing	hot springs, travertine	The area is located in the volcanic complex. Quaternary volcanic rock overlain by Holocene volcanic rock		259-271^{o}C
	Cigunung	hot springs	Sedimentary rock of Tertiary age overlies by volcanic rock of Quaternary age product of G. Galunggung eruption. Andesite intrusion of Quaternary age	NW-SE strike slip fault is prominent in this area. Normal faults control the distribution of springs	
	Cibalong	hot springs	Miocene sedimentary rock overlain by volcanic rock	Regional structures comprise of anticline and syncline trending N-S and normal faults. Normal faults control the distribution of springs	
	Ciheras-Cipatujah	hot springs	covered by Tertiary sedimentary rock overlain by recent alluvial deposit	NE-SW lineament interpreted as faults	
	Galunggung	hot springs, fumaroles, solfatara, altered ground, volcanic crater	G. Galunggung is recently active volcano. The product of eruption is found since Quaternary-recent. Depression in the crater forming caldera	caldera complex	

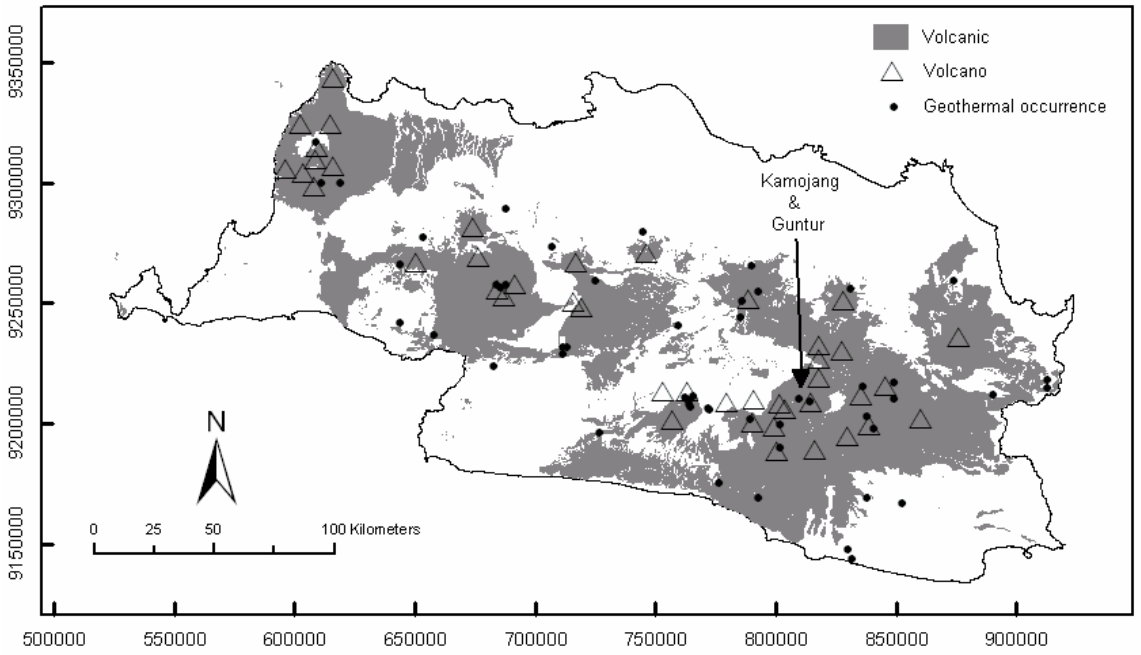

Figure 4.2: Spatial distribution of geothermal occurrences, volcanic rocks and volcanoes in West Java.

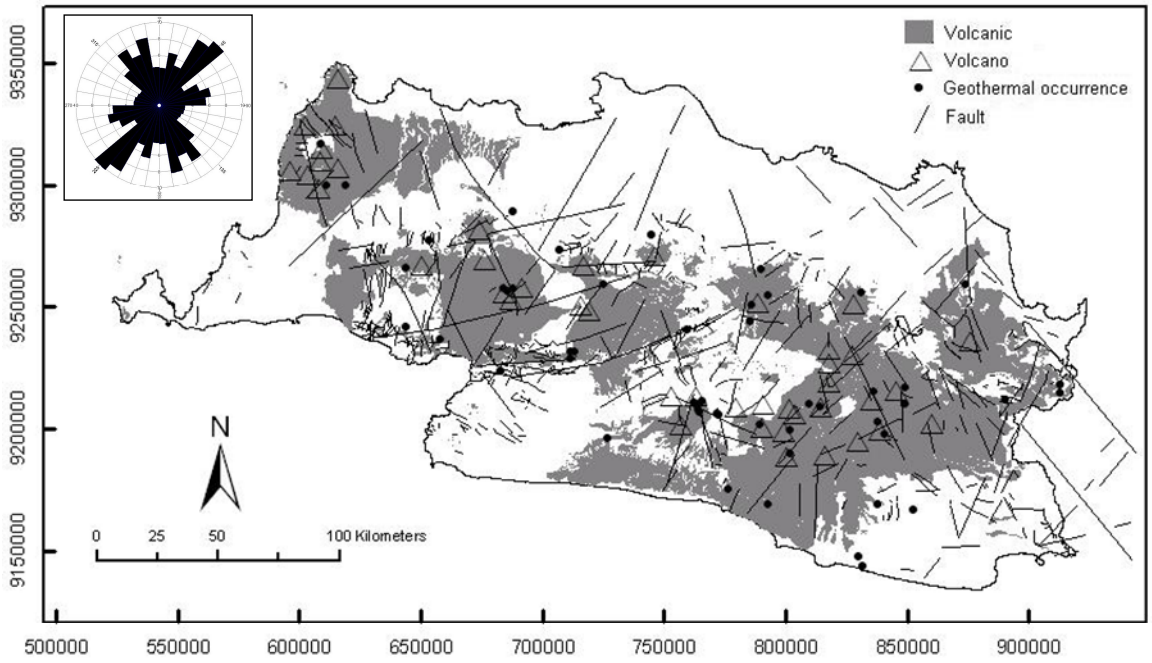

Figure 4.3: Spatial distributions of geothermal occurrences and mapped faults in West Java. Inset shows the associated rose diagram for the mapped faults.

4.1.3.3. Structural controls

Table 4.2 indicates presence of faults in the geothermal occurrences/prospects. Table 4.3 is a compilation of presence of faults in each geothermal occurrence/prospect in the study area. The data are compiled from different sources, such as published papers (as summarised in Table 4.2), reports, and the Internet, especially the official website of Indonesian Directorate of Volcanology and Geological Hazard Mitigation (from http://www.vsi.esdm.go.id/pbumi/java/). The data indicate that NE-trending and NW-trending faults are the sets of faults mostly present in the known geothermal

areas, whereas NS-trending and EW-trending faults are secondary. This observation is confirmed also by visual examination of the fault map (Figure 4.3) and the associated directional histogram (rose diagram) of the mapped faults, which shows that the dominant fault directions are NE and NW.

Table 4.3: Tabulation of presence of faults (score =1) in geothermal occurrences

Geothermal occurrences	Fault Direction							
	EW	WNW	NW	NNW	NS	NNE	NE	ENE
Awibengkok - Salak			1		1		1	
Barutunggul			1				1	
Bujal-Jasinga								
Ciarinem	1		1			1		1
Ciater		1			1			
Cibalong					1			
Cibingbin								
Cibuni Crater	1						1	
Cigunung			1					
Ciheras-Cipatujah							1	
Cikundul-Cimandiri								
Cilayu			1		1		1	
Cimanggu			1				1	
Cipacing								
Cipanas-Ciawi			1	1				
Cipanas-Pacet	1		1				1	
Cipanas-Tarogong								
Ciremai		1	1		1			
Ciseeng								
Cisolok-Cisukarame		1	1		1	1	1	
Ciwidey			1					
Danau Danu / Rawa Danau	1		1				1	
G. Endut			1		1			
G. Karang			1				1	
G. Kromong				1		1		
G. Sawal	1		1				1	
Galunggung								
Kamojang			1				1	
Karaha			1				1	
Kawah Darajat							1	
Kawah Putih			1				1	
Kawah Ratu - Salak			1		1		1	
Kiaraberes			1					1
Maribaya	1							
Pancar					1	1		
Panulisan			1					
Papandayan							1	
Patuha			1				1	
Pulosari			1				1	
Rancawalini			1				1	
Sagala Herang	1							
Saguling Rajamandala	1				1		1	
Santa	1				1		1	
Selabintana								
Subang - Kuningan	1				1			
Talaga Bodas			1					
Tampomas			1		1	1		
Tanggeung	1		1				1	
Tangkuban Parahu	1						1	
Wayang Windu			1		1		1	
Pamancalan								
Sum	12	3	28	2	14	5	25	2
Percentage (of total = 91)	13%	3%	31%	2%	15%	5%	27%	2%

4.1.3.4. Surface manifestations

The surface manifestations that are most common in the known geothermal occurrences/prospects include presence of hot springs, fumaroles, solfatara, and hydrothermally altered ground (Table 4.2). Figure 4.4 shows spatial distributions of known geothermal occurrences and hot spring occurrences.

The locations of hot springs indicate that there is heat source in the nearby locations and/or there is a structural control connected to the heat source.

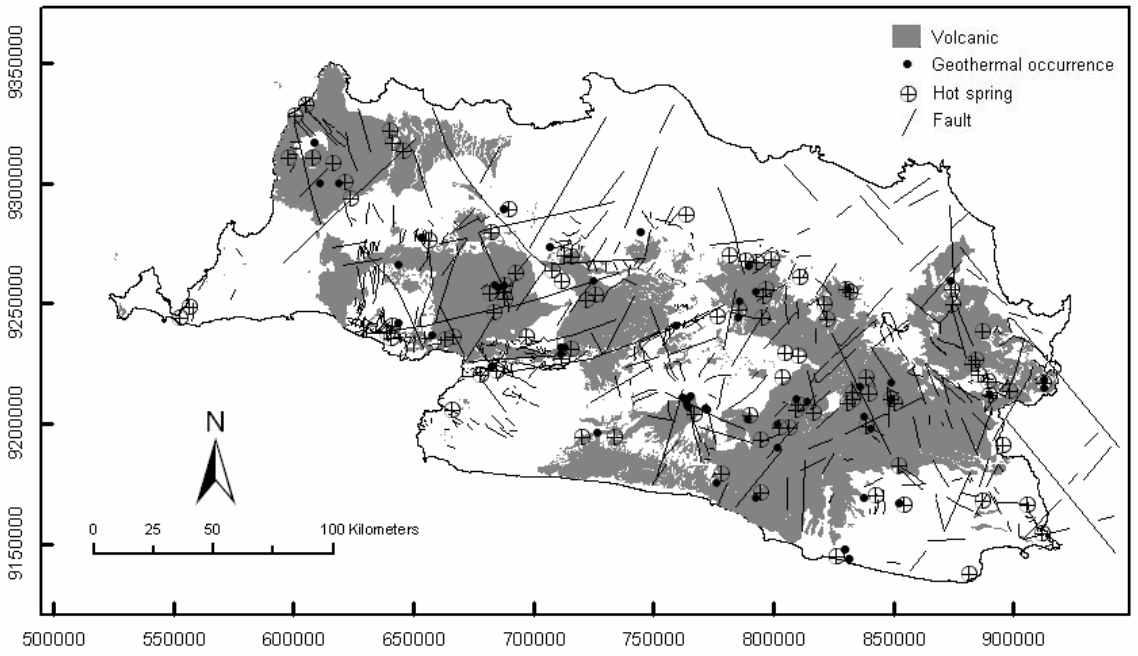

Figure 4.4: Spatial distributions of geothermal occurrences and hot springs in West Java.

4.2. Spatial analysis of indications of geothermal occurrence

Qualitative and quantitative knowledge about the spatial distributions of indicative geological features are considered important in mapping of geothermal prospectivity. In the previous section, qualitative knowledge of geological features indicative of geothermal prospectivity was presented. In this section, results of exploratory spatial analysis are presented to provide quantitative knowledge of geological features indicative of geothermal prospectivity. Two methods for exploratory spatial analysis are applied to different data sets, which represent geothermal occurrences and (based on discussion in the previous section) indicative geological features such as Quaternary volcanic centres, Quaternary volcanic rocks, mapped faults, and hot springs.

4.2.1. Spatial analytical methods

One of the methods applied is called Fry analysis, which is applied to point features (e.g., locations of geothermal occurrences) to interpret/analyze geologically meaningful spatial distribution patterns. The other method applied is called distance distribution analysis, which is applied to explore spatial associations between two sets of spatial features (e.g., geothermal occurrences versus hot spring occurrences).

4.2.1.1. Fry analysis

Fry analysis is a point pattern analysis method that uses separations between all objects of an object distribution (Fry, 1979). Fry analysis uses a geometrical method of spatial autocorrelation. The method uses all center-to-center spatial relationships (or translations) between every pair of points. Each center-to-center spatial relationship is plotted as a point in a polar diagram, as a function of direction, having a different data point as center each time, until all points have been used as centers. The resultant graph, initially named “all object separation” plot (Hanna and Fry, 1979), is commonly known as “Fry plot”. These plots display the relative position of each point to all other points viewed from a central position. Fry plots can be generated by first marking on a paper all points to be used

and a series of parallel references. On a tracing paper also with parallel references, a point to be used as origin is marked. Then that point is placed over each one of the points of the first paper, and each time every remaining points of the first paper are transferred to the second paper. During this process, both paper sheets have to maintain the same orientation (i.e., keeping lines on the tracing paper parallel to the lines on the first paper). For "***n***" data points there are $\boldsymbol{n^2}$-***n*** translations or spatial relationships. This method has been applied in regional mineral exploration to deduce structural directions that control mineralization (Vearncombe and Vearncombe, 1999; Vearncombe and Vearncombe, 2002).

The results of a Fry analysis can be interpreted from the Fry plots and also from associated rose diagrams of the plots. If there are regular patterns in terms of spacing and orientation of point objects, the Fry plot will enhance such patterns allowing an easier visual interpretation of them. High frequencies of orientation observed in the plots can reflect orientations of structures that control spatial distributions of the point objects. When Fry plots are analysed, parallel patterns can be separated at a recurrent distance from each other indicating which could be the spacing between the structural corridors with that orientation that are responsible for the pattern. Controls other than geological can also be interpreted from a Fry plot, but if there is coincidence between a geological control and the patterns visible in the plots, it can be considered that the geological control is the plausible reason for the patterns.

4.2.1.2. Distance distribution analysis

This method models spatial association between two sets of objects. The spatial association refers to distance or range of distances at which point features (e.g., geothermal occurrences) are favourably located from other point features (e.g., volcanoes) or from curvilinear features (e.g., faults). This spatial association can be regarded as spatial dependence, i.e., the locations of the points depend upon the lines or other points. This method has been used for characterizing the quantitative spatial association between mineral occurrences and curvilinear geological features. Bonham-Carter et al. (1985) statistically characterised spatial association between mineral occurrences and lineaments by measuring the distances from each mineral occurrence to the nearest lineament, and comparing the observed distance distribution to a predicted distance distribution that would be expected if a random process generated the occurrences.

The method starts with creating a map of distances from a set of evidential features (e.g., volcanic centers, faults, etc.). The map of distances is then classified into buffer zones using arbitrary distance intervals. The method then constructs a graph of distance buffer versus cumulative proportion (or percentage) of all pixels (or points) within distance buffer zones. This graph represents the expected cumulative frequency distribution of any set of (random) pixels around the evidential features under study. The method also constructs a graph of distance buffer versus cumulative proportion of pixels representing a set of target variable (e.g., geothermal occurrences) within distance buffer zones. This second graph represents the observed cumulative frequency distribution of target variable pixels around the evidential features under study. If the observed cumulative frequency distribution curve is above the expected cumulative frequency distribution curve, which means that within the distance buffer zones there is higher proportion or probability of target pixels than "random" pixels (i.e., due to chance), then it means there is positive spatial association between the set of target variable and the set of evidential features. If the observed cumulative frequency distribution curve is below the expected cumulative frequency distribution curve, which means that within the distance buffer zones there is lower proportion or probability of target pixels than "random" pixels (i.e., due to chance), then it means there is negative spatial association between the set of target variable and the set of evidential features.

The distance of optimum spatial association can be estimated by determining the difference between the observed cumulative frequency distribution curve and the expected cumulative frequency distribution curve. The distance at which there is highest difference between the two curves represents the distance of optimum spatial association. Because the strength of spatial association is inversely related to distance from evidential features (Carranza, 2002), a short distance of positive spatial association represents strong positive evidence, whereas a long distance of positive spatial association

represents weak positive evidence. Likewise, a short distance of negative spatial association represents strong negative evidence, whereas a long distance of negative spatial association represents weak negative evidence.

The distance distribution analysis was performed using ILWIS, which is a raster-based GIS software. In a raster-based GIS, spatial objects including point objects (e.g., geothermal occurrences) are represented as pixels, which have areal extents. The pixel size used in the spatial analysis is defined by the modeller according to objective/scope of study. Pixel representation of spatial objects is convenient for the distance distribution analysis, because the geothermal occurrences, although represented as point objects (i.e., by their positional coordinates), actually occupy space. So, in the distance distribution analysis a pixel size of 500×500 m is used, although this pixel size is a conservative representation of actual areas of the individual geothermal fields in the study area.

4.2.2. Spatial distribution of geothermal occurrences

The Fry analysis was carried out using all known geothermal occurrences. The 53 geothermal occurrences have 2756 translations (Figure 4.5), which are overlaid on map of study area map in order to give some geographical context about the enhanced patterns. Although each translation points have valid coordinate locations, they do not represent actual objects in the ground. The structural directions in the Fry plots are summarised in rose diagrams (Figures 4.6a and 4.6b).

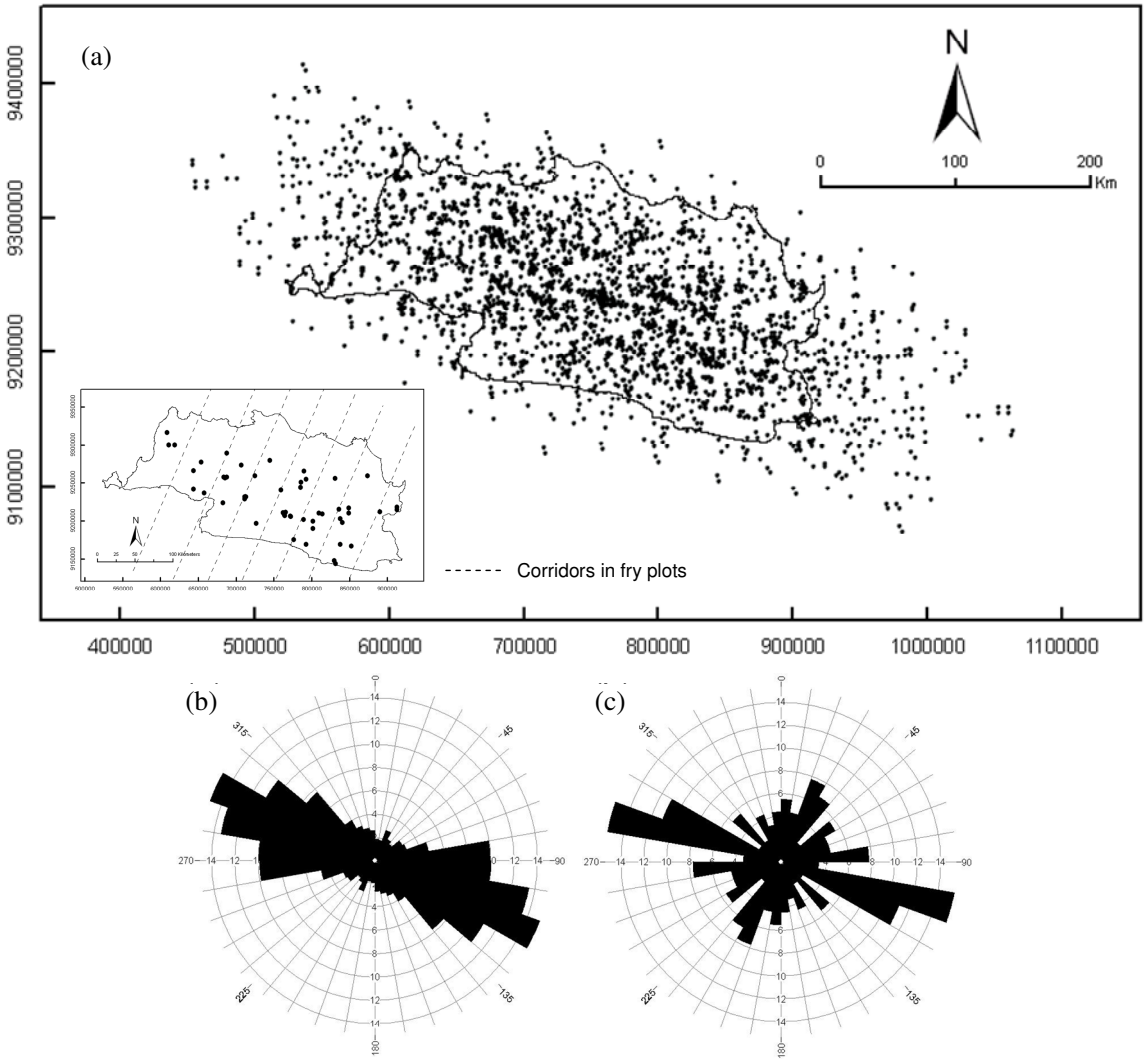

Figure 4.5: (a) Fry plot of all known geothermal occurrences (original locations are shown in inset) and (b) corresponding rose diagram of all point translations. (c) Rose of diagram of Fry points less than 30 km apart.

The point translations (Figure 4.5a) show a major WNW and minor NNE trends, which characterise the spatial distributions of geothermal occurrences. The WNW trend is not surprising because the geothermal occurrences are within Java Island, which trends WNW to roughly E-W. Therefore, this major trend could also represent bias in geothermal exploration due to the trend of Java Island. However, it can be noted in Figure 1.1 that a WNW trend also characterize the strike of the subduction zone off-shore south of Java Island and of the associated magmatic arc in the island. Therefore, the major WNW trend of the known geothermal occurrences may also be attributed to the youngest controlling structures, which have the same WNW directions, known as Java Structural Domain (Widianto et al., 2004).

The rose diagram in Figure 4.5c gives insights to trends in the fry plots of points with separation of less than 30 km. This distance was determined by another point pattern analysis (Boots and Getis, 1988) of the geothermal occurrence data to determine distance in which there is maximum probability for a neighbouring geothermal occurrence from another geothermal occurrence. The rose diagram in Figure 4.5c therefore characterizes trends between any two given geothermal occurrences. The rose diagram shows that, apart from obvious WNW trend, there is a strong secondary NE trend. This NE trend may represent structural control by NE-trending faults (see Figure 4.3).

In the Fry plot (Figure 4.5a) there is also a noticeable spacing (structural corridors?) of about 40-50 km between NNE-trending point translations. The spacing suggests that the spatial data distribution of geothermal occurrences is not random, i.e., it is clustered and follows the NNE trend. The distance between spacing reflects the distance between clusters of data. However, the reason for the NNE trend and their relation to the spatial distribution of geothermal occurrences is not understood, because there is no previous discussion in the geological literature about significant NNE-trending features in western Java.

4.2.3. Spatial distribution of Quaternary volcanoes and their spatial association with geothermal occurrences

The analysis on Quaternary volcanoes or volcanic centres in West Java was performed to determine whether or not the spatial distribution of Quaternary volcanic centres is similar to the spatial distribution of known geothermal occurrences and whether or not there is positive spatial association between the Quaternary volcanic centres and the known geothermal occurrences.

4.2.3.1. Fry analysis of Quaternary volcanic centres

The Fry plot of locations of the 43 Quaternary volcanic centres (Figure 4.6a) shows a WNW trend, which corresponds to (a) the trend of the Sunda Trench representing the destructive margin between the subducting Indo-Australian plate and the overriding Eurasian plate (Figure 1.1), (b) the trend of the magmatic arc in Java Island, and (c) the trend of the Java Structural Domain. This major trend of the Quaternary volcanoes is geologically-related. In the Fry plot, there is also a noticeable spacing of about 75 km between NE-trending point translations. The NE trend probably corresponds with NE-trending faults.

For point translations less than 36 km apart (i.e., distance of maximum probability for a neighbouring volcano from another volcano), the major trend is WNW to roughly E-W, but there is a secondary NE average trend (Figure 4.6c). This secondary NE trend also probably represents structural control on locations of volcanic centres by NE-trending faults.

The rose diagrams for the Fry plots for the Quaternary volcanic centres (Figures 4.6b and 4.6c) are quite similar to the rose diagrams of the Fry plots for the known geothermal occurrences (Figure 4.5b and 4.5c). This observation suggests that the spatial distribution of geothermal fields in the study area is controlled by the spatial distribution of Quaternary volcanoes. This also suggests that there is positive spatial association between the Quaternary volcanoes and the known geothermal occurrences.

4.2.3.2. Results of distance distribution analysis

There is positive spatial association between Quaternary volcanic centers and geothermal occurrences in West Java (Figure 4.7). The positive spatial association is optimum at 10 km. About

55% of the known geothermal occurrences are present within this distance of optimum spatial association with Quaternary volcanic centres. The "difference" curve indicates that within about 10 km of a Quaternary volcanic centre, there is about 40% higher probability of finding a geothermal occurrence than would expected due to chance. These results indicate that proximity to (within 10 km of) a Quaternary volcanic centre is a positive indication of geothermal prospectivity.

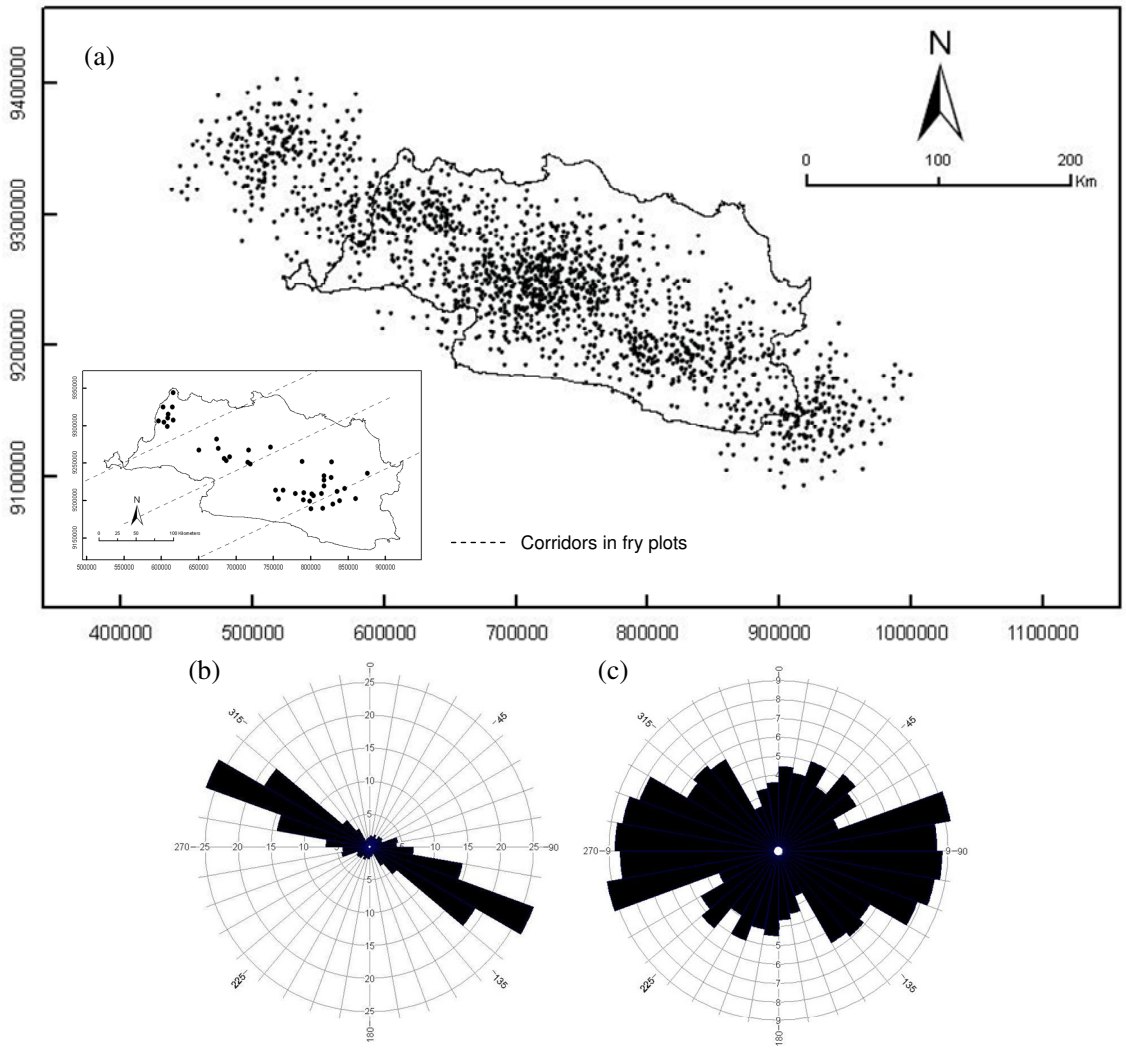

Figure 4.6: (a) Fry plot of Quaternary volcanic centres (original locations shown in inset) and (b) corresponding rose diagram of all point translations. (c) Rose of diagram of points translations less than 36 km apart.

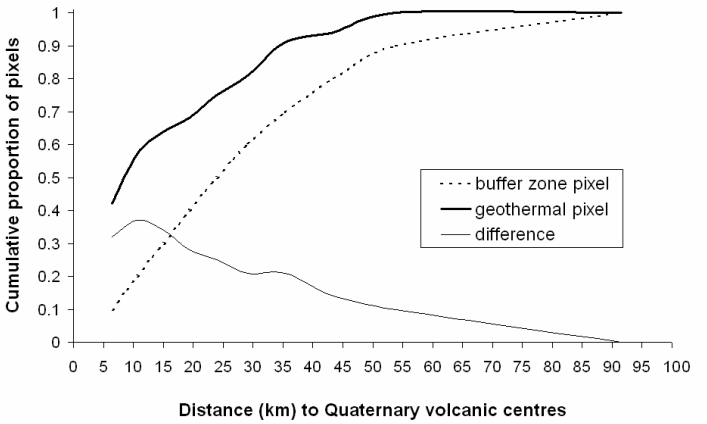

Figure 4.7: Expected cumulative frequency distribution of buffer zone pixels (around Quaternary volcanic centres) and observed cumulative frequency distribution of geothermal occurrences around Quaternary volcanic centers.

4.2.4. Spatial association of geothermal occurrences and Quaternary volcanic rocks

The spatial distributions of Quaternary volcanic rocks and geothermal occurrences are shown in Figure 4.2. Spatial association analysis is performed to explore whether or not Quaternary volcanic rocks represent positive indication of geothermal prospectivity.

There is positive spatial association between Quaternary volcanic rocks and geothermal occurrences in West Java (Figure 4.8). The positive spatial association between the Quaternary volcanic rocks and the known geothermal occurrences is optimum at 3 km. At least 90% of the known geothermal occurrences are present within the distance of optimum spatial association with Quaternary volcanic rocks. The "difference "curve indicates that within about 3 km of Quaternary volcanic rocks, there is at least 30% higher probability of finding a geothermal occurrence than would expected due to chance. These results indicate that presence of or proximity to Quaternary volcanic rocks is a positive indication of geothermal prospectivity.

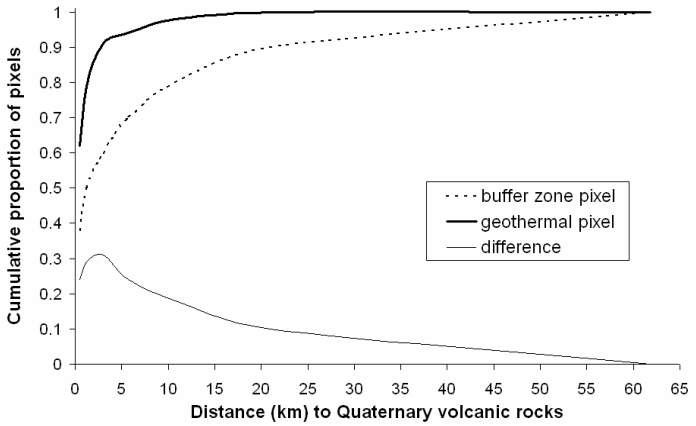

Figure 4.8: Expected cumulative frequency distribution of buffer zone pixels (in and around Quaternary volcanic rocks) and observed cumulative frequency distribution of geothermal occurrences within and around Quaternary volcanic rocks.

4.2.5. Spatial association of geothermal occurrences and mapped faults

The spatial distributions of faults and geothermal occurrences are shown in Figure 4.3. Spatial association analysis is performed to explore whether or not the mapped faults represent positive indication of geothermal prospectivity (Figure 4.9).

Figure 4.9a shows the cumulative frequency distribution curves based on all mapped faults. There is optimum positive spatial association between the known geothermal occurrences and all mapped faults at 4 km. About 75% of the known geothermal occurrences are present within this distance of optimum spatial association with all mapped faults. The "difference" curve indicates that within about 5 km of any mapped fault, there is about 20% higher probability of finding a geothermal occurrence than would expected due to chance. These results indicate that proximity to (within 4 km of) any mapped fault is a positive indication of geothermal prospectivity.

However, based on results in the previous sections (structural control in sub-section 4.1.3.3, and Fry plots of geothermal occurrences in Figure 4.5a and Quaternary volcanic centres in Figure 4.6a), the trends of most probable major structural controls are NE and WNW-NW. Therefore, a sub-set of mapped faults with NE and WNW-NW trends was created and distance distribution analysis was performed on this sub-set of mapped faults and the known geothermal occurrences. The new cumulative frequency distribution curves (Figure 4.9b) show that within 1 km of mapped faults with NE and WNW-NW trends the observed cumulative frequency distribution curve of "geothermal pixels" is slightly below the expected cumulative frequency distribution of the "buffer zone pixels". Note the slight negative value for the "difference" curve within 1 km. This suggests that within 1 km of the mapped faults with NE and WNW-NW trends there are few geothermal occurrences than would be expected due to chance. However, beyond 1 km of the mapped faults with NE and WNW-NW trends the curve for the "geothermal pixels" is above the curve for the "buffer zone pixels. This indicates that there is positive spatial association between geothermal occurrences and mapped faults with NE and WNW-NW trends. The "difference" curve indicates that the positive spatial association is optimum at about 5 km. Within 5 km from mapped faults NE and WNW-NW trends, there is about 30% higher probability of finding a geothermal occurrence than due to chance. In addition, within 5 km from mapped faults NE and WNW-NW trends, about 80% of the known geothermal occurrences are present. These observations indicate that proximity to (within 5 km of) mapped NE- and WNW-NW-trending is a positive indication of geothermal prospectivity.

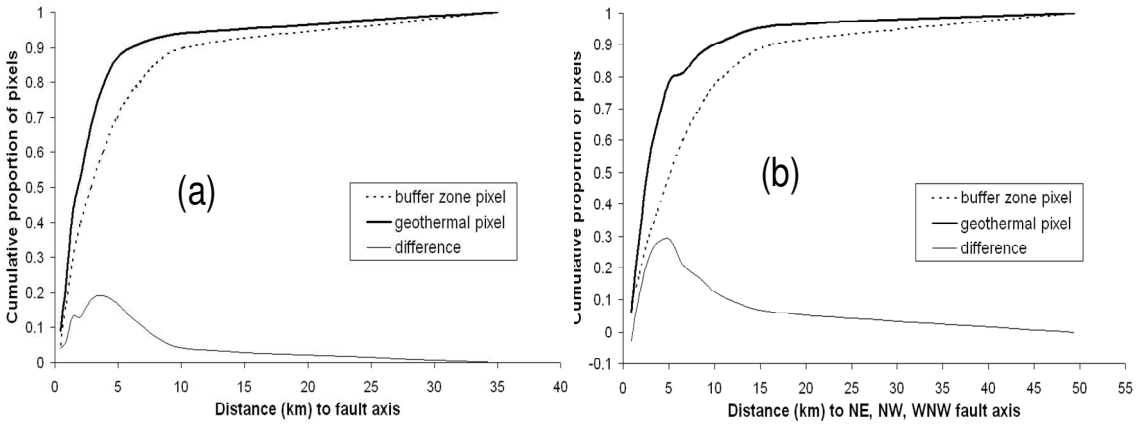

Figure 4.9: Expected cumulative frequency distribution of buffer zone pixels (around mapped faults) and observed cumulative frequency distribution of geothermal occurrences from mapped faults. (a) Using all mapped faults. (b) Using only mapped faults with NE and WNW-NW trends.

4.2.6. Spatial distribution of hot springs and their spatial association with geothermal occurrences

The analysis on hot springs was performed to determine whether or not the spatial distribution of hot springs is similar to the spatial distribution of known geothermal occurrences and whether or not there is positive spatial association between the hot springs and the known geothermal occurrences.

4.2.6.1. Fry analysis of hot springs

The Fry plot of locations of the 95 hot springs consists of 8930 translations (Figure 4.10a). The Fry plot shows major WNW to E-W trends, which are similar to the major trends in the Fry plots for the geothermal occurrences (Figure 4.5a) and Quaternary volcanic centres (Figures 4.6a). These WNW to E-W trends correspond to the trend of the Java Structural Domain. The difference with the other two Fry plots is that there are no obvious NE-trending corridors in Figure 4.10a. However, the enhanced patterns show NNW-trending corridors with spacing of about 75-80 km, or probably smaller (40-50 km) since many points are scattered between this spacing. The reason for NNW trend and the spacing, as in the case of geothermal occurrences, is not understood.

For point translations less than 30 km apart (i.e., distance of maximum probability for a neighbouring hot spring from another hot spring), a strong NW trend is observed (Figure 4.10c) aside from major NE trends. These major trends observed in Figure 4.10c probably represent structural controls on spatial distributions of hot springs by NW and NE trending faults.

The rose diagrams of the Fry plots for the hot springs are quite similar to the rose diagrams of the Fry plots for the known geothermal occurrences and for the Quaternary volcanic centres. This suggests that there is the same structural control on the spatial distributions of these geological features. This also suggests that there is positive spatial association between the hot springs and the known geothermal occurrences.

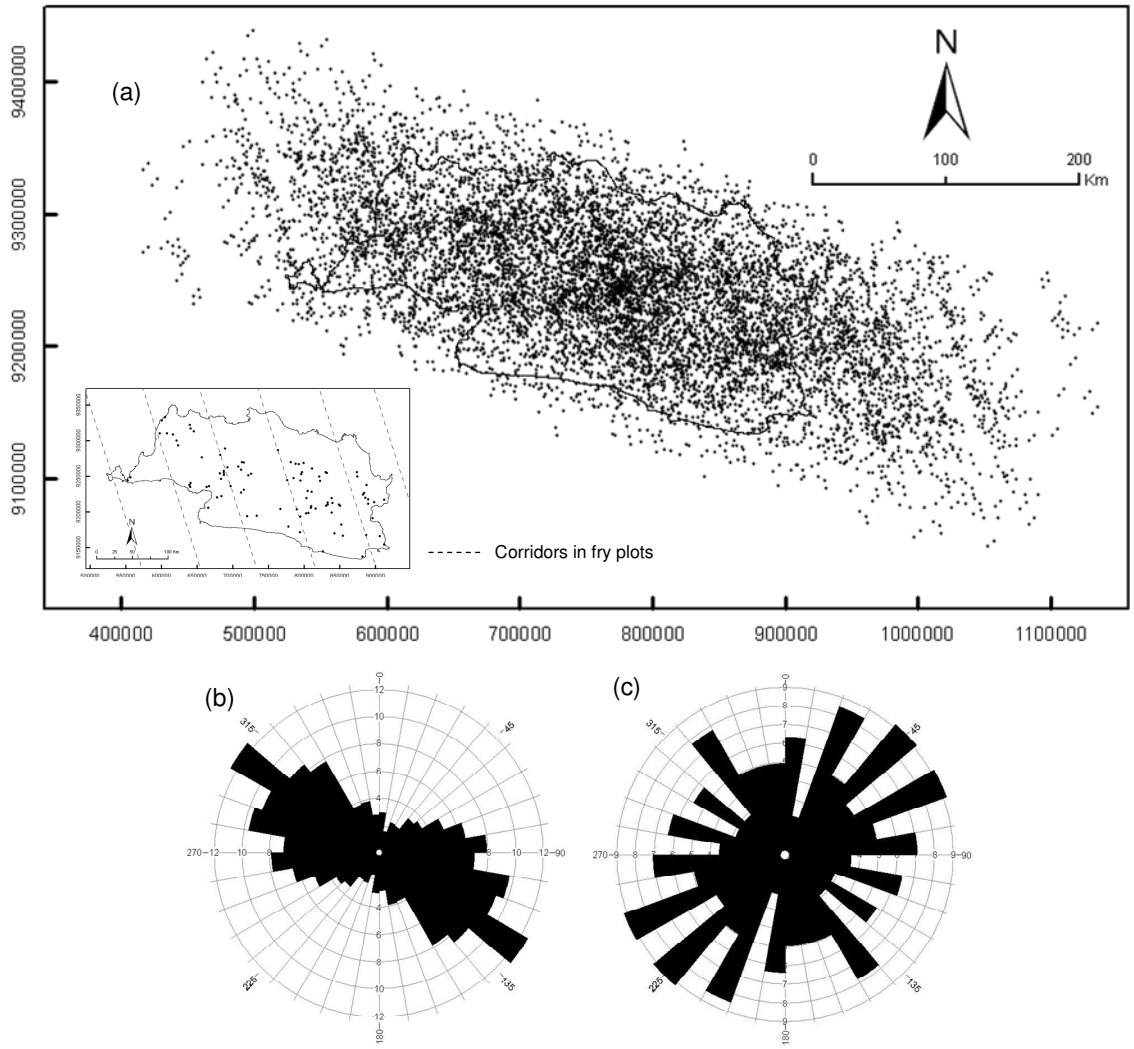

Figure 4.10: (a) Fry plot of hot springs (original locations shown in inset) and (b) corresponding rose diagram of all point translations. (c) Rose of diagram of points translations less than 30 km apart.

4.2.6.2. Results of distance distribution analysis

There is positive spatial association between hot springs and geothermal occurrences in West Java (Figure 4.11). The positive spatial association is optimum at 6 km. More than 90% of the known geothermal occurrences are present within this distance of optimum spatial association with hot springs. The "difference" curve indicates that within about 6 km of a hot springs, there is about 65% higher probability of finding a geothermal occurrence than would expected due to chance. These results indicate that proximity to (within 6 km of) hot springs is a positive indication of geothermal prospectivity.

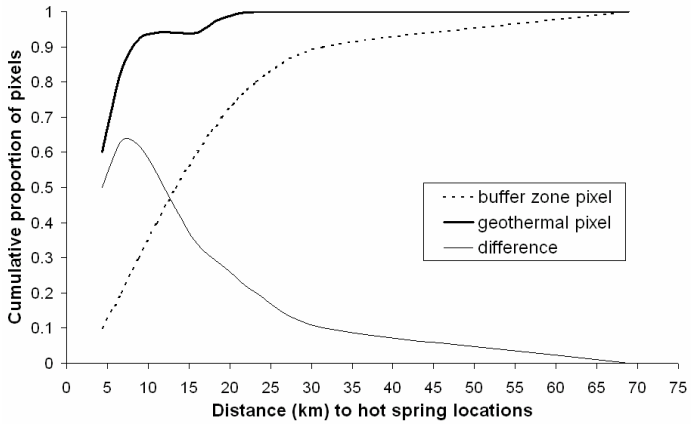

Figure 4.11: Expected cumulative frequency distribution of buffer zone pixels (around hot springs) and observed cumulative frequency distribution of geothermal occurrences around hot springs.

4.3. Conceptual model of regional-scale geothermal prospectivity

West Java is a volcanic island arc, which is mostly covered by volcanic rocks and characterized by presence of Quaternary volcanoes. Beneath the volcanic rocks, magmatic intrusions from last phases of volcanism intrude sedimentary layers. The existence of magmatic arc inland of West Java is a result of subduction of the Indo-Australian plate beneath the Eurasian plate along the Sunda Trench. This geotectonic setting provides geological conditions favourable for formation of geothermal systems. Since the study area has been undergone several phases of tectonic regimes, the resulting geological structures strongly influenced the spatial distributions of geothermal fields.

Most of the known geothermal occurrences in the study area are located within volcanic areas associated with Quaternary volcanoes, which represent plausible heat sources. The reservoir rocks are either volcanic or sedimentary rocks, and cap rocks are mostly volcanic rocks. The NW to WNW trending Java Structural Domain and the NE-trending of Meratus Structural Domain provide sets of faults that probably controlled spatial distributions of geothermal occurrences, volcanic centres, and hot springs.

The following spatial criteria therefore form a conceptual model of regional-scale geothermal prospectivity in the study area:

a) Proximity to (within 10 km of) Quaternary volcanic centres;
b) Presence of or proximity to (within 3 km of) Quaternary volcanic rocks;
c) Proximity to (within 5 km of) mapped faults with NW-WNW and NE trends;
d) Proximity to (within 6 km of) hot springs.

The distances of proximity are enclosed in brackets because these are not finite and depend on amount of data (both about geothermal occurrences and indicative geological features). For example, if there undiscovered or unrecorded geothermal occurrences, or if a sub-set of known geothermal occurrences are used in modelling (see Chapter 7), then distances of proximity could vary. The respective distances of optimum spatial association found in the distance distribution analyses could be used to create binary predictor maps, which could be overlaid on top of each other to determine intersections

of spatial criteria representing prospective ground (e.g., Carranza et al., 1999). It is considered that intersections of at least three of the four spatial criteria determine prospectivity of an area for geothermal field occurrence. However, prospectivity modelling based on binary predictor maps is simplistic because spatial criteria are given equal weights or importance with respect to model target (e.g., geothermal occurrence). In this study, a multi-class type of prospectivity modelling, with unequal weighting of spatial criteria based on known geothermal occurrences, will be presented in Chapter 7.

The conceptual model of regional-scale geothermal prospectivity will be further developed in the succeeding chapters. For example, the association between the hypothesized volcano-tectonic depression and the known geothermal occurrences will be analysed in Chapter 5. Furthermore, surface indications of geothermal prospectivity will be analysed from satellite imagery (Chapter 6).

4.4. Concluding remarks

In this chapter, information of the general characteristic of geothermal occurrences in West Java were compiled and reviewed from the geological literature and then analysed with the objective to formulate a conceptual model of regional-scale geothermal prospectivity in the study area. Fry analysis was useful in determining plausible trends of structural controls on geothermal occurrences in the area. Distance distribution analysis was useful in determining empirical spatial associations various geological features (volcanic centres, mapped faults, hot springs) and geothermal occurrences.

Based on analysis of Fry plots, it is deduced that NW and WNW-trending faults of the Java Structural Domain (which are the youngest structures in the study area) are important structural controls on the spatial distributions of geothermal occurrences, Quaternary volcanoes, and hot springs in West Java. However, the influence of older NE-trending faults of the Meratus Structural Domain seems to be important as well, as this trend consistently appears in rose diagram of all geological features discussed in this chapter.

There are general patterns of “structural corridors” in the Fry plots of geothermal occurrences (about 40-50 km between NNE trends), Quaternary volcanic centres (about 75 km between NE trends) and hot springs (about 75-80 km between NNW trends). These patterns are probably artefact related to the data distribution, although it is definitely reflect how the data are distributed in space. Further investigation on how these spatial patterns emerged and its underlying process are required to better understand them; although, this is not an objective of the present study. However, it is interesting to note that these patterns are also found in earthquake epicentres, which will be discussed in the next chapter.

Chapter 5: Analysis of Geophysical Data for Indications of Geothermal Prospectivity

This chapter describes results of processing and analyses of available geophysical datasets to investigate the hypotheses that (a) negative gravity anomalies represent terranes associated with a regional volcano-tectonic depression, which favourable to geothermal field occurrence and (b) shallow-earthquake epicentres are indicative of geothermal prospectivity. The descriptions of the results of data processing and analyses are preceded by a review or relevant literature, from which pertinent information is derived that would be useful in understanding of the results of geophysical data processing and analyses.

5.1. Indications of Geothermal Prospectivity from Gravimetry

5.1.1. Regional gravimetry in volcanic regions

Many gravimetric studies in volcanic regions elsewhere reveal caldera structures and magma intrusions that aid in understanding history of formation of these regions (e.g., Nishimura et al., 1986; Lucassen et al., 1996; Kusumoto et al., 1999; Fernandes et al., 2005). Such studies show that most calderas have a relative gravity low, which indicates lack of mass and/or depression structures (e.g., Nishimura et al., 1986; Kusumoto et al., 1999; Tamanyu and Wood, 2003).

According to Olsen and Morgan (1995), volcano-tectonic depressions are typically associated with the migration of major volcanic centres resulting in major magmatic modification of the crust and subsidence of the surface. In this case, surface subsidence is due chiefly to post-magmatic events of lithospheric cooling, widespread collapse of large calderas, and surface loading by the extensive volcanic flows rather than to extensional stresses in the crust and/or lower lithosphere. This structural arrangement could result in a broad low gravity anomaly zone (Kusumoto et al., 1999; Arana et al., 2000). In the study area, Van Bemmelen (1949) has outlined a central depression zone within the Quaternary volcanic arc along the E-W trend of Java Island (Figure 3.2) where active stratovolcano complexes are present. There is a strong Bouguer gravity low in eastern Java that is associated with this central depression (Hall, 2003; Setijadji, 2005) although the Bouguer gravity low is less pronounced in western Java (Figure 5.1). However, regional low gravity anomalies in West Java are believed to be spatially associated with the central depression.

A section with gravity interpretation (Sano, 1978) located immediately to the east of the study area (Figure 5.2) shows the general features of the sub-surface in Java Island. These anomalies were attributed by Sano (1978) to the less dense materials of Cenozoic sediments beneath the Quaternary volcanic centres, which are located within the central depression zone outlined by Van Bemmelen (1949).

5.1.2. Analysis and interpretation of gravity data

This sub-section will focus on the applied processing technique and the interpretation of Bouguer gravity anomaly of study area. Comparisons of specific geologic information, represented on geologic and tectonic maps, with corresponding gravity anomalies may provide essential information regarding the distribution of favourable terranes for geothermal occurrences (i.e., volcano-tectonic depressions). The processing method includes the usage of vertical derivative filtering to enhance shallow subsurface features. Vertical derivative will give some "optical" advantages in that some features in a map of the gravity field to be easier to spot (Parasnis, 1997). For example, adjacent maxima and minima in the gravity field are often better resolved in a derivative map than on the map of the original data.

5.1.2.1. Processing and analysis

Preliminary data examination was carried out to visualise the spatial data distribution, which could affect the subsequent gridding algorithm. The point data are not distributed evenly (Figure 3-7). Some

datasets are clustered and/or very dense, as they were collected for certain local surveys. Other datasets follow long curved lines, reflecting surveys along the roads. In addition, there are large areas in the middle without data in almost half of study area. Attempts to construct a Bouguer anomaly from the original observation values were not successful because of incompleteness in the data. Therefore, the Bouguer anomaly values already calculated for each of the gravity observation points (Figure 3.7) were used. The Bouguer anomaly values were gridded using Minimum Curvature algorithm with pixel size of 1 km. The pixel size was selected to deal with the irregularities in data distribution, while still maintaining 66% probability that there are at least two neighbouring gravity data points in one pixel (based on point pattern analysis of the point data according to method by Boots and Getis (1988)). The size of the pixel is also within the required wavelength to sample anomalies less than 10 km depth.

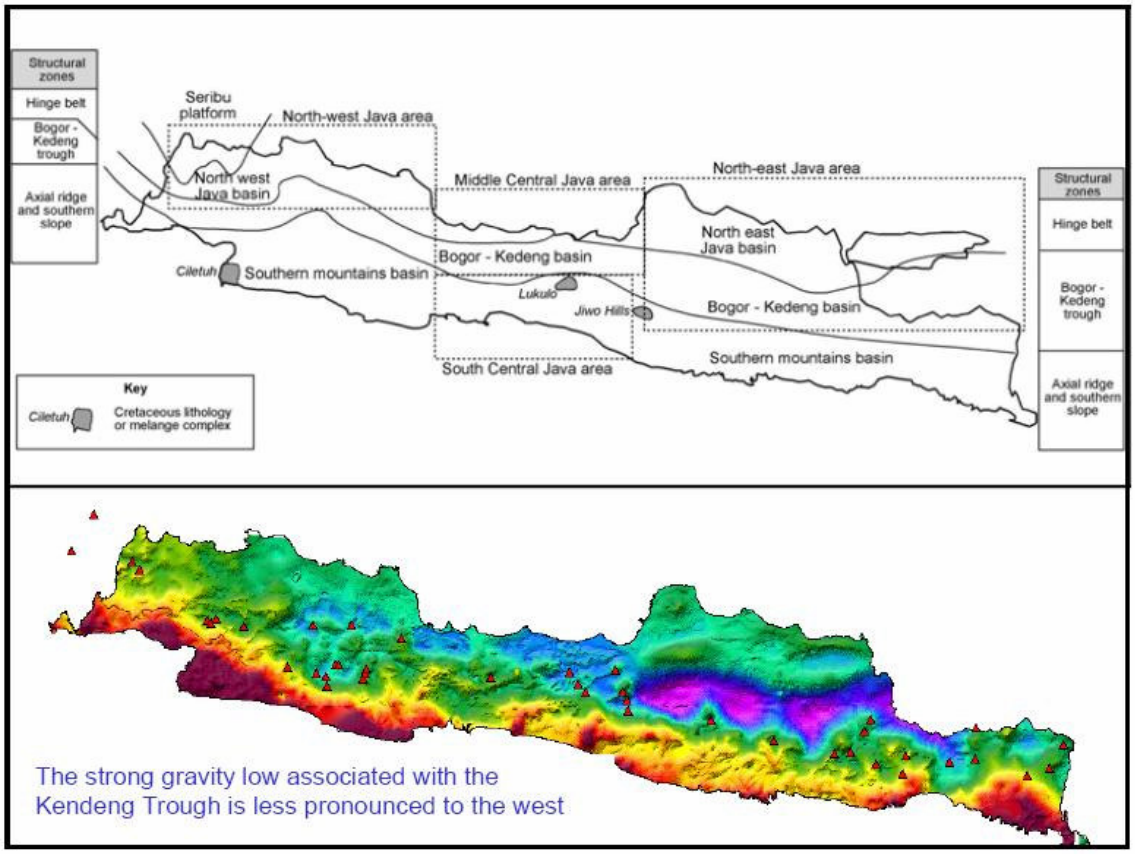

Figure 5.1: The Bogor-Kendeng Basin (Hall, 2003) or the East Java depression zone (Setijadji, 2005) and its associated gravity anomalies.

The Bouguer anomaly map (Figure 5.3) shows that the values are generally decreasing toward the north. This is consistent with the previous result of a gravity survey along a nearby cross section in the eastern part of the study area (Figure 5.2). The Southern Mountains area near Java trench are characterised by very high Bouguer anomaly values. Van Bemmelen's (1949) central depression, with more or less isolated active stratovolcano, and the folded mountain belt of Bogor anticlinorium zone are characterised by high to low Bouguer anomaly values from West to East. Finally, the Bouguer anomaly values are increasing slightly towards the north.

Figure 5.4a shows the frequency spectrum of the Bouguer gravity and the calculated depth estimate (Figure 5.4b), which is a plot of the 5-point averages of the slope of the energy spectrum (Spector and Grant, 1970). The depth estimate in Bouguer map range from 0 to 33 km, with average of 3.59 km.

In order to enhance the less pronounced low Bouguer gravity in Figures 5.3, a conventional integer vertical derivative has initially been applied to this dataset. This filter was applied to enhance the higher frequency of the Bouguer which may relate to shallow geologic features. However, 1st and 2nd vertical derivative map also enhanced the "noise" which manifested in form of bull's eyes features in the processed maps. It is typical of any high-pass filtering method, since noise mostly exists in high frequency. It is a trade-off between attenuating low frequency signal in expense of the higher one. Therefore an alternative of fractional vertical derivative filtering was applied, allowing us to enhance the high frequency signals in fractional mode. This is done by choosing the value between 0 and 1 as derivative order, rather than integer value of 1 or 2. The response of this filter on the original Bouguer map can be seen at Figure 5.4a. The high frequency content in dataset was amplified, albeit with smaller gain, at the cost of smaller attenuation in the lower frequency signal. Figure 5.4b shows the calculated depth estimate in half-vertical derivative Bouguer map range from 0 to 29 km, with average of 2.34 km. By looking at the graph, the filter has resulted in shallower depth in the Bouguer gravity data.

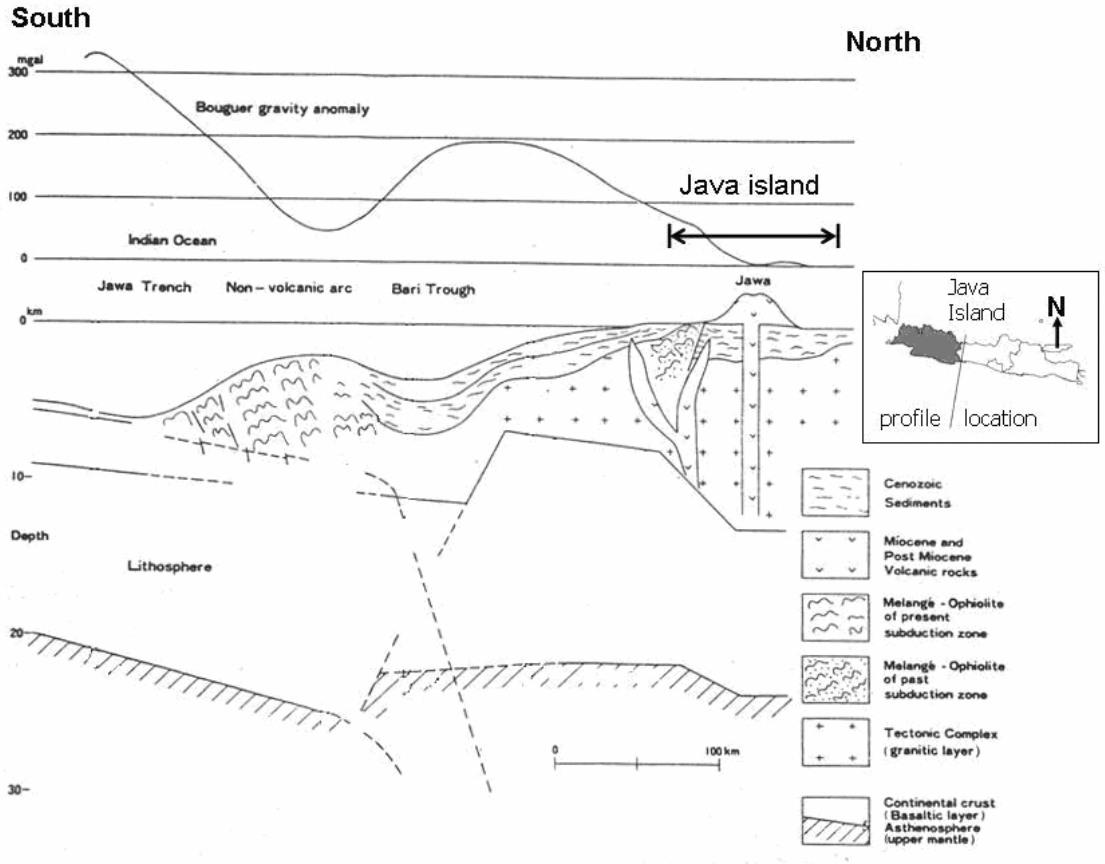

Figure 5.2: Sub-surface interpretation across Java trench and island based on gravity data (from Sano, 1978). Inset picture shows the approximate location of the profile (109 ºE).

The map output of half-vertical derivative filter is shown in Figure 5.5. In this map, longer wavelengths, which probably correspond with deeper structures, are still observed, because only very small portion of the long wavelengths are attenuated. However, the previously less pronounced features are enhanced, allowing better visualization of indications of shallower features. So, the final result of this processing is like superimposing the enhanced shallow features on top of deeper structures. In other words, the half-vertical derivative Bouguer map provides the advantage of visualizing subsurface density distribution in a "perspective" view. Both Bouguer maps, original (Figure 5.3) and filtered (Figure 5.5) were then stretched using histogram equalisation, where parts of the histogram with many pixels are stretched more than parts with few pixels. This was performed to

ensure that equal portions of the colour distribution are assigned to dominant values in the map as well as the less dominant values.

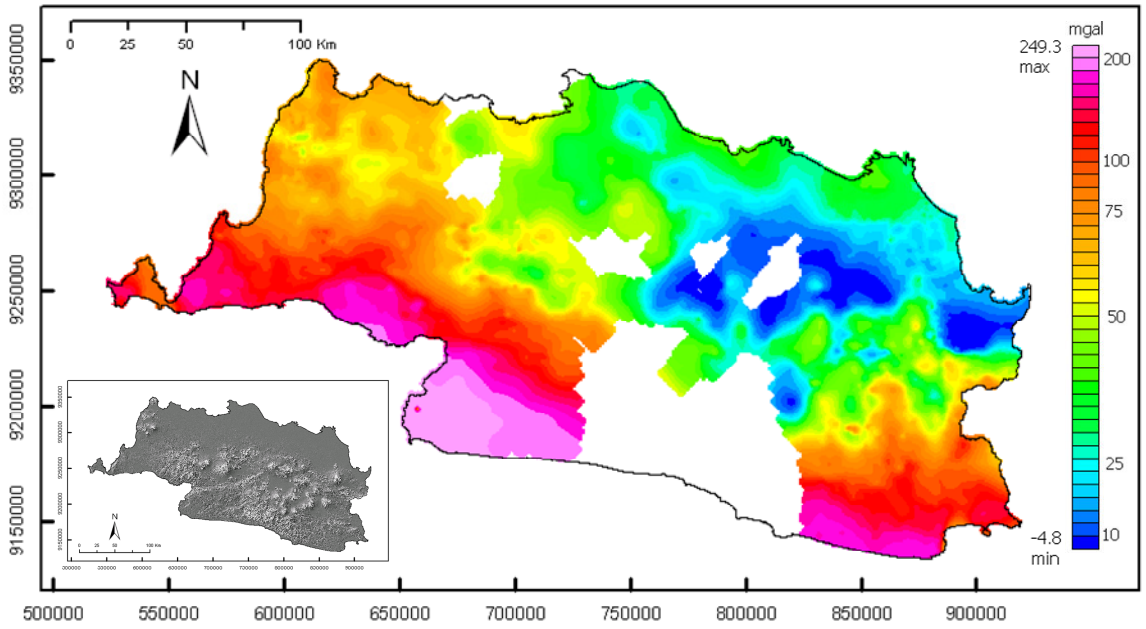

Figure 5.3: Bouguer image map. DEM-SRTM map is in inset box.

It can also be observed in Figure 5.5 that low Bouguer gravity anomalies approximately coincide with the central depression zone (see also in Figure 3.2) of Van Bemmelen (1949).

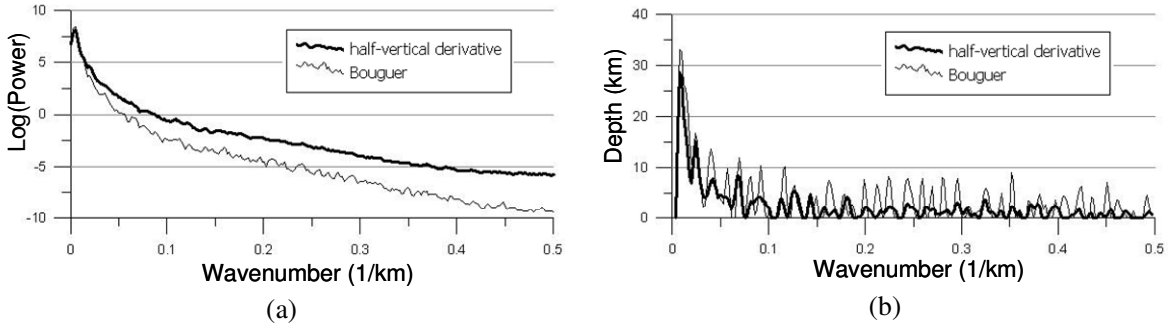

Figure 5.4: (a) Frequency spectra and (b) depth estimate of Bouguer and its half-vertical derivative

5.1.2.2. Interpretation

A suitable cross-section (line AB in Figure 5.5) was selected to give an insight on the subsurface geology based on the half-vertical derivative of Bouguer gravity values. Although the Bouguer anomalies only cover half of the map in this cross section, this profile line is the same profile AB line in Figure 3.2 and 3.5a, allowing easy comparison to be made. The gravity profile in this cross-section (Figure 5.6a) shows the Bouguer anomaly curve and the half-vertical derivative Bouguer curve. The depth of the body was then calculated using Equation 5.1 (adopted from Parasnis, 1997), assuming the causative body of massive vertical cylinder. This model is usually used for modelling geological features which has large horizontal extent, such as certain diapirs and salt domes (Parasnis, 1997). The reason for this model selection is because it is simple and has similarity in shape to the conceptual model of the causative body in geological sections of Figures 3.5a and b. For example volcanic rocks can be modelled as a layer that has certain depth from the surface, and the Cenozoic

sedimentary layer in Sano's (1978) profile (Figure 5.2) can be modelled started from a certain depth to infinity.

The cross section AB (Figure 5.6) shows the inverse correlation between topography and Bouguer gravity, suggesting the existence of a subsurface mass deficiency. The amount of low anomaly is 15 mgal compared with its surrounding. Half-vertical derivative curve gives the horizontal extent of this shallow anomaly (50 km). The andesitic characteristic of average volcanic rocks which has lower average density (2.61 g/cm3) than the average crust density (2.67 g/cm3) (taken from general reference: Telford et al., 1990), may be attributed to the low Bouguer anomaly. However, the anomaly cannot be explained by the distribution of volcanic rocks alone. Depth calculation of the anomaly results in more than the thickness of volcanic rocks, which is about 1-2 km (see Figure 3.5a). The gravity low thus requires a mass deficiency at relatively deeper layer than volcanic rocks.

$$\Delta g = 2\pi G\delta\left(z_2 - z_1 + \left(z_1^2 + a^2\right)^{1/2} - \left(z_2^2 + a^2\right)^{1/2}\right) \tag{5.1}$$

Where:

Δg	= Bouguer anomaly (mgal)
G	= 6.673 x 10^{-11} m^3 kg^{-1} s^{-2} (Gravity constant)
δ	= density contrast (g/cm^3)
a	= radius cylinder (in km)
z_1	= depth to the top of cylinder (in km)
z_2	= depth to the bottom of the cylinder (in km)

By using the same equation, 15 mgal in the profile of Bouguer anomaly values could result from a density contrast -0.2 g/cm^3, caused by a vertical cylinder body at depths from 1 to 3 km (2 km thickness). This amount of density contrast can be explained by presence of materials with average density of 2.47 g/cm^3 (as compared with average crust density 2.67 g/cm^3). If this is the case, then the Cenozoic sedimentary rocks beneath the volcanic rocks are the most plausible sources of the low gravity anomalies. This interpretation follows previous interpretation by Sano (1978).

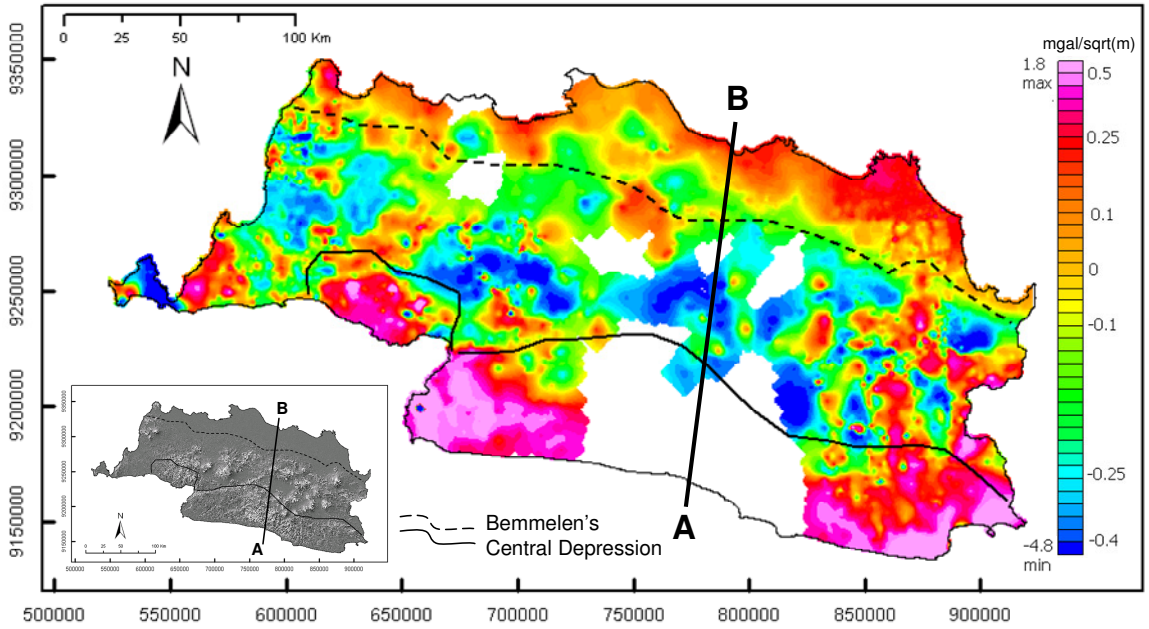

Figure 5.5: Half-vertical derivative Bouguer image map. Inset shows Van Bemmelen's (1949) central depression zones overlaid on a shaded-relief image of SRTM DEM. Line AB is a profile line for Figure 5.6.

Pakiser (1964) in his study on the southern Cascade Range – Lassen Volcanic National Park, California, investigated the cause of a large gravity low in that area. He postulated several probable geologic structures that may cause the low gravity. The low density mass could be made up of: (1) a batholith of silicic rock, (2) a thick accumulation of low density sedimentary deposits, (3) a low density mass caused by thermal expansion of crustal rocks by heat from igneous activity, (4) a volcano-tectonic depression filled with volcanic material of low average density, or some combination of these. Similar geological conditions in Lassen Volcanic National Park that cause large low Bouguer anomalies are also probably present in the study area, such as huge fault trough bounded by fractures transverse to the direction of the mountain range, and has subsided to great depths, and then later filled with immense accumulation of volcanic rocks and closed in building the two giant volcanoes (Pakiser, 1964). In West Java, Dam (1994) mentioned the existence of deep-seated E-W trending rupture through the central part of volcanic arc, with the northern part subsiding down and northward, causing faulting and dislocation of the anticlinal central arc. Thus, based on literature reviews of geological and geophysical investigations in Java Island (Sano, 1978; Dam, 1994; Hall, 2003; Setijadji, 2005), it is hypothesized that the low Bouguer gravity in West Java is due to a regional E-W trending volcano-tectonic depression that exist in the West Java.

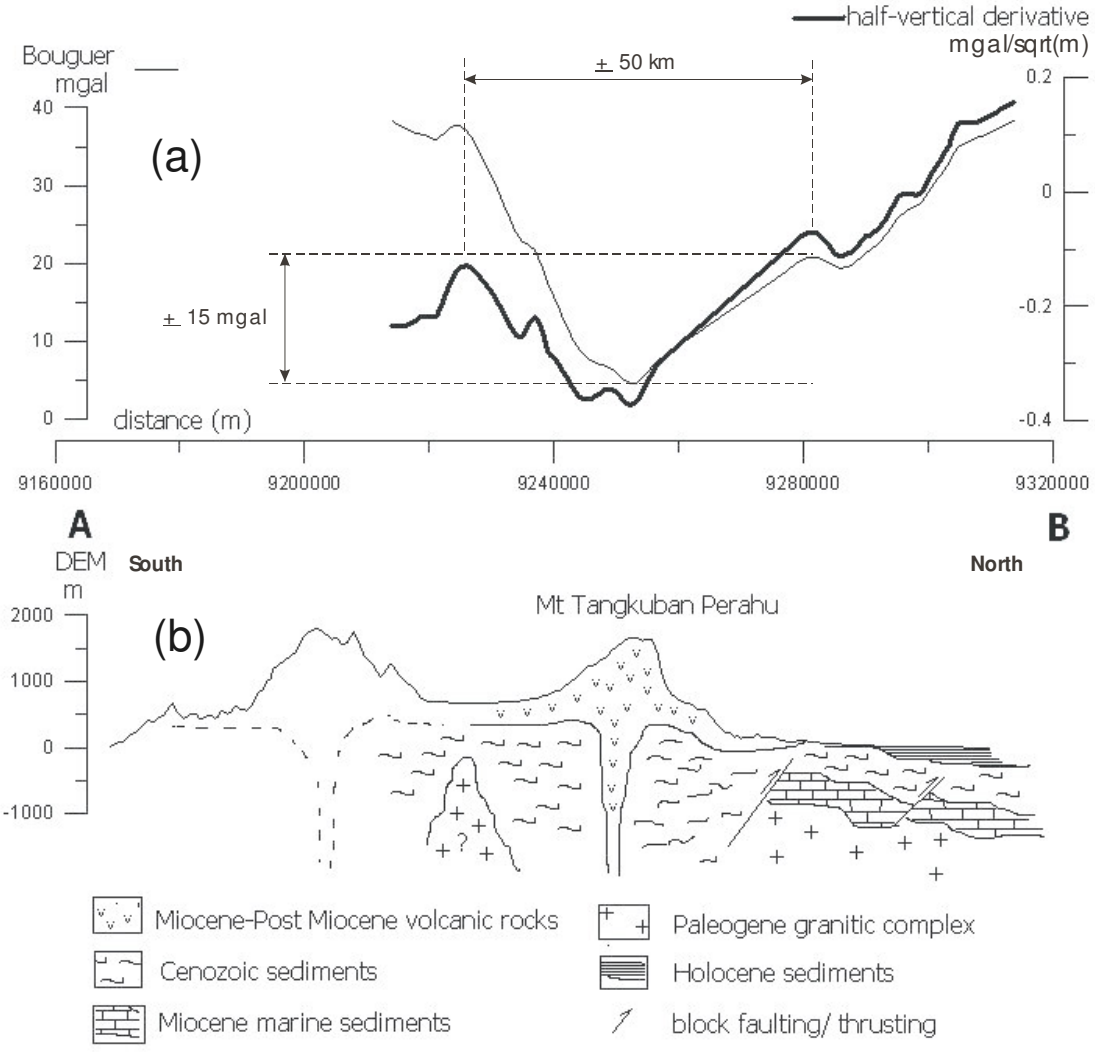

Figure 5.6: Cross section AB in Figure 5.5, (a) Bouguer anomaly (thin line) showing the total anomaly and half-vertical Bouguer anomaly (bold line) in exaggerated vertical scale, showing the anomaly due to shallow subsurface bodies, (b) schematic subsurface interpretation of Bouguer gravity across West Java (exaggerated vertical scale).

5.1.2.3. Outline of boundary of volcano-tectonic depression

Based on the preceding discussion, boundary of the hypothesized E-W trending volcano-tectonic depression is outlined based on the following argument. If low half-vertical derivatives of Bouguer anomaly values in West Java suggest presence of an E-W trending volcanic-tectonic depression (Figure 5.5) and if volcanic centres in West Java occur mostly (say, >50%) within this volcanic-tectonic depression, then the boundary of such volcano-tectonic depression could be outlined using the Bouguer anomaly values and locations of volcanic centres as constraints. So, to outline the boundary of the hypothesized E-W trending volcano-tectonic terrane, the principle behind the distance distribution analysis (see sub-section 4.2.1.2) is applied by using classes of Bouguer anomaly values (instead of classes of distances to geological features) and locations of volcanic centres (instead of locations of geothermal occurrences).

The range of Bouguer anomaly values was partitioned into 20 classes using 5-percentile intervals of the data. The cumulative frequencies of pixels within classes of increasing Bouguer anomaly values were determined to define an expected cumulative frequency distribution curve. The cumulative frequencies of "volcanic centre" pixels within classes of increasing Bouguer anomaly values were also determined to define an observed cumulative frequency distribution curve. A "difference" curve of the observed minus the expected cumulative frequencies was also determined. Figure 5.7 shows that the observed cumulative frequency distribution curve is above the expected cumulative frequency distribution curve. This implies that the volcanic centres have positive spatial association with low Bouguer anomaly values. The "difference" curve is highest at -0.153. About 65% of the volcanic centres occur in zones with Bouguer anomaly values of ≤-0.153.

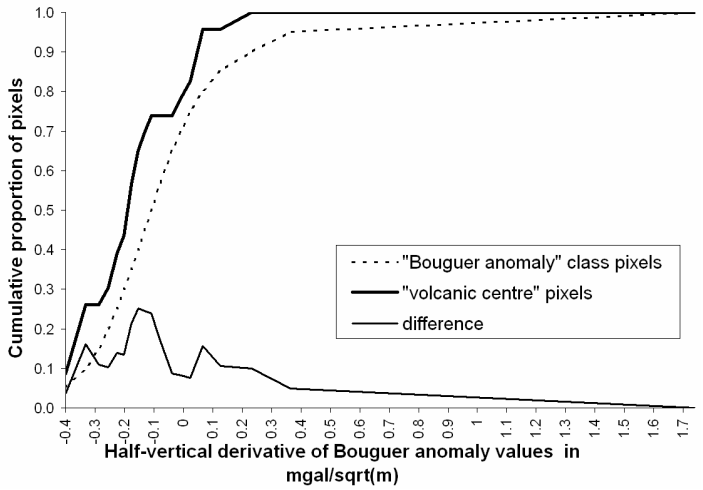

Figure 5.7: Expected cumulative frequency distribution of "Bouguer anomaly" class pixels and observed cumulative frequency distribution of volcanic centres in "Bouguer anomaly" classes.

The value of -0.153 was then used as a threshold to distinguish between "low" and "high" Bouguer anomaly values. Because of missing data and probably because irregular characteristics of the subsurface as reflected by the Bouguer anomaly values, the pattern of only "low" Bouguer anomaly values is irregular (figure 5.8a). However, a zone with "predominantly low" Bouguer anomaly values can be delineated as shown in Figure 5.8a. In Figure 5.8b, it is shown that such zone with "predominantly low" Bouguer anomaly values roughly coincides with Van Bemmelen's (1949) central depression. Therefore, the boundary of such zone with "predominantly low" is also considered boundary of the hypothesized E-W trending volcano-tectonic depression.

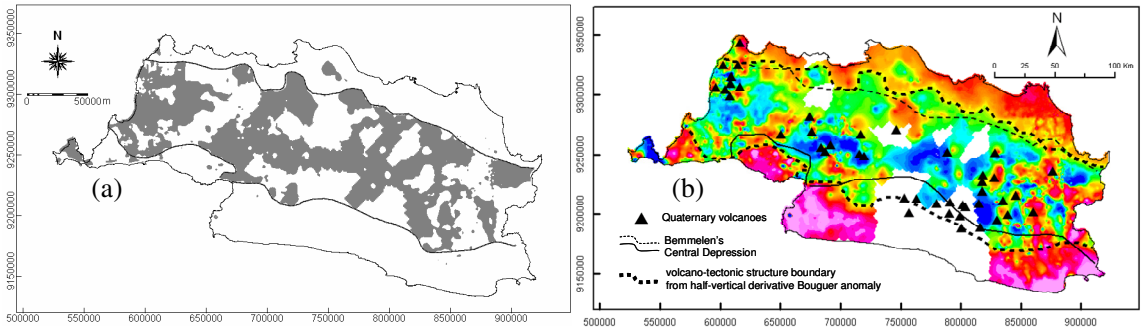

Figure 5.8: West Java: (a) zone of "predominantly low" Bouguer anomaly values (shown in grey), which probably coincides with hypothesized volcano-tectonic depression; (b) half-vertical derivative of Bouguer anomaly values, boundary of hypothesized volcano-tectonic depression (bold dashed lines), and Van Bemmelen's (1949) central depression.

5.1.3. Spatial association between volcano-tectonic depression and geothermal occurrences

The hypothesized volcano-tectonic depression is filled by Cenozoic sediments (Thamrin, 1985), upon which were Quaternary volcanic rocks were deposited. The sediments within the hypothesized volcano-tectonic depression are potential reservoir rocks of geothermal energy, whereas the overlying volcanic rocks could act as cap rocks. The hypothesized volcano-tectonic depression is a spatial indicator of geothermal prospectivity. Distance distribution analysis was performed to explore whether or not presence of or proximity to boundary of hypothesized volcano-tectonic depression represents a positive indication of geothermal prospectivity.

Figure 5.9 indicates that there is positive spatial association between volcano-tectonic depression and geothermal occurrences. The positive spatial association between the volcano-tectonic depression and the known geothermal occurrences is optimum at 6.6 km. About 90% of the known geothermal occurrences are present within the distance of optimum spatial association with volcano-tectonic depression. The "difference "curve indicates that within 6.6 km of the volcano-tectonic depression, there is about 20% higher probability of finding a geothermal occurrence than would expected due to chance. These results indicate that presence of or proximity to interpreted volcano-tectonic depression is a positive indication of geothermal prospectivity.

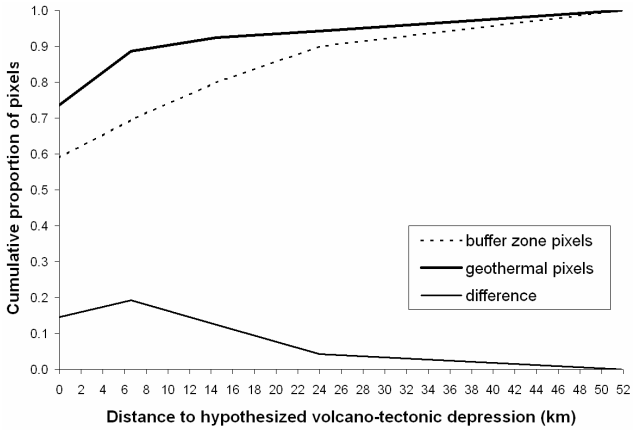

Figure 5.9: Expected cumulative frequency distribution of buffer zone pixels (within and around volcano-tectonic depression) and observed cumulative frequency distribution of geothermal occurrences within and around volcano-tectonic depression.

5.2. Indications of Geothermal Prospectivity from Seismicity

5.2.1. Regional seismicity and geothermal systems

Earthquakes mostly occur in brittle materials along tectonic plate margins and below a certain temperature threshold (Rybach, 1981; Bodri et al., 1991; Bodri and Iizuka, 1993). Hanus and Vanek (1989), in their study of seismotectonics in Circum-Pacific subduction zones, concluded that the seismically active fracture zones seem to be the main import path for solutions liberated from the zone of subduction. This has been proven by the location of practically all hot springs in Mexico and Ecuador. In addition, clusters of earthquakes, referred to as seismically active columns, found beneath active volcanoes of western Java in lithospheric wedges above subducting slabs. These clusters of earthquakes occur only beneath volcanoes along deep-rooted seismically active fracture zones (Špicák et al., 2005). Earthquakes in these clusters beneath volcanoes are interpreted as events induced by magma transport through lithospheric wedges that were subcritically pre-stressed by plate convergence. The investigation by Špicák et al. (2005) supports the concept that a subducted oceanic lithosphere is the source region for the primary magma, to which calc-alkaline volcanoes at convergent plate margins are associated with. Gulyás and Hédervári (1976) concluded that there is relationship between the depth of primary magma chambers (sources of andesitic magma) in western Java and the seismic energy concentration beneath the volcanoes. Thus, there is strong relationship between subduction zones, volcanoes, earthquake epicentres distribution (Rubie and Hilst, 2001) and geothermal occurrences.

Sibson (1987) discussed the importance of earthquake rupturing as a mineralising agent in hydrothermal systems; that the ruptures act as vertical pipe like conduits for enhanced fluid flow. Foulger (1982) concluded that in many cases the location of a geothermal area coincides with an area where regional stress is being released at a different rate to the surrounding area. The differences in seismicity of different geothermal areas may hence reflect differences in the regional tectonics of the areas in question. Majer and McEvilly (1979) noted, however, that earthquakes tended to occur at the edges of, and not within, the zones of geothermal production. This may be attributed to the inverse correlation between earthquake numbers and sizes with temperature (e.g., Ehara, 1987; Bodri and Iizuka, 1993; Simiyu and Malin, 2000), which suggests that there is less seismicity observed within high temperature areas. The reason of these phenomena is related with the fact that the crust's strength increases linearly with increasing pressure but decreases exponentially with increasing temperature (Simiyu and Malin, 2000). However, many studies also show that recent intrusions are associated with high levels of earthquake activity (Doi et al., 2000; Zhao, 2001; Tanaka et al., 2002; Špicák et al., 2005). Thus, earthquake activities are controlled by crustal temperature, tectonic stress, and magma movement. For example, in Central Kyushu, Japan, the presence of hot crust is also accompanied by the change in the tectonic stress field, resulting in high seismic activity in this area (Ehara, 1987).

5.2.2. Spatial analysis of earthquake epicentre data

Spatial analysis was performed to determine and whether or not there is positive spatial association between the earthquake epicentres and the known geothermal occurrences. The spatial analysis of the earthquake epicentres in West Java was also performed to determine whether or not the spatial distribution of earthquake epicentres is similar to the spatial distribution of known geothermal occurrences. However, it should be remarked that the earthquake epicenters dataset used in this study is a mixture between different datasets compiled from two agencies (i.e., National Seismological Centre and Volcanological Centre); consequently the location of seismometer and its radius of measurement are according to their acquisition purposes.

5.2.2.1. Results of Fry analysis

The Fry plot of locations of the 127 earthquake epicentres (Figure 5.10a) shows a major WNW trend, which corresponds to (a) the trend of the subduction zone along Sunda Trench offshore south of Java Island, (b) the trend of the magmatic arc in the island, and (c) the trend of Java Structural Domain. This major trend of the earthquake epicentres depicted in the Fry plot is therefore geologically-related.

There is a secondary but obvious NE trend in the Fry plot, which is probably related with NE-trending faults. There are subtle spacings of about 70-90 km between NE-trending point translations. This is a similar observation in the Fry plots of the Quaternary volcanoes (See sub-section 4.2.3.1 and Figure 4.6), which reduces the possibility that such spacings in the Fry plots are artefacts of the data. Note also that the amount of this spacing is similar to Fry plot points of Quaternary volcanoes (75 km). Although the spacings in the Fry plots are difficult to explain, the similarities in the Fry plots of earth epicentres and Quaternary volcanoes and the discussion in the review of literature presented above (section 5.2.1) suggest that spatial distributions of earthquake epicentres and Quaternary volcanoes in West Java are controlled by the same tectonic process.

For point translations less than 47 km apart (i.e., distance of maximum probability for a neighbouring earthquake epicentre from another earthquake epicentre), NE is the major trend (Figure 5.9c), whereas the WNW trend is minor. This spatial pattern is also similar to the spatial patterns found for the geothermal occurrences, hot springs and Quaternary volcanoes (see Chapter 4). These similarities in spatial patterns of the different geological features studied here suggest a common principal structural control on their spatial distributions in the study area. The similarity of spatial patterns of the earthquake epicentres and the geothermal occurrences also suggest that there is positive spatial association between the earthquake epicentres and the known geothermal occurrences.

5.2.2.2. Results of distance distribution analysis

Within 4 km of earthquake epicentres the observed cumulative frequency distribution curve of “geothermal pixels” is slightly below the expected cumulative frequency distribution of the “buffer zone pixels” (figure 5.11). Note the slight negative value for the “difference” curve at 4 km. This suggests that within 4 km of earthquake epicentres there are few geothermal occurrences than would be expected due to chance. However, beyond 4 km of earthquake epicentres curve for the “geothermal pixels” is above the curve for the “buffer zone pixels. This indicates that there is positive spatial association between earthquake epicentres and geothermal occurrences. The positive spatial association is optimum at 16 km. About 77% of the known geothermal occurrences are present within this distance of optimum spatial association with Quaternary volcanic centres. The “difference” curve indicates that within about 16 km of earthquake epicentres, there is about 17% higher chance of finding a geothermal occurrence than would expected due to chance. These results indicate that proximity to earthquake epicentres is a positive evidence of geothermal prospectivity.

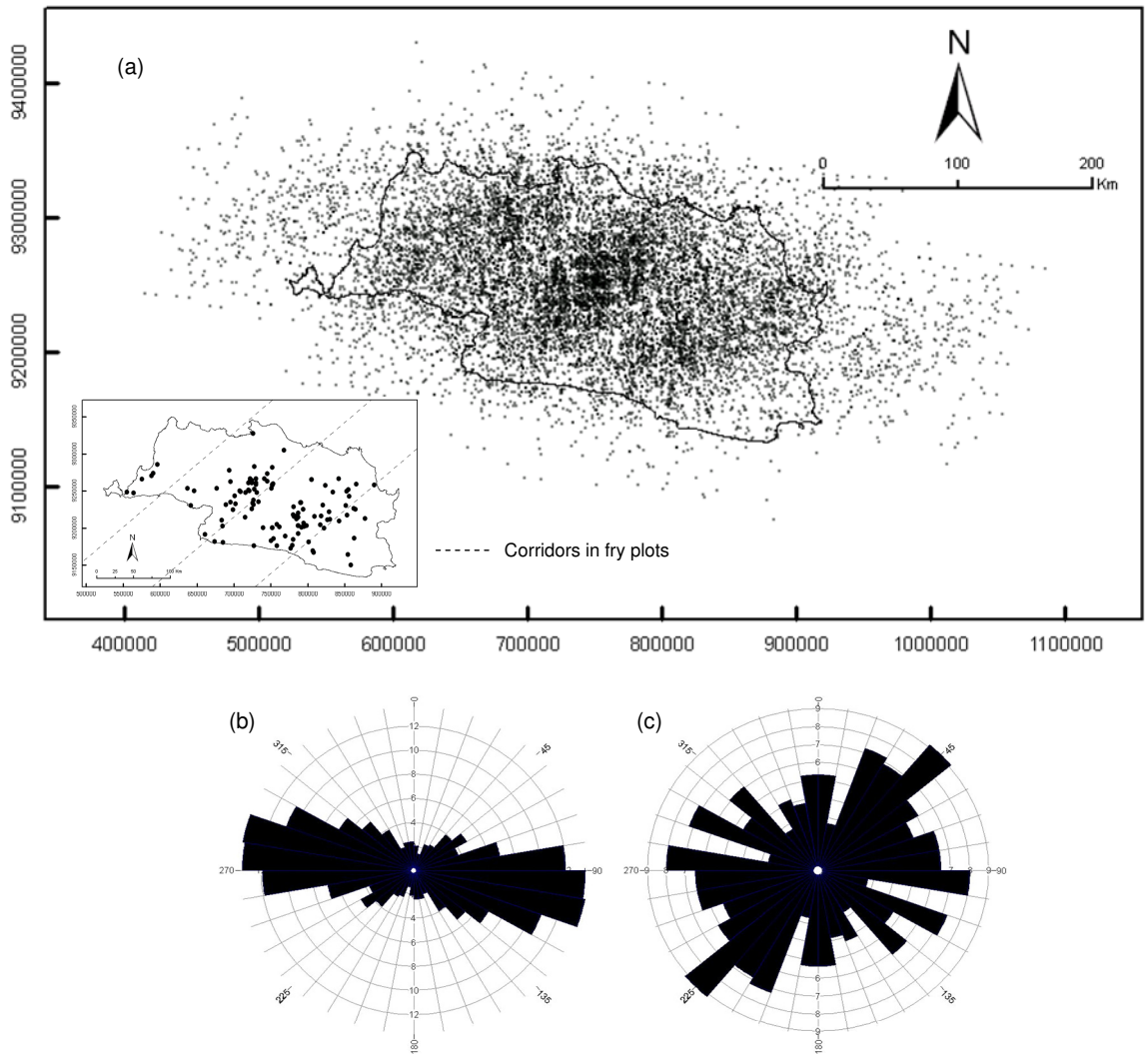

Figure 5.10: (a) Fry plot of earthquake epicentres (inset shows original locations of earthquake epicentres) and (b) corresponding rose diagram of all point translations. (c) Rose diagram of point translations less than 47 km apart.

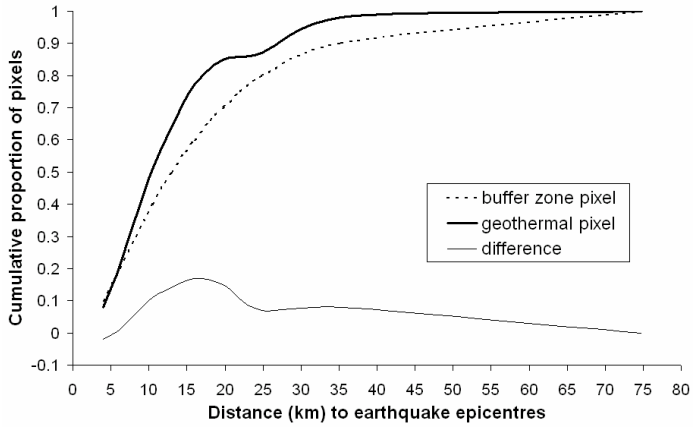

Figure 5.11: Expected cumulative frequency distribution of buffer zone pixels (around earthquake epicentres) and observed cumulative frequency distribution of geothermal occurrences around earthquake epicentres.

5.3. Discussion and concluding remarks

A half-vertical derivative filter was applied to the gravity data to enhance shallow features in geological environments associated with geothermal systems. Analysis of the derivative gravity data leads to interpretation of volcano-tectonic depressions, which provide conditions favourable for formation of geothermal reservoirs. Structural features such as half-grabens and subsidence basins are commonly found in volcano-tectonic depressions. These structural controls may act as conduit paths for rising hot fluids or provide places for sedimentary or volcanic materials, deposited as permeable layers that might lead to the formation of geothermal reservoir systems. In the study area, favourable conditions provided by the volcano-tectonic depressions are permeable volcano-sedimentary layers as reservoir rocks, faults, and fractures as conduits for geothermal fluids, and volcanic rocks as cap rocks.

The influence of earthquakes on geothermal prospectivity in the study area has been investigated empirically through spatial analysis. There is similarity between earthquake epicentre and Quaternary volcano data clustering in West Java, which caused the spacing pattern in the Fry plots. Furthermore, there is similarity of earthquake epicentres short distance NE trend with the one found in geothermal occurrences, hot springs, and volcanoes. These observations suggest that the distribution of spatial location of these data is controlled by the same principal structural control (i.e., tectonic process and volcanism). Further investigation about the underlying process might still be needed.

There is strong relationship between subduction zones and spatial distributions of volcanoes, earthquake epicentres, and geothermal occurrences. Earthquake activities are controlled by crustal temperature, tectonic stress, and magma movement. Seismically active fracture zones seem to be the main import path for geothermal solutions and intrusions are often accompanied by high seismicity activities. These geological environments may provide favourable terranes for geothermal systems.

The following spatial criteria are therefore included in the conceptual model of geothermal prospectivity presented in Chapter 4: (a) presence of or proximity to (within 6.6 km of) volcano-tectonic depressions; and (b) proximity to (within 16 km of) earthquake epicentres. The conceptual model of geothermal prospectivity now developed consists of six spatial criteria. The respective distances of optimum spatial association found in the distance distribution analyses (Chapter 4 and in this chapter) could be used to create binary predictor maps, which could be overlaid on top of each other to determine intersections of spatial criteria representing prospective ground (e.g., Carranza et al., 1999). It is considered that intersections of at least four of the six spatial criteria determine prospectivity of an area for geothermal field occurrence. However, prospectivity modelling based on binary predictor maps is simplistic because spatial criteria are given equal weights or importance with respect to model target (e.g., geothermal occurrence). In this study, a multi-class type of prospectivity modelling, with unequal weighting of spatial criteria based on known geothermal occurrences, will be presented in Chapter 7. Before that, the conceptual model of geothermal prospectivity will be developed further depending on results of remote sensing of surface indications of geothermal occurrences (Chapter 6).

Chapter 6: Analysis of Landsat TM data for Indications of Geothermal Prospectivity

In Table 4.2, it is indicated that there are hydrothermal alterations in some of the geothermal prospects. One type of alteration, which is distinct from silica sinters or travertine deposits, generally consists of clay minerals such as kaolinite, illite, and smectites (e.g., Utami, 2000). Clay alteration of is present in prospects such as Tangkuban Parahu, Patuha, Cibuni crate, Wayang Windu, Panulisan, G. Sawal, Talaga Bodas, Papandayan, Cilayu, Ciarinem, Kawah Darajat, and Galunggung. Aside from the clay alteration in some of the geothermal prospects, it is also indicated in Table 4.2 that there are iron-oxide alterations in some of the prospects (Cimanggu, Rancawalini, Barutunggul, Panulisan, Cilayu, Ciater, Sagala Herang, Santa, Congeang-Cileungsing, and G. Tampomas).

Outcropping, altered rocks characterized by clay and iron-oxide group of minerals are, in general, amenable to remote detection using spaceborne multispectral imagery such as Landsat TM data. This chapter reports on the results of analysis of Landsat TM data to map areas where altered rocks are possibly present. The spatial associations between areas possibly containing altered rocks and the known geothermal occurrences are then quantified to determine whether or not the remotely-sensed altered rocks are positive indications of geothermal occurrences in the study area.

6.1. Remote detection of presence of altered rocks

It is indicated in section 3.5.6 that all the Landsat TM scenes were not acquired on the same date, and Figure 3.12 shows that one scene (p122r65) is most affected by haze. More importantly, as indicated in Figure 3.12, the study area is characterized mostly my vegetation cover because of the predominance of red in the colour composite image. Because of these factors, the individual Landsat TM scenes are pre-processed separately. To address the problem of remote detection of altered rocks in the presence of vegetation, the software defoliant technique (Fraser and Green, 1987) is applied.

6.1.1. Pre-processing Landsat TM bands

Image pre-processing of the Landsat TM data included only haze correction by a simple dark-object subtraction method (Richards, 1999). Haze is due to particulates present in the atmosphere, which obscures the spectral response of ground objects and has an additive noisy effect on the image brightness. The simple dark-objection subtraction method relies on the assumption that there should be black pixels (e.g., shadows, fresh water bodies) in an image and these pixels should have a DN (digital number) value of zero (i.e., no reflectance). Due to haze, however, these black or dark objects have DN values greater than zero. The simple dark-objection subtraction method thus involves subtracting a constant DN value from a certain digital image. This constant DN value is the lowest (i.e. pertaining to the darkest pixels) in a certain digital image and is determined from a histogram of the DN values of that image.

6.1.2. Application of the software defoliant technique

The software defoliant technique is essentially a directed principal components (DPC) analysis of two band ratio images (Fraser and Green, 1987). Two pairs of bands are selected such that one pair of bands produce band ratios that represent presence of the material of interest (e.g., altered rocks), the spectral response of which suffers interference from the spectral response of another type of material (i.e., vegetation). The other pair of bands should therefore produce band ratios that represent presence of the spectrally interfering material. The software defoliant technique has been adopted/adapted with relative success to detect clay-altered and iron-oxide-altered rocks in vegetated areas (e.g., Craig et al., 1999; Carranza and Hale, 2002a; Almeida and de Souza Filho, 2004). In this study, the modified technique developed by (2002a) is adopted because their study area in the Philippines and the study area here have similar tropical vegetation density characteristics.

So, two suitable pairs of Landsat TM bands are first selected according to the following criteria. Band ratios for vegetation must be theoretically high (i.e., greater than 1) in either of the input images. Band ratios for material of interest must be theoretically high (i.e., greater than 1) in one of the input images and theoretically low (i.e., less than 1) in the other input image. Two band ratio images are then input into DPC analysis. The DPCs are then interpreted as follows. The DPC with higher eigenvalues and with loadings having similar signs on both input band ratio images explains presence of vegetation. The other DPC, with lower eigenvalues and with loadings of different signs on either of the input band ratio images, explains the presence of the material of interest. For the DPC explaining the presence of the material of interest, the sign of the loadings on either of the input band ratio images indicates whether or not the material of interest will be represented by a high DPC score in an output image. A positive loading on the input band ratio image in which band ratios for the material of interest is theoretically high indicates that the presence of the material of interest will be represented by high DPC scores in an output image. A negative loading on the input band ratio image in which band ratios for material of interest is theoretically high indicates that the presence of the material of interest will be represented by low DPC scores in an output image. If the DPC explaining the presence of the material of interest has a negative loading on the input band ratio image in which band ratios for material of interest is theoretically high, then the corresponding DPC scores must be negated (i.e., multiplied by -1) in order to represent the material of interest by high DPC scores. It is important to state here that the DPC scores are interpreted here to indicate only relative degrees of presence of material of interest. This is mainly because in a 30×30 m pixel of Landsat TM imagery, it can be expected that there several other types of materials that could be present but not accounted for in the DPC analysis.

Fraser and Green (1987) recommend that the band ratios are computed from unstretched data and then the computed band ratios are standardised through a histogram equalisation stretch so that in an input image the values range from 0 to 255 and have an average of approximately 128. The software defoliant technique should also be performed on individual scenes (or sets of data), because the method is essentially scene-dependent (Fraser and Green, 1987).

6.1.2.1. Detection of relative degree of presence of clay alteration

Based on typical reflectance curves for vegetation and clay (Figure 6.1), the pairs of bands band4:band5 and band5:band7 were selected, because these two pairs of bands will both produce theoretically high ratios for vegetation but band4:band5 ratio will be theoretically low for clay and band5:band7 ratio will be theoretically high for clay. Another reason for selecting bands 4, 5 and 7 is that spectral features of vegetation and most clay minerals are in the infrared regions of the electromagnetic (EM) spectrum where these three Landsat TM bands are positioned (Spatz, 1997; Sabins, 1999).

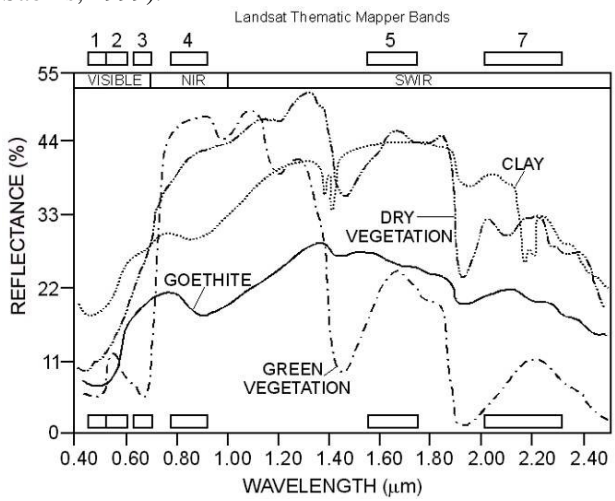

Figure 6.1: Typical reflectance spectra of vegetation, iron-oxides and clays (from Fraser and Green, 1987). The positions of Landsat TM bands are also shown.

For Landsat TM scene Path 121 Row 64, DPC2 explains presence of clay alteration (Table 6.1). The positive sign of loading on band5:band7 means that relative degrees of presence of clay alteration will be depicted as high DPC2 scores.

Table 6.1: Directed principal components (DPC) analysis of band ratio images of Landsat TM scene Path 121 Row 64 for clay alteration detection by application of the software defoliant technique. The DPC with loadings in bold explains presence of clay alteration.

Principal components	Eigenvectors		Eigenvalues (%)
	band4:band5	band5:band 7	
DPC1	0.707	0.707	85.23
DPC2	**-0.707**	**0.707**	14.77

For Landsat TM scene Path 121 Row 65, DPC2 explains presence of clay alteration (Table 6.2). The negative sign of loading on band5:band7 means that relative degrees of presence of clay alteration will be depicted as low DPC2 scores. The DPC2 scores are thus negated to depict relative degrees of presence of clay alteration as high DPC2 scores.

Table 6.2: Directed principal components (DPC) analysis of band ratio images of Landsat TM scene Path 121 Row 65 for clay alteration detection by application of the software defoliant technique. The DPC with loadings in bold explains presence of clay alteration.

Principal components	Eigenvectors		Eigenvalues (%)
	band4:band5	band5:band 7	
DPC1	0.707	0.707	86.55
DPC2	**0.707**	**-0.707**	13.45

For Landsat TM scene Path 122 Row 64, DPC2 explains presence of clay alteration (Table 6.3). The positive sign of loading on band5:band7 means that relative degrees of presence of clay alteration will be depicted as high DPC2 scores.

Table 6.3: Directed principal components (DPC) analysis of band ratio images of Landsat TM scene Path 122 Row 64 for clay alteration detection by application of the software defoliant technique. The DPC with loadings in bold explains presence of clay alteration.

Principal components	Eigenvectors		Eigenvalues (%)
	band4:band5	band5:band 7	
DPC1	0.707	0.707	75.84
DPC2	**-0.707**	**0.707**	24.16

For Landsat TM scene Path 122 Row 65, DPC2 explains presence of clay alteration (Table 6.4). The positive sign of loading on band5:band7 means that relative degrees of presence of clay alteration will be depicted as high DPC2 scores.

Table 6.4: Directed principal components (DPC) analysis of band ratio images of Landsat TM scene Path 122 Row 64 for clay alteration detection by application of the software defoliant technique. The DPC with loadings in bold explains presence of clay alteration.

Principal components	Eigenvectors		Eigenvalues (%)
	band4:band5	band5:band 7	
DPC1	0.707	0.707	86.16
DPC2	**-0.707**	**0.707**	13.84

For Landsat TM scene Path 123 Row 64, DPC2 explains presence of clay alteration (Table 6.5). The positive sign of loading on band5:band7 means that relative degrees of presence of clay alteration will be depicted as high DPC2 scores.

Table 6.5: Directed principal components (DPC) analysis of band ratio images of Landsat TM scene Path 122 Row 64 for clay alteration detection by application of the software defoliant technique. The DPC with loadings in bold explains presence of clay alteration.

Principal components	Eigenvectors		Eigenvalues (%)
	band4:band5	band5:band 7	
DPC1	0.707	0.707	81.29
DPC2	**-0.707**	**0.707**	18.71

For Landsat TM scene Path 123 Row 64, DPC2 explains presence of clay alteration (Table 6.6). The negative sign of loading on band5:band7 means that relative degrees of presence of clay alteration will be depicted as low DPC2 scores. The DPC2 scores are thus negated to depict relative degrees of presence of clay alteration as high DPC2 scores.

Table 6.6: Directed principal components (DPC) analysis of band ratio images of Landsat TM scene Path 122 Row 64 for clay alteration detection by application of the software defoliant technique. The DPC with loadings in bold explains presence of clay alteration.

Principal components	Eigenvectors		Eigenvalues (%)
	band4:band5	band5:band 7	
DPC1	0.707	0.707	75.37
DPC2	**0.707**	**-0.707**	24.63

6.1.2.2. Detection of relative degree of presence of iron-oxide alteration

Judging from the reflectance curves of green vegetation and goethite (a typical iron-oxide mineral in weathered altered rocks) and the position of Landsat TM bands (Figure 6.1), the pairs of bands band4:band5 and band5:band7, which were selected for clay detection, will both produce theoretically high ratios for vegetation and band4:band5 ratios will be theoretically low for goethite and band5:band7 ratios will be theoretically high for goethite. So, the pairs of bands band4:band5 and band5:band7 would basically be applicable also for iron-oxide detection. However, spectral features of either vegetation or iron-oxides are in the visible to near-infrared regions of the electromagnetic spectrum (Spatz, 1997; Sabins, 1999). So, suitable pairs of Landsat TM bands for iron-oxide detection should be selected from among bands 1, 2, 3 and 4. Accordingly, based on the reflectance curves of green vegetation and goethite (a typical iron-oxide mineral in weathered altered rocks) and the position of Landsat TM bands (Figure 6.1), the pairs of bands band2:band3 and band4:band1 were selected, because these two pairs of bands will both produce theoretically high ratios for vegetation but band2:band3 ratios will be theoretically low for goethite and band4:band1 ratios will be theoretically high for goethite.

For Landsat TM scene Path 121 Row 64, DPC2 explains presence of iron-oxide alteration (Table 6.7). The negative sign of loading on band4:band1 means that relative degrees of presence of iron-oxide alteration will be depicted as low DPC2 scores. The DPC2 scores are thus negated to depict relative degrees of presence of iron-oxide alteration as high DPC2 scores.

Table 6.7: Directed principal components (DPC) analysis of band ratio images of Landsat TM scene Path 121 Row 64 for iron-oxide alteration detection by application of the software defoliant technique. The DPC with loadings in bold explains presence of iron-oxide alteration.

Principal components	Eigenvectors		Eigenvalues (%)
	band 2:band3	band4:band1	
DPC1	0.707	0.707	82.56
DPC2	**0.707**	**-0.707**	17.44

For Landsat TM scene Path 121 Row 65, DPC2 explains presence of iron-oxide alteration (Table 6.8). The positive sign of loading on band4:band1 means that relative degrees of presence of iron-oxide alteration will be depicted as high DPC2 scores.

Table 6.8: Directed principal components (DPC) analysis of band ratio images of Landsat TM scene Path 121 Row 65 for iron-oxide alteration detection by application of the software defoliant technique. The DPC with loadings in bold explains presence of iron-oxide alteration.

Principal Components	Eigenvectors		Eigenvalues (%)
	band 2:band3	band4:band1	
DPC1	0.707	0.707	76.57
DPC2	**-0.707**	**0.707**	23.43

For Landsat TM scene Path 122 Row 64, DPC2 explains presence of iron-oxide alteration (Table 6.9). The negative sign of loading on band4:band1 means that relative degrees of presence of iron-oxide alteration will be depicted as low DPC2 scores. The DPC2 scores are thus negated to depict relative degrees of presence of iron-oxide alteration as high DPC2 scores.

Table 6.9: Directed principal components (DPC) analysis of band ratio images of Landsat TM scene Path 122 Row 64 for iron-oxide alteration detection by application of the software defoliant technique. The DPC with loadings in bold explains presence of iron-oxide alteration.

Principal components	Eigenvectors		Eigenvalues (%)
	band 2:band3	band4:band1	
DPC1	0.707	0.707	83.32
DPC2	**0.707**	**-0.707**	16.68

For Landsat TM scene Path 122 Row 65, DPC2 explains presence of iron-oxide alteration (Table 6.10). The negative sign of loading on band4:band1 means that relative degrees of presence of iron-oxide alteration will be depicted as low DPC2 scores. The DPC2 scores are thus negated to depict relative degrees of presence of iron-oxide alteration as high DPC2 scores.

Table 6.10: Directed principal components (DPC) analysis of band ratio images of Landsat TM scene Path 122 Row 65 for iron-oxide alteration detection by application of the software defoliant technique. The DPC with loadings in bold explains presence of iron-oxide alteration.

Principal components	Eigenvectors		Eigenvalues (%)
	band 2:band3	band4:band1	
DPC1	0.706	0.708	70.82
DPC2	**0.708**	**-0.706**	29.18

For Landsat TM scene Path 123 Row 64, DPC2 explains presence of iron-oxide alteration (Table 6.11). The negative sign of loading on band4:band1 means that relative degrees of presence of iron-oxide alteration will be depicted as low DPC2 scores. The DPC2 scores are thus negated to depict relative degrees of presence of iron-oxide alteration as high DPC2 scores.

Table 6.11: Directed principal components (DPC) analysis of band ratio images of Landsat TM scene Path 123 Row 64 for iron-oxide alteration detection by application of the software defoliant technique. The DPC with loadings in bold explains presence of iron-oxide alteration.

Principal components	Eigenvectors		Eigenvalues (%)
	band 2:band3	band4:band1	
DPC1	0.706	0.708	84.07
DPC2	**0.708**	**-0.706**	15.93

For Landsat TM scene Path 123 Row 65, DPC2 explains presence of iron-oxide alteration (Table 6.12). The negative sign of loading on band4:band1 means that relative degrees of presence of iron-oxide alteration will be depicted as low DPC2 scores. The DPC2 scores are thus negated to depict relative degrees of presence of iron-oxide alteration as high DPC2 scores.

Table 6.12: Directed principal components (DPC) analysis of band ratio images of Landsat TM scene Path 123 Row 65 for iron-oxide alteration detection by application of the software defoliant technique. The DPC with loadings in bold explains presence of iron-oxide alteration.

Principal components	Eigenvectors		Eigenvalues (%)
	band 2:band3	band4:band1	
DPC1	0.707	0.708	71.42
DPC2	**0.708**	**-0.707**	28.58

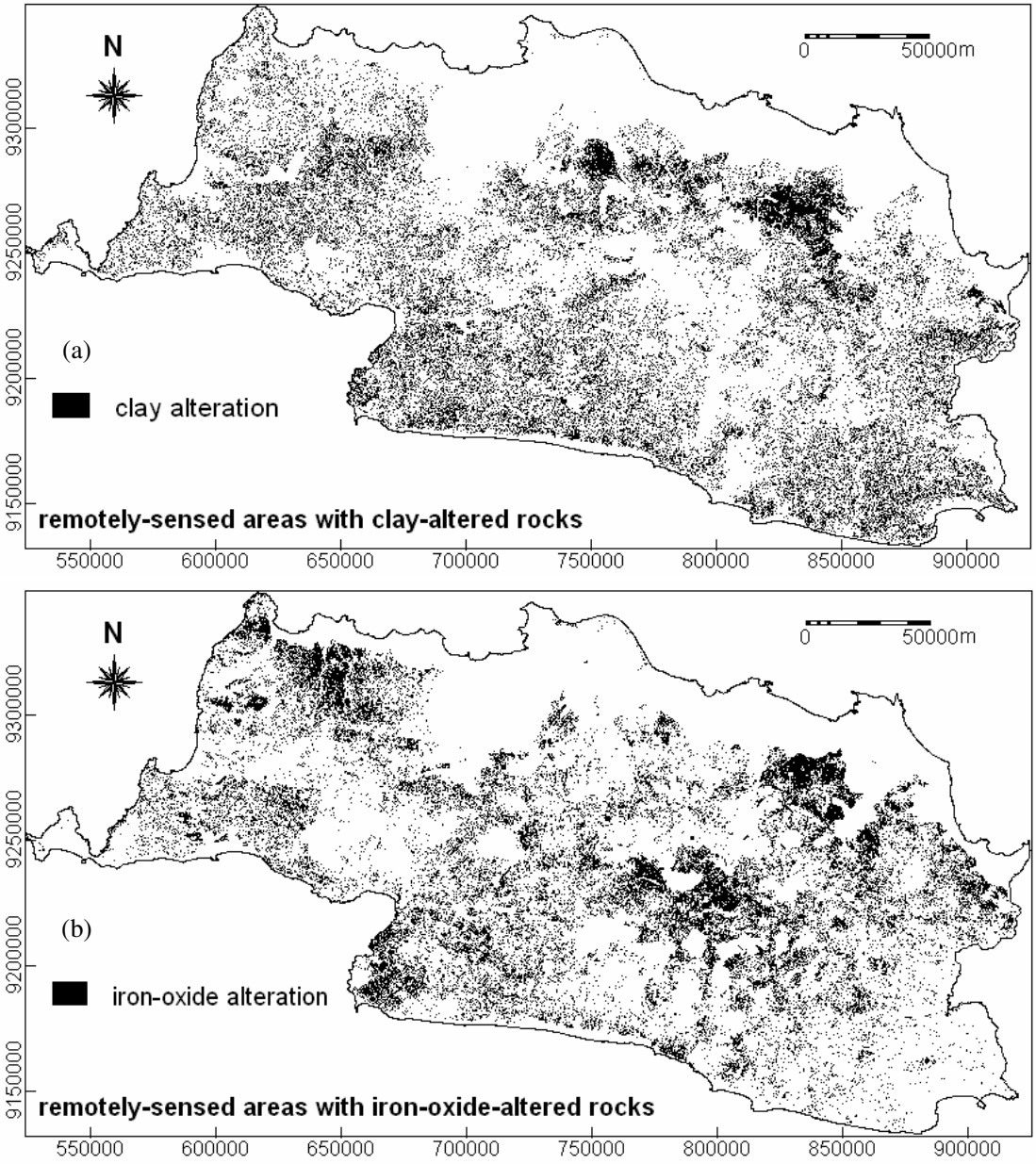

Figure 6.2: Remotely-sensed areas with (a) clay alteration and (b) iron-oxide alteration.

6.1.3. Mapping of areas possibly containing altered rocks

The images of calculated DPC2 scores (negated or not), which represent relative degrees of presence of altered rocks in 30×30 m pixels, are transformed into images with 500×500 m pixel size. This transformation is important because a pixel of 500×500 m pixel size was used in the spatial analyses of indications of geothermal occurrences (Chapter 4) and will be used in the integration modelling of geothermal prospectivity (Chapter 7). The transformed images of DPC2 scores thus represent relative degrees of presence of altered rocks in 500×500 m pixels. The transformation was performed by using a bi-cubic re-sampling algorithm (ITC-ILWIS, 2001).

In each of the re-sampled images of DPC2 scores, pixels pertaining to areas of surficial deposits (see Figure 3.9) were masked out, because surficial deposits (e.g., alluvium) are mostly transported materials and therefore DPC2 scores in these areas do not reflect presence of in-situ altered rocks. Remaining DPC2 scores greater than the 75th percentile in an image were then considered to represent presence of altered rocks. Maps of areas with altered rocks that were derived from each of the individual Landsat TM scenes where then mosaicked to form a seamless map of altered rocks for the whole study area. Figure 6.2 shows the remotely-sensed areas where clay-altered rocks and iron-oxide-altered are probably present.

6.2. Spatial association between remotely-sensed presence of alteration and geothermal occurrences

The presence of altered rocks on the surface does not necessarily mean that a geothermal field is present directly at depths. A plausible reason for this is that the altered rocks on the surface and the geothermal reservoir at depths are linked via an inclined fault system (see Figure 2.2a). Therefore, proximity to outcropping altered rocks is also a consideration in prospecting for geothermal resource. To determine whether or not proximity to remotely-sensed areas with altered rocks is a positive indication of geothermal prospectivity, distance distribution analysis (described in Chapter 4) is performed.

6.2.1. Spatial association between geothermal occurrences and remotely-sensed clay alteration

About 22% of the geothermal occurrences are present within (i.e., zero kilometers from) areas of remotely-sensed clay alteration. There is positive spatial association between areas with remotely-sensed clay alteration and geothermal occurrences in West Java (Figure 6.3). The positive spatial association between areas with remotely-sensed clay alteration and the known geothermal occurrences is optimum at 1 km. About 95% of the known geothermal occurrences are present within the distance of optimum spatial association with areas containing remotely-sensed clay alteration. The “difference “curve indicates that within about 1 km of areas with remotely-sensed clay alteration, there is about 19% higher chance of finding a geothermal occurrence than would expected due to chance. These results indicate that proximity to areas with remotely-sensed clay alteration is a positive indication of geothermal prospectivity.

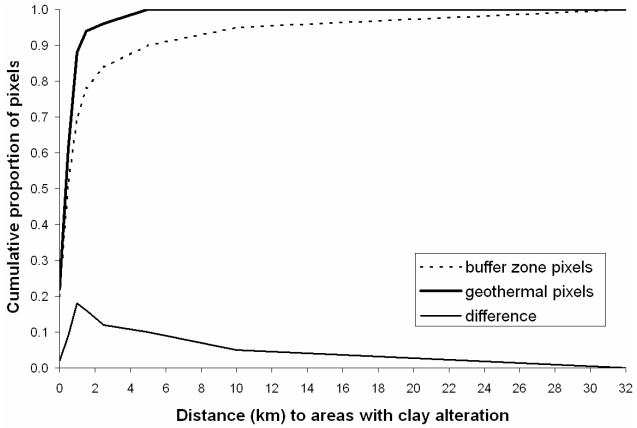

Figure 6.3: Expected cumulative frequency distribution of buffer zone pixels (around areas with remotely-sensed clay alteration) and observed cumulative frequency distribution of geothermal occurrences from areas with remotely-sensed clay alteration.

6.2.2. Spatial association between geothermal occurrences and remotely-sensed iron-oxide alteration

About 12% of the geothermal occurrences are present within (i.e., zero kilometers from) areas of remotely-sensed iron-oxide alteration. Within 1 km of areas of remotely-sensed iron-oxide alteration, the expected cumulative frequency distribution of buffer zone pixels around areas with remotely-sensed iron-oxide alteration is slightly above the observed cumulative frequency distribution of geothermal occurrences (Figure 6.4). This means that there is negative spatial association between the known geothermal occurrences and areas with remotely-sensed iron-oxide alteration. However, the position of two cumulative frequency distribution curves relative to each other changes beyond 1 km. This indicates that beyond 1 km of areas with remotely-sensed iron-oxide alteration there is higher probability of finding a geothermal occurrence than would be expected due to chance. This increased probability of finding a geothermal occurrence away from areas with remotely-sensed iron-oxide alteration is optimum at about 2.5 km. However, even at this regionally short distance of 2.5 km from areas with remotely-sensed iron-oxide alteration, there is only about 9% higher probability of finding a geothermal occurrence than would be expected due to chance. This means that proximity to areas with remotely-sensed iron-oxide alteration is not a positive indication of geothermal prospectivity.

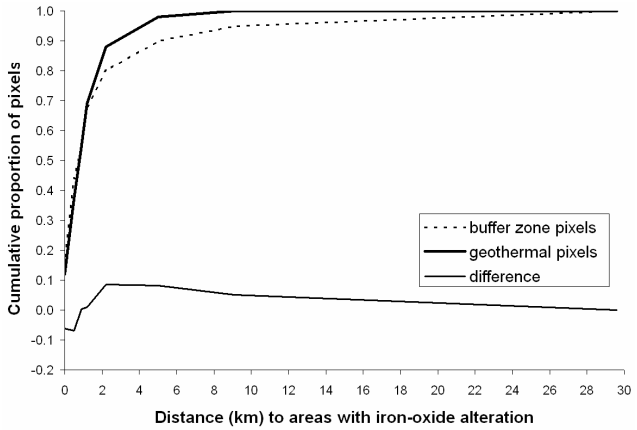

Figure 6.4: Expected cumulative frequency distribution of buffer zone pixels (around areas with iron-oxide alteration) and observed cumulative frequency distribution of geothermal occurrences from areas with iron-oxide alteration.

6.3. Discussion and concluding remarks

The analysis presented here shows that Landsat TM data could provide regional-scale geo-information about altered rocks that could be used for regional-scale mapping of geothermal prospectivity. Because of lack of temporal Landsat TM data, especially at anniversary dates/months, the remote sensing technique proposed by Nash and Hernandez (2001) could not be adopted/adapted here. The method of Nash and Hernandez (2001) involves temporal Landsat TM datasets for change-detection of vegetation characteristics to detect vegetation anomalies associated with to geothermal activities. Nevertheless, the application of software defoliant technique (Fraser and Green, 1987) results in enhancement of presence of clay-altered and iron-oxide-altered rocks in certain areas.

The results of analyses of spatial associations between geothermal occurrences and areas containing altered rocks are consistent with the information summarised in Table 4.2. This consistency is indicated by the higher proportion of geothermal occurrences associated with clay-altered rocks than the proportion of geothermal occurrences associated with iron-oxide-altered rocks. This observation suggests that the remotely-sensed alteration by the software defoliant technique (Fraser and Green, 1987) is fairly reliable. However, it cannot be neglected that there is uncertainty in the remotely-sensed information about areas with clay and/or iron-oxide alteration. It is difficult to quantify this uncertainty here because of lack of ground-truth data. However, in the next chapter, where development of a model of geothermal prospectivity will be described, the integration modelling method based on evidential belief functions will be applied because this method is able to handle datasets that inherently contain uncertainty.

The results of the spatial association analysis indicate that presence of or proximity to (within 1 km of) remotely-sensed clay alteration is a positive indication of geothermal prospectivity. Therefore, this is an additional spatial criterion to the conceptual model of geothermal prospectivity, which now has seven spatial criteria. The respective distances of optimum spatial association found in the distance distribution analyses (Chapters 4 and 5 and in this chapter) could be used to create binary predictor maps, which could be overlaid on top of each other to determine intersections of spatial criteria representing prospective ground (e.g., Carranza et al., 1999). It is considered that intersections of at least four of the seven spatial criteria determine prospectivity of an area for geothermal field occurrence. However, prospectivity modelling based on binary predictor maps is simplistic because spatial criteria are given equal weights or importance with respect to model target (e.g., geothermal occurrence). In this study, a multi-class type of prospectivity modelling, with unequal weighting of spatial criteria based on known geothermal occurrences, will be presented in the next chapter.

Chapter 7: Regional-Scale Predictive Modelling of Geothermal Prospectivity

The objective of this section is to create a regional-scale predictive map of geothermal prospectivity for West Java. From the results of studies presented in Chapters 4 to 6, the following spatial criteria form a conceptual model of regional-scale geothermal prospectivity in the study area:

a) Proximity to Quaternary volcanic centres;
b) Presence of or proximity to Quaternary volcanic rocks;
c) Proximity to mapped faults with NW-WNW and NE trends;
d) Proximity to hot springs;
e) Presence of or proximity to hypothesized volcano-tectonic depression;
f) Proximity to earthquake epicentres; and
g) Presence of or proximity to areas with remotely-sensed clay alteration.

Multi-class proximity maps representing these spatial criteria are created and used in the predictive modelling via application of evidential belief functions (EBFs), which are considered to be adequate for representation and management of uncertainty in exploration data (An et al., 1994).

7.1. Evidential belief functions

The Dempster-Shafer theory of evidence provides framework for estimation of EBFs (Dempster, 1967); Shafer, 1976), which are integrated according to Dempster's (1968) rule of combination. The following discussion, adopted from Carranza et al. (2005), for the application of EBF in this research is simplified and informal, because the theoretical formalization of EBFs is very involved.

Estimation of EBFs for spatial data is always in relation to a proposition, which in this case study is: ***"This location contains a geothermal occurrence based on given spatial evidence"***. The EBFs are ***Bel*** (degree of belief), ***Dis*** (degree of disbelief), ***Unc*** (degree of uncertainty), and ***Pls*** (degree of plausibility) (Figure 7.1). ***Bel*** and ***Pls*** represent, respectively, lower and upper probabilities that evidence supports a proposition (Dempster, 1967). Thus, ***Pls*** is often greater than or sometimes equal to ***Bel***. ***Unc*** is equal to ***Pls–Bel*** and represents ignorance (or doubt) of one's belief in the proposition based on a given evidence. If ***Unc***=0, then ***Bel=Pls***. ***Dis*** is belief that the proposition is false based on given evidence; it is equal to 1–***Pls*** or 1–***Unc–Bel***. Thus, ***Bel+Unc+Dis***=1. However, if ***Bel***=0, then ***Dis***=0 because there can be no disbelief if there is no belief; there can only be uncertainty. Interestingly, if ***Unc***=0, then ***Bel+Dis***=1, as in probability approach. The ***Bel***, ***Unc,*** and ***Dis*** are the EBFs used to integrate evidences according to Dempster's rule of combination (1968).

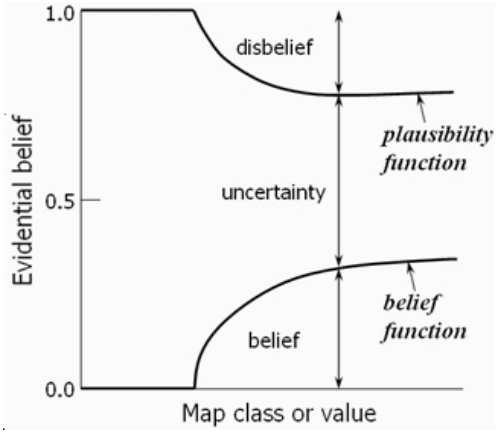

Figure 7.1: Schematic relationships of EBFs (modified after Wright and Bonham-Carter, 1996)

In mineral prospectivity mapping, procedures for data-driven estimation of EBFs proposed by Chung and Fabbri (1993) and An, Moon and Bonham-Carter (1994) are appropriate if locations of both mineralized and unmineralized zones are sufficiently known. In the case when locations of

mineralized zones are fairly known but locations of "truly" unmineralized zones are insufficiently known, Carranza and Hale (2003) proposed similar but different data-driven estimation procedures, which are adapted here for geothermal prospectivity mapping as explained below.

Suppose an exploration area *T* consists of *N(T)* total number of unit cells or pixels and geothermal occurrences *D* in *N(D)* number of pixels. Suppose further that evidence maps X_i (i=1,2,…,n), with C_{ij} (j=1,2,…,m) classes of attributes, have been created for certain spatial criteria. By overlaying binary map of *D* on each evidential map, number of C_{ij} pixels overlapping with pixels containing *D* [i.e., $N(C_{ij} \cap D)$] and number of C_{ij} pixels not overlapping with pixels containing *D* [i.e., $N(C_{ij}) - N(C_{ij} \cap D)$] are determined. The EBFs can then be estimated as follows, based on Carranza and Hale (2003).

$$Bel_{C_{ij}} = \frac{W_{C_{ij}D}}{\sum_{j=1}^{m} W_{C_{ij}D}} \tag{7.1}$$

$$\text{where } W_{C_{ij}D} = \frac{\dfrac{N(C_{ij} \cap D)}{N(C_{ij})}}{\dfrac{N(D) - N(C_{ij} \cap D)}{N(T) - N(C_{ij})}}. \tag{7.1a}$$

The numerator in Equation 7.1a to estimate parameter $W_{C_{ij}D}$ is conditional probability that *D* exists given presence of C_{ij}, which means that *D* occurs more (or is more present) in C_{ij} than would be expected due to chance. The denominator to estimate parameter $W_{C_{ij}D}$ is conditional probability that *D* exists given absence of C_{ij}, which means that *D* occurs more outside (or is more absent in) C_{ij} than would be expected due to chance. The parameter $W_{C_{ij}D}$ is, therefore, weight of C_{ij} in terms of *D* being more present than absent as may be expected due to chance. Thus, the degree of belief for C_{ij}, $Bel_{C_{ij}}$, as defined in Equation 7.1, is relative strength of $W_{C_{ij}D}$ for every j^{th} C_{ij} class of evidence in map X_i.

$$Dis_{C_{ij}} = \frac{W_{C_{ij}\overline{D}}}{\sum_{j=1}^{m} W_{C_{ij}\overline{D}}} \tag{7.2}$$

$$\text{where } W_{C_{ij}\overline{D}} = \frac{\dfrac{N(C_{ij}) - N(C_{ij} \cap D)}{N(C_{ij})}}{\dfrac{N(T) - N(D) - [N(C_{ij}) - N(C_{ij} \cap D)]}{N(T) - N(C_{ij})}}. \tag{7.2a}$$

The numerator in Equation 7.2a to estimate parameter $W_{C_{ij}\overline{D}}$ is conditional probability that *D* does not exist given presence of C_{ij}, which means that *D* occurs less (or is more absent) in C_{ij} than would be expected due to chance. The denominator to estimate parameter $W_{C_{ij}\overline{D}}$ is conditional probability that *D* does not exist given absence of C_{ij}, which means that *D* occurs less outside (or is more present in) C_{ij} than would be expected due to chance. This means that parameter $W_{C_{ij}\overline{D}}$ is weight of C_{ij} in terms of *D* being more absent than present as may be expected due to chance. Thus, the degree of disbelief for C_{ij}, $Dis_{C_{ij}}$, as defined in Equation 2, is relative strength of $W_{C_{ij}\overline{D}}$ for every j^{th} C_{ij} class of evidence in map X_i.

Equations 7.1 and 7.2 for data-driven estimation of ***Bel*** and ***Dis***, respectively, were developed and demonstrated by Carranza and Hale (2003) based on recommendations by (Chung and Fabbri, 1993) to take into account not only (a) spatial association between an evidential map layer and target geothermal occurrences but also (b) spatial relationships between classes of evidences in an evidential map layer. Note that, if for C_{ij} estimated $W_{C_{ij}D} = 0$, which means that $Bel_{C_{ij}} = 0$, then the corresponding estimated $W_{C_{ij}\overline{D}}$ should be re-set to zero, even if it is not, so that the corresponding $Dis_{C_{ij}} = 0$ according to Figure 4.5. ***Unc*** and ***Pls*** can then be estimated, respectively, as:

$$Unc_{C_{ij}} = 1 - Bel_{C_{ij}} - Dis_{C_{ij}} \tag{7.3}$$

$$Pls_{C_{ij}} = Bel_{C_{ij}} + Unc_{C_{ij}} \text{ or } Pls_{C_{ij}} = 1 - Dis_{C_{ij}} \tag{7.4}$$

Estimates of EBFs are usually held in attribute tables associated with spatial evidence maps X_i maps so that attribute maps of EBFs for X_i can be readily created. Maps of EBFs for X_1 can then be combined with maps of EBFs for X_2 according to Dempster's (1968) rule of combination in order to generate an integrated map of EBFs. The formulas for combining maps of EBFs of two evidential maps (X_1 and X_2) are the following (adopted from Wright and Bonham-Carter, 1996):

$$Bel_{X_1X_2} = \frac{Bel_{X_1}Bel_{X_2} + Bel_{X_1}Unc_{X_2} + Bel_{X_2}Unc_{X_1}}{\beta} \tag{7.5}$$

$$Dis_{X_1X_2} = \frac{Dis_{X_1}Dis_{X_2} + Dis_{X_1}Unc_{X_2} + Dis_{X_2}Unc_{X_1}}{\beta} \tag{7.6}$$

$$Unc_{X_1X_2} = \frac{Unc_{X_1}Unc_{X2}}{\beta} \tag{7.7}$$

where $\beta = 1 - Bel_{X_1}Dis_{X_2} - Dis_{X_1}Bel_{X_2}$ is a normalizing factor to ensure that $Bel + Unc + Dis = 1$. $Pls_{X_1X_2}$ is estimated according to Equation 4. Only maps of EBFs of two spatial evidences can be combined each time; maps of EBFs representing $X_3, \ldots, X_n$ are combined one after another by repeated applications of Equations 5 to 7. Note however that the formulas for combining EBFs of two spatial evidences are commutative and associative, which means that different groups or orders of evidence combinations do not affect the final result. Final combination of maps of EBFs results in integrated ***Bel***, ***Dis***, ***Unc*** and ***Pls*** for the proposition based on given spatial evidences.

7.2. Estimation of EBFs of geothermal prospectivity

To estimate EBFs of geothermal prospectivity, a pixel (or unit cell) size of 500×500 m is used, which is the same pixel used in the distance distribution analysis (sub-section 4.2.1.2). This pixel size is used because it represents each geothermal field occurrence as one, and only one, pixel. The pixel size used also means that regional-scale prospectivity for geothermal field occurrence is estimated for every 500×500 m cell in the study area, given several sets of evidential maps.

Estimates of EBFs, particularly *Bel* values, reflect spatial associations between indicative geological features and target spatial objects, e.g., geothermal occurrences (Carranza, 2002; Carranza and Hale, 2003). Therefore, results of EBF estimations are compared with results of distance distribution analyses presented in the preceding chapters. However, within a map layer of indicative geological features, estimates of EBFs also represent weights of relative importance of individual map classes in support or lack of support for the proposition of geothermal occurrence.

7.2.1. Preparation of evidential maps

An evidential map for each set of indicative geological features, according to the formulated conceptual model of geothermal prospectivity, was prepared in a 2-step procedure. First, a map of distances to indicative geological features was created. Second, a map of proximity to indicative geological features was created by partitioning values in a distance map into a number of proximity classes using 10-percentile intervals. Some of the distance maps do not result into 10 proximity

classes because the geological features (e.g., zero distances from volcanic rocks) represent more than 10 percentile of the area. For each proximity map i, $N(C_{ij})$ (i.e., number of pixels in each j=1,2,…,m proximity classes) and $N(T)$ (i.e., total number of pixels) are determined. The other parameters needed to estimate the EBFs (see Equations 7.1a and 7.2a) are then determined by overlaying map of training data with a map of proximity to indicative geological features.

7.2.2. Preparation of map of training geothermal field occurrences

The set of 53 known occurrences of geothermal fields was split into two sub-sets by random selection from the whole data set. One sub-set consists about 75% (or 40) of the 53 known geothermal occurrences, whereas the other sub-set consists about 25% (or 13) of the 53 known geothermal occurrences (e.g., Carranza et al., 2005). The map of each sub-set of geothermal field occurrences was rasterized using a 500×500 m pixel size. The map of 40 geothermal occurrences was used as training data for estimation of EBFs. The map of 13 geothermal occurrences was later used to validate the model of geothermal prospectivity.

7.2.3. Estimated EBFs of evidential maps

In the descriptions of results below, references are made only to *Bel* (degrees of belief), *Dis* (degrees of disbelief), and *Unc* (degrees of uncertainty). The reason for is that these three EBFs are the ones used in Dempster's (1968) rule of combination and also because *Pls* (degrees of plausibility) can be estimated easily from any two of these three EBFs. The results of EBF estimations are also compared with the results of distance distribution analysis, because the EBFs, most particularly *Bel*, reflect spatial association between indicative features and target variables (Carranza, 2002; Carranza and Hale, 2003; Carranza et al., 2005). However, estimated EBFs also reflect relative importance or weight of each class in an evidential map layer with respect to the target variable (which in this case is geothermal occurrences).

7.2.3.1. Estimated EBFs of proximity to Quaternary volcanic centres

Table 7.1 shows that within 8.1 km of Quaternary volcanic centres, the degrees of belief are higher and the degrees of uncertainty are lower than beyond 8.1 km of Quaternary volcanic centres. The results here are similar to the results of distance distribution analysis, which showed 10 km as distance of optimum positive spatial association between Quaternary volcanic centres and the 53 geothermal occurrences (Figure 4.7). The results also show that within 8.1 km of Quaternary volcano centres the degrees of belief are greater than the degrees of disbelief. The results therefore indicate that zones within 8.1 km of Quaternary volcanic centres support the proposition of geothermal occurrence. Geologically, the results suggest that heat sources of the Quaternary volcanoes and the geothermal occurrences are the same.

Table 7.1: Estimated EBFs of proximity to Quaternary volcanic centres, West Java. [$N(T)$=187474], [$N(D)$=40].

Proximity to Quaternary volcanic centres (km)	$N(C_{ij})$	$N(C_{ij} \cap D)$	*Bel*	*Dis*	*Unc*
0.0 – 8.1	18653	21	0.6808	0.1249	0.1943
8.1 – 12.7	18502	5	0.0888	0.1250	0.7862
12.7 – 17.7	19084	1	0.0154	0.1250	0.8596
17.7 – 22.8	18543	2	0.0326	0.1250	0.8424
22.8 – 28.0	18799	1	0.0157	0.1250	0.8593
28.0 – 33.3	18953	4	0.0672	0.1250	0.8078
33.6 – 40.3	18781	3	0.0496	0.1250	0.8254
40.3 – 49.0	18678	3	0.0499	0.1250	0.8251
49.0 – 60.4	18788	0	0.0000	0.0000	1.0000
60.4 – 100.0	18836	0	0.0000	0.0000	1.0000

7.2.3.2. Estimated EBFs of presence of or proximity to Quaternary volcanic rocks

Within and up to 3 km away from Quaternary volcanic rocks, the degrees of belief are higher and the degrees of uncertainty are lower than beyond 3 km away from Quaternary volcanic rocks (Table 7.2). These results are similar to the results of distance distribution analysis, which showed 3 km as distance of optimum positive spatial association between the Quaternary volcanic centres and the 53 geothermal occurrences (Figure 4.8). The results also show that within and up to 3 km away from Quaternary volcanic rocks the degrees of belief are greater than the degrees of disbelief. The results therefore indicate that zones within and up to 3 km away from Quaternary volcanic rocks support the proposition of geothermal occurrence. These results could mean that Quaternary volcanic rocks are important controls for the occurrence of geothermal fields, because they serve as cap rocks for trapping the heat beneath the ground.

Table 7.2: Estimated EBFs of presence of or proximity to Quaternary volcanic rocks, West Java. [$N(T)$=187474], [$N(D)$=40].

Proximity to Quaternary volcanic rocks (km)	$N(C_{ij})$	$N(C_{ij} \bigcap D)$	*Bel*	*Dis*	*Unc*
0.0	71114	23	0.3547	0.1666	0.4787
0.0 – 1.3	22015	7	0.2553	0.1666	0.5781
1.3 – 3.0	19001	5	0.2029	0.1666	0.6305
3.0 – 5.8	19152	2	0.0741	0.1667	0.7592
5.8 – 10.8	18606	2	0.0765	0.1667	0.7568
10.8 – 20.7	18969	1	0.0365	0.1667	0.7968
20.7 – 61.2	18760	0	0.0000	0.0000	1.0000

7.2.3.3. Estimated EBFs of proximity to mapped NE- and WNW-NW-trending faults

Within 3.8 km of mapped NE- and WNW-NW-trending faults, the degrees of belief and degrees of uncertainty are higher and lower, respectively, than beyond 3.8 km of mapped NE- and WNW-NW-trending faults (Table 7.3). These results are consistent with the results of distance distribution analysis (Figure 4.9), which showed about 5 km as distance of optimum positive spatial association of geothermal occurrences with mapped NE- and WNW-NW-trending faults. The results also show that within 3.8 km of mapped NE- and WNW-NW-trending faults the degrees of belief are mostly greater than the degrees of disbelief. The results therefore show that mapped NE- and WNW-NW-trending faults support the proposition of geothermal occurrence. Geologically, the results could mean that NE- and WNW-NW-trending fault systems control occurrence of geothermal fields, although the results also suggest that geothermal fields do not spatially coincide with the mapped NE- and WNW-NW-trending faults but probably along faults/fractures that are subsidiary to (and located within 3.8 km of) the mapped NE- and WNW-NW-trending faults.

Table 7.3: Estimated EBFs of proximity to mapped NE- and WNW-NW-trending faults, West Java. [$N(T)$=187474], [$N(D)$=40].

Proximity to mapped faults (km)	$N(C_{ij})$	$N(C_{ij} \bigcap D)$	*Bel*	*Dis*	*Unc*
0.0 – 0.9	16791	4	0.1020	0.1000	0.7980
0.9 – 1.8	16536	10	0.3112	0.1000	0.5888
1.8 – 2.8	22146	5	0.0963	0.1000	0.8037
2.8 – 3.8	16331	7	0.2008	0.1000	0.6992
3.8 – 5.2	21571	4	0.0772	0.1000	0.8228
5.2 – 6.5	18384	1	0.0213	0.1000	0.8787
6.5 – 8.4	19498	3	0.0631	0.1000	0.8369
8.4 – 10.9	18675	2	0.0430	0.1000	0.8570
10.9 – 16.4	18808	2	0.0426	0.1000	0.8574
16.4 – 47.7	18877	2	0.0425	0.1000	0.8575

7.2.3.4. Estimated EBFs of proximity to hot springs

Table 7.4 shows that within 9 km of hot springs, the degrees of belief are much higher and the degrees of uncertainty are much lower than beyond 9 km of hot springs. The results here are similar to the results of the distance distribution analysis, which showed about 6 km as distance of positive optimum spatial association between hot springs and 53 geothermal occurrences (Figure 4.11). The

results here also show that within 9 km of hot springs the degrees of belief are greater than the degrees of disbelief. The results therefore indicate that proximity to hot springs supports the proposition of geothermal occurrence, because such geological features are surface manifestations of geothermal fields at depths.

Table 7.4: Estimated EBFs of proximity to hot springs, West Java. [$N(T)$=187474], [$N(D)$=40].

Proximity to hot springs (km)	$N(C_{ij})$	$N(C_{ij} \bigcap D)$	*Bel*	*Dis*	*Unc*
0.0 – 4.4	18440	12	0.3215	0.1249	0.5536
4.4 – 6.8	19029	14	0.3900	0.1249	0.4851
6.8 – 9.0	18300	6	0.1335	0.1250	0.7415
9.0 – 11.2	18719	3	0.0598	0.1250	0.8152
11.2 – 13.6	19054	0	0.0000	0.0000	1.0000
13.6 – 16.3	18620	1	0.0190	0.1250	0.8560
16.3 – 19.4	18892	1	0.0187	0.1250	0.8563
19.4 – 24.0	18972	1	0.0186	0.1250	0.8564
24.0 – 32.3	18715	2	0.0388	0.1250	0.8362
32.3 – 69.3	18876	0	0.0000	0.0000	1.0000

7.2.3.5. Estimated EBFs of presence of or proximity to volcano-tectonic depression

Within and up to 6.6 km away from the hypothesized volcano-tectonic depression, the degrees of belief are higher and the degrees of uncertainty are lower than beyond 6.6 km away from the hypothesized volcano-tectonic depression (Table 7.2). These results are consistent with the results of distance distribution analysis, which showed 6.6 km as distance of optimum positive spatial association between the hypothesized volcano-tectonic depression and the 53 geothermal occurrences (Figure 5.9). The results here also show that within and up to 6.6 km away from the hypothesized volcano-tectonic depression the degrees of belief are greater than the degrees of disbelief. The results therefore show that zones within and up to 6.6 km away from the hypothesized volcano-tectonic depression support the proposition of geothermal occurrence. Geologically, the results suggest that the Cenozoic sediments that filled the hypothesized volcano-tectonic depression, which were later overlain by Quaternary volcanic rocks, are probable reservoir rocks of geothermal fields in the study area.

Table 7.5: Estimated EBFs of presence of or proximity to hypothesized volcano-tectonic depression, West Java. [$N(T)$=187474], [$N(D)$=40].

Proximity to boundaries of volcano-tectonic depression (km)	$N(C_{ij})$	$N(C_{ij} \bigcap D)$	*Bel*	*Dis*	*Unc*
0.0	110618	28	0.3532	0.2000	0.4468
0.0 – 6.6	19831	7	0.3903	0.2000	0.4097
6.6 – 14.5	19612	1	0.0478	0.2000	0.7522
14.5 – 24.0	18779	1	0.0501	0.2000	0.7499
24.0 – 51.8	18777	3	0.1586	0.2000	0.6414

7.2.3.6. Estimated EBFs of proximity to earthquake epicenters

Within 4 km of earthquake epicentres, there is very low degree of belief and very high degree of uncertainty within 4 km of earthquake epicentres (Table 7.6). Within 4-15.9 km of earthquake epicentres, the degrees of belief and degrees of uncertainty are mostly higher and lower, respectively, than beyond 15.9 km of earthquake epicentres. These results here are similar to the results of distance distribution analysis (Figure 5.11), which showed that (a) within 4 km of earthquake epicentres there is a slight negative spatial association with geothermal occurrences and (b) distance of optimum positive spatial association of earthquake epicentres with geothermal occurrences is 16 km. The results here also show that within 4-15.9 km of earthquake epicentres the degrees of belief are mostly greater than the degrees of disbelief. The results here therefore show that zones within 4-15.9 km of earthquake epicentres support the proposition of geothermal occurrence. These results are consistent with observations of Major and McEvilly (1979) that earthquakes tend to occur at edges of, but not within, geothermal production zones.

Table 7.6: Estimated EBFs of proximity to earthquake epicentres, West Java. [$N(T)$=187474], [$N(D)$=40].

Proximity to earthquake epicentres (km)	$N(C_{ij})$	$N(C_{ij} \bigcap D)$	*Bel*	*Dis*	*Unc*
0.0 – 4.0	18060	3	0.0728	0.1250	0.8022
4.0– 6.2	19379	6	0.1466	0.1250	0.7284
6.2 – 9.3	18333	7	0.1874	0.1250	0.6876
9.3 – 10.4	18554	5	0.1246	0.1250	0.7504
10.4 – 12.9	19218	3	0.0680	0.1250	0.8070
12.9 – 15.9	18783	7	0.1825	0.1250	0.6925
15.9 – 19.7	18726	4	0.0959	0.1250	0.7791
19.7 – 24.7	18901	0	0.0000	0.0000	1.0000
24.7 – 35.1	18879	5	0.1222	0.1250	0.7528
35.1 – 75.0	18784	0	0.0000	0.0000	1.0000

7.2.3.7. Estimated EBFs of presence of or proximity to remotely-sensed clay alteration

Within areas with remotely-sensed clay alteration the degree of belief is less than the degree of disbelief. Outside but only up to 1.8 km of areas with remotely-sensed clay alteration the degrees of belief are mostly greater than the degrees of disbelief (Table 7.7). The results of distance distribution analysis, on the other hand, showed that within 1 km of areas with remotely-sensed clay alteration there is optimum positive spatial association with geothermal occurrences (Figure 6.3). So, the results here and the results of the distance distribution analysis are quite similar because within about 1 km of areas with remotely-sensed clay alteration the degrees of belief are highest and the degrees of uncertainty are lowest. Nevertheless, the results here suggest that presence of or proximity to areas with remotely-sensed clay alteration does not strongly support the proposition of geothermal occurrence. Practically, the results could mean that the remotely-sensed clay alteration could be related either to hydrothermal alteration associated with geothermal systems or to chemical weathering of lithologies not spatially or genetically related with geothermal systems.

Table 7.7: Estimated EBFs of presence of or proximity to areas with remotely-sensed clay alteration, West Java. [$N(T)$=187474], [$N(D)$=40].

Proximity to clay alteration (km)	$N(C_{ij})$	$N(C_{ij} \bigcap D)$	*Bel*	*Dis*	*Unc*
0.0	35817	6	0.1284	0.2000	0.6716
0.0 – 0.5	60334	14	0.1951	0.2000	0.6049
0.5 – 1.0	32698	11	0.3086	0.2000	0.4914
1.0 – 1.8	20122	5	0.2042	0.2000	0.5958
1.8 – 5.2	19600	4	0.1636	0.2000	0.6364
5.2 – 31.9	19046	0	0.0000	0.0000	1.0000

7.3. Integration of EBFs of geothermal prospectivity

The EBFs were estimated and are held in attribute tables of evidential maps. In order to integrate the EBFs of proximity classes in evidential maps representing spatial criteria of geothermal prospectivity, attribute maps of *Bel*, *Dis,* and *Unc* for each evidential layer were first created. Maps of integrated *Bel*, integrated *Dis*, and integrated *Unc* were then derived by application of Equations 7.5 to 7.7. A map of integrated *Pls* was created using Equation 7.4. Maps of integrated EBFs of multi-class evidential layers are displayed in grey-scale.

Three sets of maps of integrated EBFs were created. One set of maps of integrated EBFs was created for all the seven evidential layers. A second set of maps of integrated EBFs was created using all except the evidential layer of presence of or proximity to hypothesized volcano-tectonic depression. A third set of maps of integrated EBFs was created using all except the evidential layer of presence of or proximity to remotely-sensed clay alteration. The reason for creating the first set of maps of EBFs is to determine usefulness of integrating all relevant evidential data/information in geothermal prospectivity mapping. The reason for creating the second and third sets of maps of EBFs is to determine usefulness of derivative but relevant evidential information (e.g., hypothesized volcano-tectonic depression or remotely-sensed clay alteration) in geothermal prospectivity mapping.

7.3.1. Integrated EBFs of all evidential layers

The grey-scale maps of integrated EBFs of all multi-class evidential layers are displayed in Figure 7.2. There are several circular patterns with very high degrees of belief (Figure 7.2a) and very high degrees of plausibility (Figure 7.2d). These circular patterns have low degrees of disbelief (Figure 7.2b) and low degrees of uncertainty (Figure 7.2c). Other circular patterns with intermediate degrees of belief (Figure 7.2a) have corresponding intermediate degrees of disbelief and intermediate degrees of uncertainty. The circular patterns with intermediate to very high degrees of belief are related with proximity to Quaternary volcanic centres (see Figure 4.2) and with proximity to hot springs (see Figure 4.4), but they are not related proximity to earthquake epicentres (see Figure 3.8). Because most of the training geothermal occurrences fall within circular patterns with intermediate to very high degrees of belief, the maps of integrated EBFs suggest that proximity to Quaternary volcanic centres and proximity hot springs strongly support the proposition of geothermal prospectivity, whereas proximity to earthquake epicentres weakly support the proposition of geothermal prospectivity.

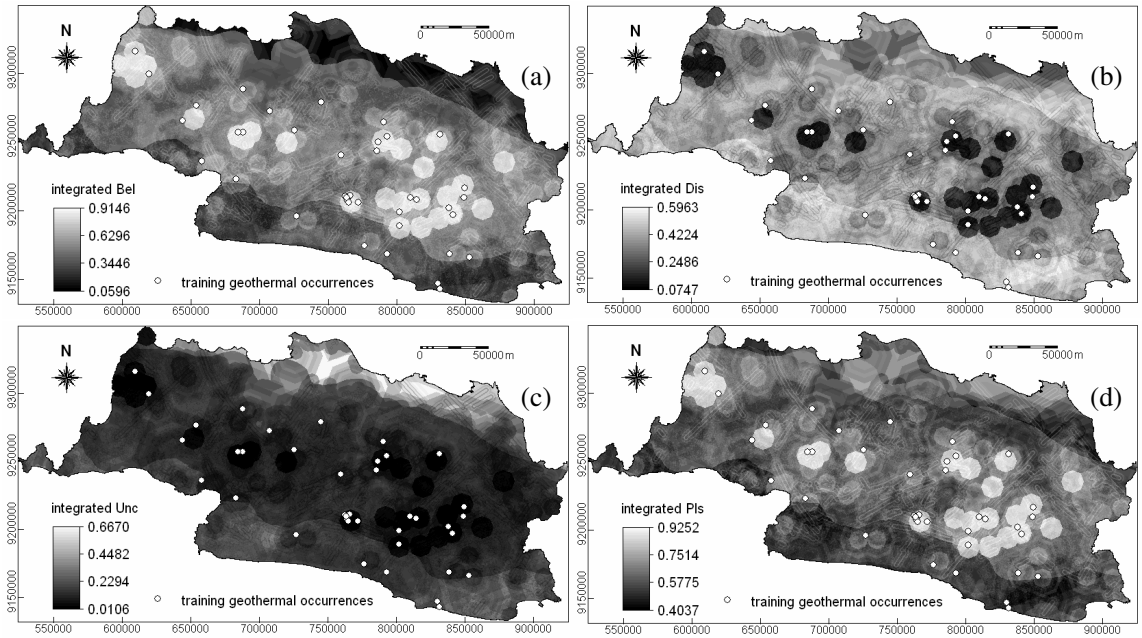

Figure 7.2: Maps of integrated EBFs inclusive of all seven evidential layers, West Java: (a) integrated *Bel*, (b) integrated *Dis*, (c) integrated *Unc*, and (d) integrated *Pls*.

There is a WNW trending zone along the length of West Java, which is characterised mainly by intermediate degrees of belief, intermediate degrees of disbelief, low degrees of uncertainty, and intermediate degrees of plausibility (Figure 7.2). This WNW trending zone reflects the hypothesized volcano-tectonic depression. All of the circular patterns with intermediate to very high degrees of belief lie within this WNW trending zone. These observations imply that presence of or proximity to the hypothesized volcano-tectonic depression moderately supports the proposition of geothermal prospectivity.

Within the WNW trending zone mentioned above, there are linear patterns with mostly intermediate degrees of belief and with low degrees of uncertainty that either intersect or do not intersect with the circular patterns mentioned above. These linear patterns reflect proximity to mapped NE- and WNW-NW-trending faults. Many of the training geothermal occurrences fall within circular patterns that are intersected by linear patterns and many training geothermal occurrences lie on or close to but also away from the linear patterns. These observations suggest that proximity to mapped NE- and WNW-NW-trending faults moderately support the proposition of geothermal prospectivity.

The maps of integrated EBFs vaguely reflect patterns of the Quaternary volcanic rocks. However, in the southern parts of the study area between 700000E and 810000E there are zones of low to intermediate degrees of belief (Figure 7.2a), which are underlain by Quaternary volcanic rocks (see

Figure 4.2). These observations suggest that presence of or proximity to Quaternary volcanic rocks weakly to moderately support the proposition of prospectivity mapping.

The maps of integrated EBFs do not show obvious patterns that reflect areas with remotely-sensed clay alteration. This observation suggests that presence of or proximity to remotely-sensed clay alteration weakly support the proposition of geothermal prospectivity.

The remarks given above about the different evidential layers' relative degree of support to the proposition of geothermal prospectivity will be further evaluated later based on the classified prospectivity maps.

7.3.2. Integrated EBFs exclusive of remotely-sensed clay alteration evidential layer

The maps of integrated EBFs using all except the remotely-sensed clay alteration evidential layer (Figure 7.3) display very similar characteristics with the maps of integrated EBFs inclusive of all evidential layers. Therefore, the same remarks can be given about the relative degree of support to the proposition of geothermal prospectivity provided by the different evidential layers except the remotely-sensed clay alteration evidential layer. However, by removing the remotely-sensed clay alteration evidential layer, the maximum degree of belief in Figure 7.3a is only slightly lower than the maximum degree of belief in Figure 7.2a but there is no difference between the maximum degrees in Figures 7.3c and 7.2c. This observation further suggests that presence of or proximity to remotely-sensed clay alteration weakly supports the proposition of geothermal prospectivity, because removing it from the integrated evidential layers does not result in drastic changes in the integrated EBFs. This remark about the quality of the remotely-sensed clay alteration evidential layer will be further evaluated later based on the classified prospectivity maps. Likewise, because of the strong similarities between the maps of integrated EBFs shown in Figures 7.2 and 7.3, the remarks given above about the relative degree of support to the proposition of geothermal prospectivity provided by the other evidential layers will be further evaluated later based on the classified prospectivity maps.

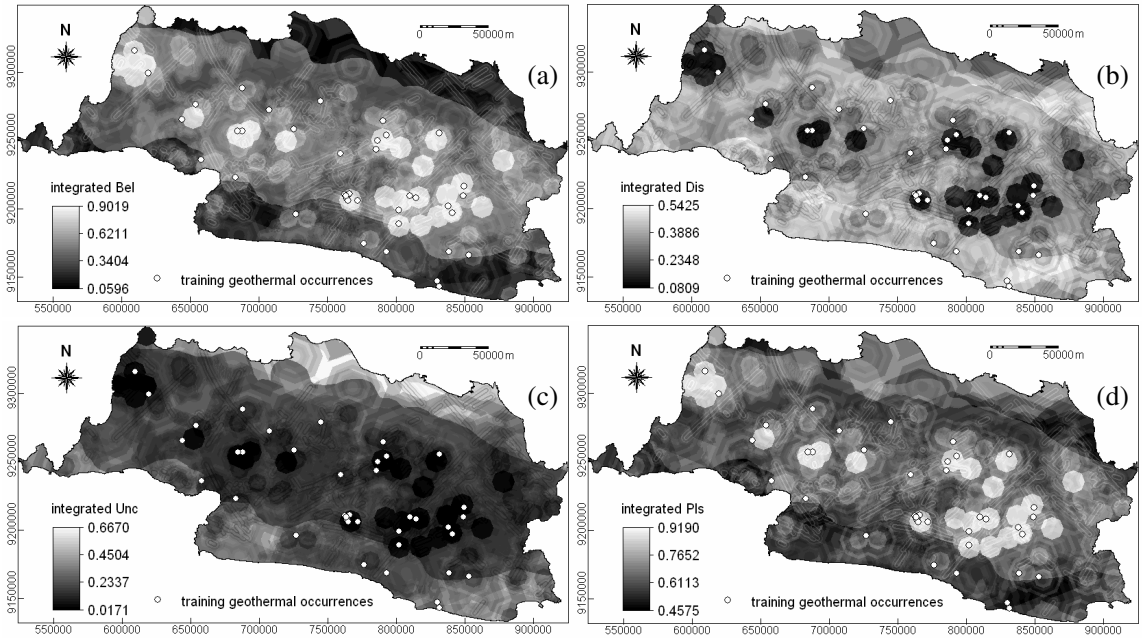

Figure 7.3: Maps of integrated EBFs using six evidential layers (i.e., exclusive of remotely-sensed clay alteration evidential layer), West Java: (a) integrated *Bel*, (b) integrated *Dis*, (c) integrated *Unc*, and (d) integrated *Pls*.

7.3.3. Integrated EBFs exclusive of hypothesized volcano-tectonic depression evidential layer

The maps of integrated EBFs integrated EBFs using all except the hypothesized volcano-tectonic depression evidential layer (Figure 7.4) are also show several similarities with the maps of integrated EBFs using all evidential layers (Figure 7.2). Therefore, the same remarks can be made about the relative degree of support to the proposition of geothermal prospectivity provided by the different evidential layers except the hypothesized volcano-tectonic depression evidential layer. However, a clear difference between the maps of integrated EBFs shown in Figures 7.2 and 7.4 is that the maps of integrated EBFs shown in Figure 7.4 do not shows patterns reflecting the hypothesized volcano-tectonic depression. By removing the hypothesized volcano-tectonic depression evidential layer, the maximum degree of belief in Figure 7.4a is clearly lower than the maximum degree of belief in Figure 7.2a and the maximum degree of uncertainty in Figure 7.4c is clearly much higher that the maximum degree of uncertainty in Figure 7.2c. These observations suggest that the hypothesized volcano-tectonic depression evidential layer provides moderate to strong support for the proposition of geothermal prospectivity because removing it from the integrated evidential layers results in drastic decrease in integrated degrees of belief and drastic increase in integrated degrees of uncertainty. This remark about the quality of the hypothesized volcano-tectonic depression evidential will be further evaluated later based on the classified prospectivity maps. Likewise, because of the several similarities between the maps of integrated EBFs shown in Figures 7.2 and 7.4, the remarks given above about the relative degree of support to the proposition of geothermal prospectivity provided by the other evidential layers will be further evaluated later based on the classified prospectivity maps.

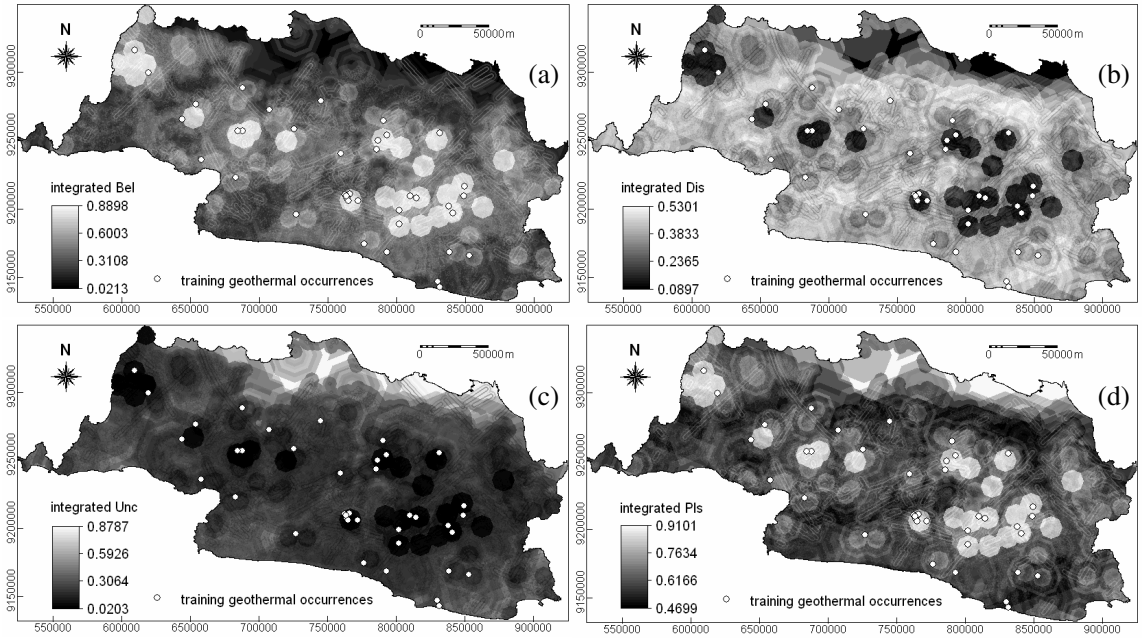

Figure 7.4: Maps of integrated EBFs using six evidential layers (i.e., exclusive of hypothesized volcano-tectonic depression evidential layer), West Java: (a) integrated *Bel*, (b) integrated *Dis*, (c) integrated *Unc*, and (d) integrated *Pls*.

7.4. Classification and validation of predictive models of geothermal prospectivity

As can be seen from Figures 7.2 to 7.4, integrated degrees of belief and integrated degrees of plausibility reflect spatial association with the geothermal occurrences. However, integrated degrees of plausibility include integrated degrees of uncertainty. Maps of integrated degrees of belief are therefore used to classify geothermal prospectivity.

Degree of geothermal prospectivity was categorised into five classes by using 20-percentile intervals of the degrees of belief. The 0-20 percentile range of integrated degrees of belief is considered to represent very low prospectivity. The 20-40 percentile range of integrated degrees of belief is considered to represent low prospectivity. The 40-60 percentile range of integrated degrees of belief is considered to represent intermediate or moderate prospectivity. The 60-80 percentile range of integrated degrees of belief is considered to represent high prospectivity. The 80-100 percentile range of integrated degrees of belief is considered to represent very high prospectivity. This scheme of classifying degree of geothermal prospectivity was uniformly applied to the three sets of maps of integrated degrees of belief (Figures 7.2a, 7.3a, and 7.4a). The reason for this is that the three different geothermal prospectivity maps can also be validated in a uniform way and therefore can be compared properly.

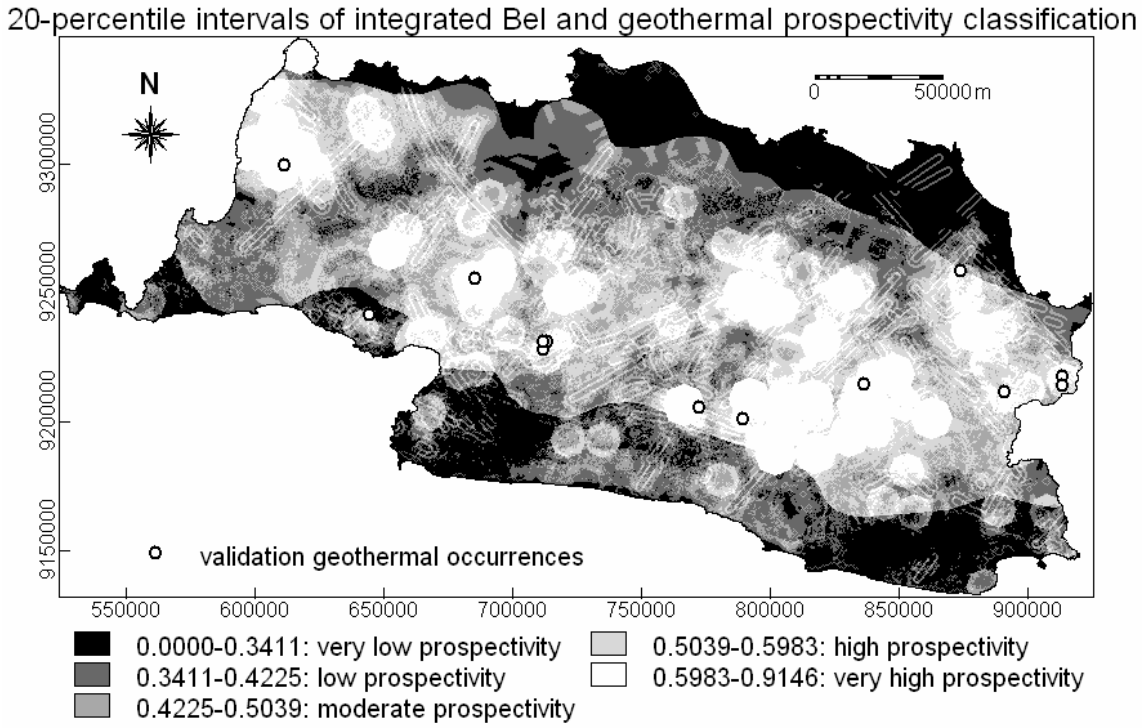

Figure 7.5: Geothermal prospectivity map based on integrated *Bel* using all seven evidential layers.

The classified geothermal prospectivity map based of all evidential layers (Figures 7.5) and the classified geothermal prospectivity map exclusive of the remotely-sensed clay alteration evidential layer (Figure 7.6) are very similar. They both show circular zones with very high prospectivity reflecting proximity to Quaternary volcanic centres and circular zones with moderate to very high prospectivity reflecting proximity to hot springs. This observation indicates that proximity to Quaternary volcanic centres and proximity to hot springs provide strong support to the proposition of geothermal prospectivity. The classified geothermal prospectivity maps in Figures 7.5 and 7.6 also show that zones with moderate to very high prospectivity are located within the area occupied by the hypothesized volcano-tectonic depression. This observation indicates that presence of or proximity to the hypothesized volcano-tectonic depression provides moderate to strong support to the proposition of geothermal prospectivity. Another similarity between Figures 7.5 and 7.6 is that they both show NE- and WNW-NW-trending linear patterns with moderate to high prospectivity, except where the linear patterns intersect with circular patterns due to proximity to Quaternary volcanic centres and to hot springs. This indicates that proximity to mapped NE- and WNW-NW-trending faults provides moderate support for the proposition of geothermal prospectivity. Another similarity between Figures 7.5 and 7.6 is that patterns with low to high prospectivity, which reflect presence of or proximity Quaternary volcanic rocks, are obvious mainly in the southern portions of the study area between

700000E and 810000E. This indicates that presence of or proximity to Quaternary volcanic rocks provides weak to moderate support to the proposition of geothermal prospectivity. Another similarity between Figures 7.5 and 7.6 is that they both do not show patterns of any degree of prospectivity that reflect proximity to earthquake epicentres. This indicates that proximity to earthquake epicentres provides weak support to the proposition of geothermal prospectivity. The main difference between the geothermal prospectivity maps shown in Figures 7.5 and 7.6 is that the geothermal prospectivity map shown in Figure 7.6 does not exhibit "fine-texture" patterns, which reflect the patterns of the remotely-sensed clay alteration. Because of the high degree of similarity between the classified geothermal prospectivity maps shown in Figures 7.5 and 7.6, except that "fine-texture" patterns reflecting presence of or proximity to remotely-sensed clay alteration are absent in Figure 7.6, it can be interpreted that the presence of or proximity to remotely-sensed clay alteration provides weak support to the proposition of geothermal prospectivity. This final remark about the quality of presence of or proximity to remotely-sensed clay alteration as evidential layer for geothermal prospectivity will be further evaluated based on results of validation of the prospectivity maps.

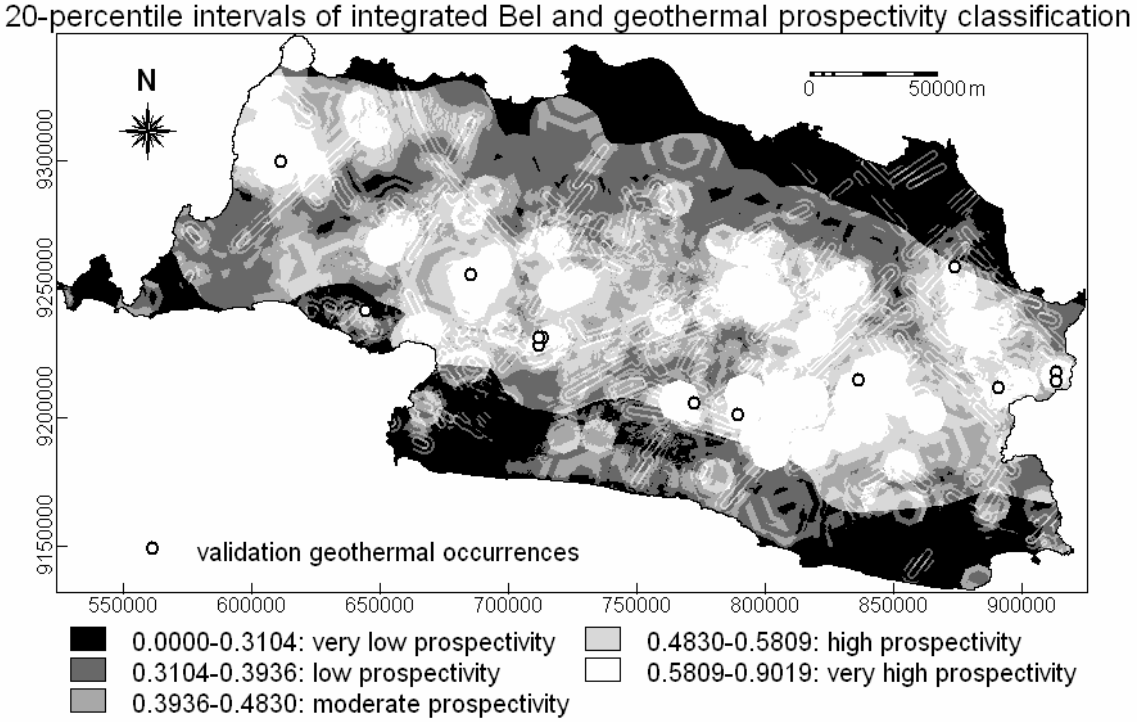

Figure 7.6: Geothermal prospectivity map based on integrated *Bel* using six evidential layers (i.e., exclusive of remotely-sensed clay alteration evidential layer).

The classified geothermal prospectivity map inclusive of all evidential layers (Figures 7.5) and the classified geothermal prospectivity map exclusive of the remotely-sensed clay alteration evidential layer (Figure 7.7) also show several similarities. They both show circular zones with very high prospectivity reflecting proximity to Quaternary volcanic centres and circular zones with moderate to very high prospectivity reflecting proximity to hot springs. This indicates that proximity to Quaternary volcanic centres and proximity to hot springs provide strong support to the proposition of geothermal prospectivity. Another similarity between Figures 7.5 and 7.7 is that they both show NE- and WNW-NW-trending linear patterns with moderate to high prospectivity, except where the linear patterns intersect with circular patterns due to proximity to Quaternary volcanic centres and to hot springs. This indicates that proximity to mapped NE- and WNW-NW-trending faults provide moderate support to the proposition of geothermal prospectivity. Another similarity between Figures 7.5 and 7.7 is that they both do not show patterns of any degree of prospectivity that reflect proximity to earthquake epicentres. This indicates that proximity to earthquake epicentres provides weak support to the

proposition of geothermal prospectivity. Another similarity between Figures 7.5 and 7.7 is that they both show "fine texture" patterns, which reflect presence of or proximity to remotely-sensed clay alteration, having mostly low to moderate prospectivity. This indicates that presence of or proximity to remotely-sensed clay alteration provides weak support to the proposition of geothermal prospectivity. A clear difference between Figures 7.5 and 7.7 is that Figure 7.7 shows patterns with mainly moderate prospectivity, which reflects presence of or proximity to Quaternary volcanic rocks. This indicates that presence of or proximity to Quaternary volcanic rocks provides moderate support to the proposition of geothermal prospectivity. Another clear difference between Figures 7.5 and 7.7 is that Figure 7.7 does not exhibit an E-W trending zone, which reflects the pattern of the hypothesized volcano-tectonic depression. Exclusion of the evidential layer of volcano-tectonic depression results in obvious change in the distribution of high prospective zones. This indicates that presence of or proximity to the hypothesized volcano-tectonic depression provides moderate to strong support to the proposition of geothermal prospectivity. This final remark about the quality of presence of or proximity to the hypothesized volcano-tectonic depression as evidential layer for geothermal prospectivity will be further evaluated based on results of validation of the prospectivity maps.

The classified geothermal prospectivity map exclusive of the remotely-sensed clay alteration evidential layer (Figures 7.6) and the classified geothermal prospectivity map exclusive of the hypothesized volcano-tectonic depression evidential layer (Figure 7.7) are also similar and different in the same ways as integrated EBFs (between Figure 7.3 and 7.4). Therefore, the same remarks can be given about the quality of the different evidential layers for geothermal prospectivity mapping. However, because only two evidential layers were excluded in the analysis, the results of validation of the three different prospectivity maps will be used as a final reference to remark further about the quality of presence of or proximity to the hypothesized volcano-tectonic depression evidential layer and the quality of presence of or proximity to remotely-sensed clay alteration evidential layer.

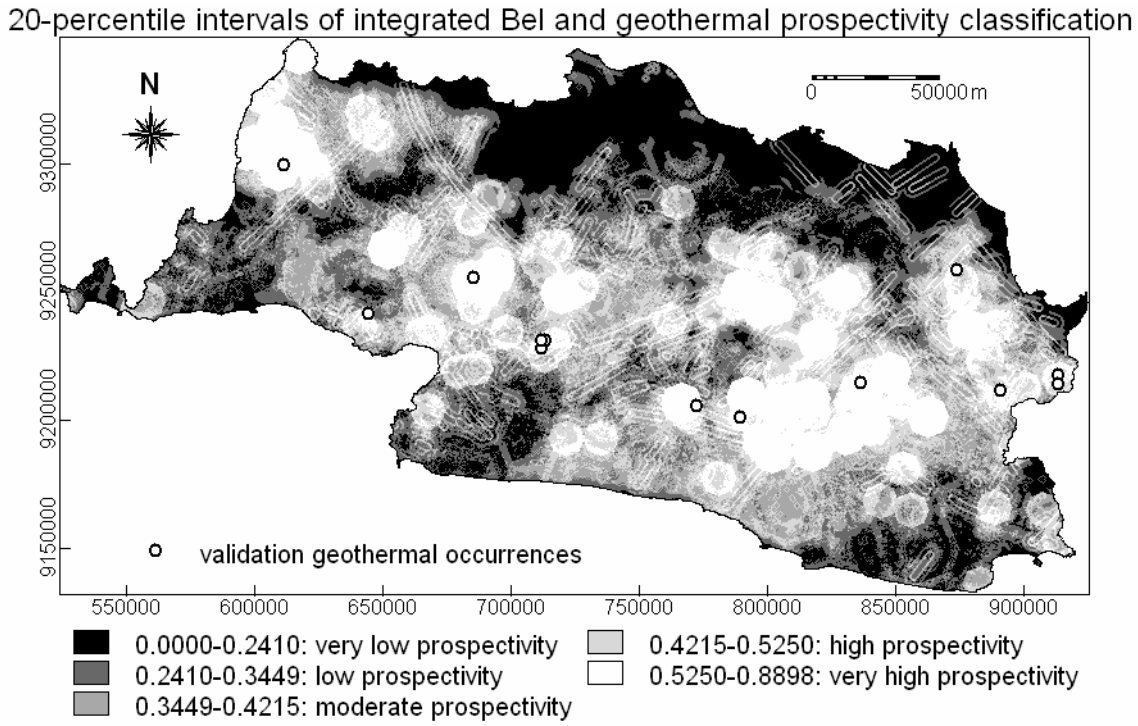

Figure 7.7: Geothermal prospectivity map based on integrated *Bel* using six evidential layers (i.e., exclusive of hypothesized volcano-tectonic depression evidential layer).

To validate the geothermal prospectivity maps, the training geothermal occurrences and the validation geothermal occurrences are overlaid on the prospectivity maps and then two parameters are estimated: (1) success rate; and (2) prediction rate. Success rate is estimated as percentage of training geothermal occurrences that are delineated in a prospectivity class. Prediction rate is estimated as percentage of validation geothermal occurrences that are delineated in a prospectivity class. The areas covered by the different prospectivity classes are not used to compare the geothermal prospectivity maps, because the classification was based on 20-percentile intervals of integrated degrees of belief and therefore areas of different prospectivity classes cover 20% of the study area. The estimated success rates and prediction rates of prospectivity classes in the different geothermal prospectivity maps are shown in Table 7.8.

Table 7.8: Success rates and prediction rates of geothermal prospectivity maps based on classification of integrated degrees of belief.

Geothermal prospectivity class	Prospectivity map inclusive of all evidential layers (Figure 7.5)		Prospectivity map exclusive of remotely-sensed clay alteration evidential layer (Figure 7.6)		Prospectivity map exclusive of hypothesized volcano-tectonic depression evidential layer (Figure 7.7)	
	Success rate (%)	Prediction rate (%)	Success rate (%)	Prediction rate (%)	Success rate (%)	Prediction rate (%)
Very high prospectivity	70.0	84.6	72.5	84.6	67.5	76.9
High prospectivity	20.0	7.7	12.5	15.4	20.0	23.1
Moderate prospectivity	5.0	7.7	10.0	-	7.5	-
Low prospectivity	-	-	-	-	2.5	-
Very low prospectivity	5.0	-	5.0	-	2.5	-

By removing the remotely-sensed clay alteration evidential layer (Figure 7.6), the prediction rate of the very high prospectivity class remains the same at 86.6%. However, by removing the remotely-sensed clay alteration evidential layer, the success rate of the very high prospectivity class increases from 70.0% to 72.5% and the prediction rate of the high prediction class increases from, 7.7% to 15.4%. This indicates that presence of or proximity to remotely-sensed clay alteration provides weak support to the proposition of geothermal prospectivity and could be excluded in geothermal prospectivity mapping.

By removing the hypothesized volcano-tectonic depression evidential layer (Figure 7.7), the success rate of the very high prospectivity class decreases from 70.0% to 67.5% and the prediction rate of the very high prospectivity decreases from 84.6% to 76.9%. By removing the hypothesized volcano-tectonic depression evidential layer, however, the prediction rate of high prospectivity class increases from 7.7% to 23.1%. In general, these results indicate that presence of or proximity to the hypothesized volcano-tectonic depression provides moderate to strong support to the proposition of geothermal prospectivity and should not be excluded in geothermal prospectivity mapping.

The validation results therefore show that the geothermal prospectivity map exclusive of remotely-sensed clay alteration evidential layer (Figure 7.6) is the best among the three geothermal prospectivity maps.

7.5. Discussion and concluding remarks

Proximity to Quaternary volcanoes and proximity to hot springs provide strong support to the proposition of geothermal prospectivity, because these geological features directly indicate the presence of heat sources for geothermal fields. Presence of or proximity to Quaternary volcanic rocks provides weak to moderate support to the proposition of geothermal prospectivity, because although the volcanic rocks could act as cap rocks of geothermal reservoirs, its spatial distribution does not always related to geothermal fields. Presence of or proximity to the hypothesized volcano-tectonic depression provides moderate support to the proposition of geothermal prospectivity, because this regional geological feature is probably filled with sedimentary rocks that act as reservoir rocks of geothermal fluids. Proximity to mapped NE- and WNW-NW-trending faults provides weak to moderate support to the proposition of geothermal prospectivity, because not all but only faults actually provide structural controls on geothermal systems or probably because regional faults are not

adequately mapped. Therefore, other geoscience data (e.g., regional aeromagnetics) could be useful for structural interpretations in support of geothermal prospectivity mapping. Presence of or proximity to remotely-sensed clay alteration provides weak support to the proposition of geothermal prospectivity, probably because the application of the software defoliant technique or the use of Landsat TM data did not result in accurate detection of clay alteration and probably because not all remotely-sensed are actually hydrothermal in origin but also to surficial weathering. Therefore, other techniques of hydrothermal alteration mapping in dense tropical vegetation (e.g., Carranza and Hale, 2002a) could be tested in the study area, but it is necessary to have proper training and validation data. Proximity to earthquake epicentres provides weak support to the proposition of geothermal prospectivity, probably because the earthquake epicentre data available are insufficient to properly quantify spatial association between such geological features and geothermal occurrences. A more complete data and/or different representation of earthquake epicenter (e.g., its density map), might be required to further test the usefulness of this type of data in geothermal prospectivity mapping.

In general, most of the very high prospectivity zones delineated in this study are located inside the published geothermal prospect areas, including the geothermal prospect areas that were previously considered as questionable (Figure 7.8). However, the best geothermal prospectivity map created here is able to reduce targets for exploration by focusing on zones proximal to Quaternary volcanic centres and to hot springs. This difference can be explained by the fact that the geothermal prospectivity modelling presented here is based on geothermal occurrences, many of which have been discovered after 1970 when the map of geothermal prospect areas was published. There is no literature found describing how the published map of geothermal prospect areas was constructed, since it is found only in map form, although there are locations of hot spring indicated in the map (Figure 3.6). These locations of hot springs are the same data used in this study. So, actually the map of the geothermal prospects published in 1970 and the present map of geothermal prospectivity are not comparable in terms of their efficiency, because the amount and quality of data used are conceivably different between about 35 year ago and now. The point intended to be made here is that spatial data analysis and integration is a potential tool for geothermal prospectivity mapping, but adequate datasets are required.

The results of the study, however, show that use of available public domain geoscience data allows delineation of zones prospective for geothermal exploration. The geothermal prospectivity maps (i.e., classified maps of integrated degrees of belief) clearly indicate that zones proximal to Quaternary volcanic centres and to hot springs and zones within the hypothesized volcano-tectonic depression and Quaternary volcanic rocks are where geothermal fields are mostly likely to occur. The results of integration of maps of EBFs of evidential layers conforms with the observation of Suryantini et al. (2005b) that most geothermal prospects are spatially associated with the Quaternary volcanoes, which are subduction related, whereas non-prospective areas are in the back arc regions whose genetic relationship with subduction is questionable. Suryantini et al. (2005b) also noticed that high enthalpy geothermal fields are also associated with large number of Quaternary volcanic cones clustering in restricted areas. Few geothermal fields, mostly of minor economic importance, are located far beyond the domains of active volcanoes.

The results of the study therefore show that public domain geoscience datasets, which are mostly kept in archives, can be further used for geothermal prospectivity mapping where the regional geological tectonic is recognized to be favourable for occurrence of geothermal systems. If there are no data on geothermal occurrences, then knowledge-driven approaches such as those applied to mineral potential mapping (e.g., Carranza et al., 1999; Prol-Ledesma, 2000; Carranza and Hale, 2001) could probably be used to model geothermal prospectivity. Alternatively, if there are no data on geothermal occurrences but the geotectonic setting is similar to the study areas, then the spatial associations between geothermal occurrences and indicative geological association quantified in this study could probably be used as bases for knowledge-driven prospectivity modelling. If there are data of geothermal occurrences, then these can be used in data-driven approaches to geothermal prospectivity mapping such as the application of EBFs demonstrated here. In relation to this, the best geothermal prospectivity map created in this study is based only on a randomly sub-set of the geothermal occurrence data available. Determining the best prospectivity map would actually require what is called a jackknife approach (Chung and Agterberg, 1979), whereby one occurrence is removed

from the occurrence data and all remaining occurrences are used in prospectivity modelling. In this study, with 53 geothermal occurrences, it would mean that the best prospectivity map should be evaluated from among 52 different prospectivity maps. The jackknife procedure would certainly take much longer. Since time is limited to carry out this research only one sub-set of the geothermal occurrence of the data was used, but a large proportion (75%) of the data was used so that spatial association between the geothermal occurrences and the indicative geological features are adequately quantified.

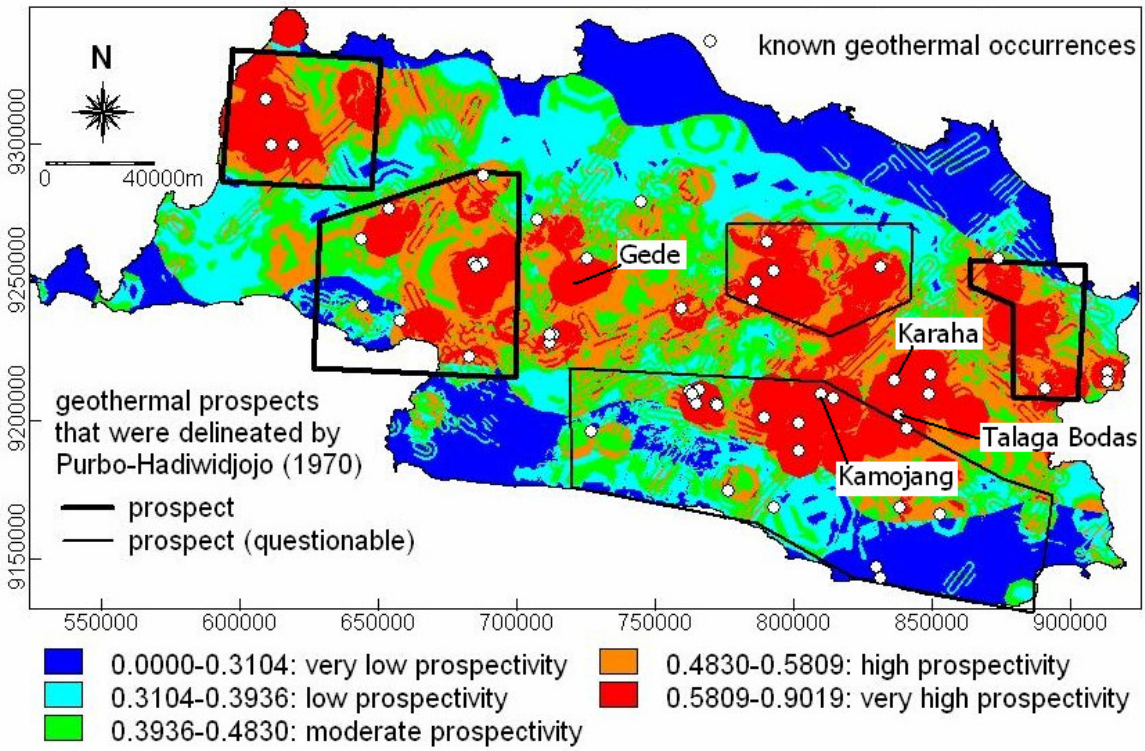

Figure 7.8: The best geothermal prospectivity map (also shown in Figure 7.6) and boundaries of published geothermal prospect areas (Purbo-Hadiwidjojo, 1970). Locations of some well known geothermal areas are annotated for reference in the text.

With 53 geothermal occurrences, the study area is indeed a well-explored region for geothermal resources. However, the best geothermal prospectivity map created here (Figure 7.8) suggests that undiscovered geothermal fields might still be present in certain zones in the area. For example, a zone with very high prospectivity to the south of Gede and zone with very high prospectivity to the east of Talaga Bodas require further field investigation.

Chapter 8: Conclusions and Recommendations

8.1. Conclusions

1. The regional geo-tectonic setting of West Java provides favourable conditions for occurrences of geothermal fields that can be utilised as energy resources. These favourable conditions are mostly caused by volcanism associated with the subduction history in this area. Volcanism due to ascending magma chambers resulted in several stratovolcano edifices, providing potential heat sources for geothermal fields. Its volcanic pyroclastic product and sedimentary materials provide potential reservoir for geothermal fields. The distribution of volcanic rocks that covers a wide area provides cap rock that can trap the heat beneath the ground. The resulting structural features, in the form of half-grabens and subsidence basins developed within the volcanic arc, provide structural control and potential reservoirs for geothermal fields.
2. Fry analyses show that the spatial distributions of Quaternary volcanoes, earthquake epicentres, geothermal occurrences, and hot springs have common regional NW and WNW trends, which could be associated with (a) the trend of the Sunda Trench, (b) the trend of the magmatic arc in Java Island, and (c) the trend of the Java Structural Domain. The corresponding rose diagrams of the Fry plots also reveal NE trends in the spatial distributions of Quaternary volcanoes, earthquake epicentres, geothermal occurrences, and hot springs. The NE trends are explainable by structural controls due to NE-trending faults. Furthermore, the Fry analyses enhanced general patterns of clustering in the spatial distributions Quaternary volcanoes, earthquake epicentres, geothermal occurrences, and hot springs. The results of Fry analyses imply that the Quaternary volcanoes, earthquake epicentres, hot springs, and geothermal occurrences have common principal structural controls, which are interpreted to be volcanism and tectonic processes.
3. Distance distribution analyses indicate positive spatial associations between known geothermal occurrences and individual sets of geological features in the study area. The results of the distribution analyses enabled definition of conceptual model of geothermal prospectivity.
4. Analysis of the derivative gravity data leads to interpretation of a regional E-W trending volcano-tectonic depression, which could have provided the conditions favourable for formation of geothermal fields. These favourable conditions provided by the volcano-tectonic depression are permeable volcano-sedimentary layers that could act as reservoir rocks, faults/fractures as conduits for geothermal fluids, and volcanic rocks as cap rocks.
5. There is consistency between the results of analyses of spatial associations between geothermal occurrences and areas containing remotely-sensed altered rocks and the compilation of information about characteristics of geothermal prospects, which indicate that geothermal occurrences are more associated with clay alteration than with iron-oxide alteration. This consistency in the spatial data analysis and in the information from the literature suggests that the remotely-sensed alteration by the software defoliant technique is fairly reliable. However, results of the predictive modelling of geothermal prospectivity indicate that the remotely-sensed clay alteration is an inefficient evidential layer, and therefore could be excluded in regional-scale geothermal prospectivity mapping. The most likely reason for this is that the remotely-sensed clay alteration could be either due to hydrothermal alteration in geothermal systems or simply to surface chemical weathering in areas away from geothermal systems.
6. Predictive mapping of geothermal prospectivity based on application of data-driven evidential belief functions allows representation of uncertainty as well as weights of relative importance of evidential data layers with respect to known geothermal occurrences. The geothermal prospectivity maps produced in this study clearly indicate that highly prospective zones are those that are proximal to Quaternary volcanic centres, hot springs, within or proximal to the hypothesized volcano-tectonic depression and covered by Quaternary volcanic rocks. The uncertainty maps indicate that the number of spatial evidence layers is sufficient to provide support for the proposition that a geothermal field exists.

7. The study area has been extensively explored for many years. Existing exploration and geothermal occurrence data are considered representative for this area, although details for each geothermal field are fragmentary, sometimes confidential, and mostly extracted from public domain source. The results of this study demonstrate the ability and usefulness of spatial analysis in constructing the conceptual models of relevant and available public domain geosciences data set for regional-scale geothermal prospectivity mapping. The use of available public domain data has proved useful to delineate prospective zones in the study area.

8.2. Recommendations

1. Further investigation is required to determine geological processes that could be associated with the presence of NNE-trending clusters of geothermal occurrences and NNW-trending clusters of hot springs in the study area.
2. Further work is recommended to whether or not predictive mapping of geothermal prospectivity could be improved by incorporating other relevant geoscience datasets, such as geochemical and hydrological data, which are not available in this study.
3. Due to time limitation, the author was not able to experiment incorporation of a density map of faults/fracture (as suggested by Soengkono, 2000) and density map of earthquake epicentres and volcanoes (as suggested by observation of Suryantini, 2005b) in the predictive modelling of geothermal prospectivity.
4. The procedures conducted in this study could also be applied elsewhere, particularly in areas along the Sunda trench where similar geological and tectonic settings could provide favourable conditions for occurrences of geothermal fields. These favourable conditions are mostly caused by volcanism associated with the subduction history in these areas.

References

Almeida, T.I.R. and de Souza Filho, C.R., 2004. Principal component analysis applied to feature-oriented band ratios of hyperspectral data: a tool for vegetation studies. International Journal of Remote Sensing, vol. 25, no. 22, pp. 5005-5023.

Alzwar, M., 1986. Geothermal Energy Potential Related to Active Volcanism in Indonesia. Geothermics, 15(5-6): 601-607.

Arana, V. et al., 2000. Internal Structure of Tenerife (Canary Islands) Based on Gravity, Aeromagnetic and Volcanological Data. 103: 43-64.

Bauman, P., Oesmerle, H., Sumintadireja, P. and Wibisono, 1972. Stratigraphic Correlations in the Tertiary of Java and Sumatra. 1st Annual Convention, Indonesia Petroleum Association, Indonesia.

Bates, R.L. and Jackson, J.A., 1987. Glossary of Geology, 3rd edition. American Geological Institute, Falls Church, Virginia, 788 pp.

Van Bemmelen, R.W., 1949. The geology of Indonesia: Vol. IA General Geology of Indonesia and Adjacent Archipelagoes. Martinus Nijhoff, The Hague.

Berrino, G., 2000. Combined Gravimetry in The Observation of Volcanic Processes in Southern Italy. Journal of Geodynamics, 30: 371-388.

Bertani, R., 2005. World Geothermal Power Generation in The Period 2001-2005, Geothermics, In Press, Corrected Proof, Available online 25 October 2005 (www.sciencedirect.com/science/article/B6VCN-4HDG98T-1/2/5c9419c332aad39cd8c02f7301a47b91).

Bodri, B., Iizuka, S. and Hayakawa, M., 1991. Geothermal and Rheological Implications of Intracontinental Earthquakes beneath the Kanto-Tokai Region, Central Japan. Tectonophysics, 194(4): 337-347.

Bodri, B. and Iizuka, S., 1993. Earthquake Cutoff Depth as a Possible Geothermometer - Applications to Central Japan. Tectonophysics, 225(1-2): 63-78.

Bogie, I. and Lawless, J., 2000. Application of Mineral Deposit Concepts to Geothermal Exploration, World Geothermal Congress. International Geothermal Association / IGA, Kyushu - Tohoku, Japan.

Boots, B.N. and Getis, A., 1988. Point Pattern Analysis. Sage University Scientific Geography Series no.8. Sage Publications, Beverly Hills.

Bonham-Carter, G.F., 1994. Geographic Information Systems for Geoscientists: Modelling with GIS. Pergamon, 398 pp.

Bonham-Carter, G.F., Rencz, A.N. and Harris, J.R., 1985. Spatial Relationship of Gold Occurrence With Lineaments Derived from Landsat and Seasat Imagery, Meguma Group, Nova Scotia, 4th Thematic Conference on Remote Sensing for Exploration Geology, San Francisco, pp. 755-768.

Boots, B.N. and Getis, A., 1988. Point Pattern Analysis. Sage University Scientific Geography Series no.8. Sage Publications, Beverly Hills.

Caglar, I. and Isseven, T., 2004. Two-dimensional geoelectrical structure of the Goynuk geothermal area, northwest Anatolia, Turkey. Journal of Volcanology and Geothermal Research, 134(3): 183-197.

Carranza, E.J.M., Mangaoang, J.C. and Hale, M., 1999. Application of mineral exploration models and GIS to generate mineral potential maps as input for optimum land-use planning in the Philippines. Natural Resources Research, 8(2): 165-173.

Carranza, E.J.M. and Hale, M., 2001. Geologically constrained fuzzy mapping of gold mineralization potential, Baguio district, Philippines, Natural Resources Research, 10(2): 125-136.

Carranza, E.J.M., 2002. Geologically-Constrained Mineral Potential Mapping (Examples from the Philippines). PhD Thesis, Technical University of Delft, The Netherlands. ITC (International Institute for Geo-Information Science and Earth Observation) Publication No. 86, Enschede, The Netherlands, 480 pp.

Carranza, E.J.M. and Hale, M., 2002a. Mineral Imaging with Landsat Thematic Mapper Data for Hydrothermal Alteration Mapping in Heavily Vegetated Terrane. Int. J. Remote Sensing, 23(22): 4827-4852.

Carranza, E.J.M. and Hale, M., 2002b. Spatial Association of Mineral Occurrences and Curvilinear Geological Features. Mathematical Geology, 34(2): 199-217.

Carranza, E.J.M. and Hale, M., 2003. Evidential belief functions for data-driven geologically constrained mapping of gold potential, Baguio district, Philippines. Ore Geology Reviews, 22(1-2): 117-132.

Carranza, E.J.M., Woldai, T. and Chikambwe, E.M., 2005. Application of Data-Driven Evidential Belief Functions to Prospectivity Mapping for Aquamarine-Bearing Pegmatites, Lundazi District, Zambia. Natural Resources Research, 14(1): 47-63.

Cas, R.A.F. and Wright, J.V., 1987. Volcanic Successions, Modern and Ancient. Allen and Unwin, London, 528 pp.

Chung, C.F. and Agterberg, F.P., 1979. Regression models for estimating mineral resources from geologic map data, Mathematical Geology, 12(5): 473-488.

Chung, C.F. and Fabbri, A.G., 1993. The Representation of Geoscience Information for Data Integration. Nonrenewable Resources, 12(2): 122-139.

Coles, D., Vichabian, Y, Fleming, R., DesAutels, C., Briggs, V., Vermeesch, P., Arrell, J.R., Lorraine Lisiecki, L., Kessler, T., Hooper, H., Jensen, E., Sogade, J. and Morgan, F.D., 2004. Spatial Decision Analysis of Geothermal Resource sites in the Qualibou Caldera, Saint Lucia, Lesser Antilles. Geothermics, 33: 277-308.

Coolbaugh, M.R., Raines, G., Shevenell, L., Minor, T., Sawatzky, D. and Oppliger, G., 2004. Regional Assessment of Exploration Potential for Geothermal Systems in the Great Basin Using a Geographic Information System (GIS) - Part II. Great Basin Center for Geothermal Energy, http://www.unr.edu/geothermal.

Craig, M.A., Wilford, J. R. and Tapley, I.J., 1999. Regolith-landform mapping in the Gawler Craton – an alternative approach. MESA Journal, vol. 12, January 1999, pp. 17-21.

CSUI, 2006. The Physical Earth. Charles Sturt University Initiative (CSUI), http://hsc.csu.edu.au/physics/options/geophysics/3066/PHY951net.htm#net2.

Dam, M.A.C., 1994. The Late Quaternary Evolution of the Bandung Basin, West Java, Indonesia. PhD Thesis, Vrije Universiteit, Amsterdam, The Netherlands, 252 pp.

Dardji, N., Villemin, T. and Rampuoux, J.P., 1994. Paleostresses and Strike-Slip Movement: The Cimandiri Fault Zone, West Java, Indonesia. J. SE Asian Earth Sci., 9(1/2): 3-11.

Dickson, M.H. and Fanelli, M., 2004. What is Geothermal Energy? International Geothermal Association (IGA); http://iga.igg.cnr.it/geo/geoenergy.php.

Dijk, A.I.J.M.v., 2002. Water and Sediment Dynamics in Bench-Terraced Agricultural Steeplands in West Java, Indonesia. PhD Thesis, Vrije Universiteit, Amsterdam, The Netherlands, 369 pp.

Doi, N. et al., 2000. Seismic Activity in the Kakkonda Geothermal System Characterised by The Quaternary Kakkonda Granite, Japan, World Geothermal Congress. International Geothermal Association / IGA, Kyushu - Tohoku, Japan.

Drury, S.A., 1993. Image Interpretation in Geology. Chapman & Hall, 283 pp.

Edwards, L.M., Chilingar, G.V., III, H.H.R. and Fertl, W.H., 1982. Handbook of Geothermal Energy. Gulf Publishing Company, 613 pp.

Ehara, S., 1987. Thermal Structure and Seismic Activity in Central Kyushu, Japan. Tectonophysics, 159(3-4): 269-278.

Elder, J., 1981. Geothermal Systems. Academic Press Inc. Ltd, London, 508 pp.

Faulds, J.E., Garside, L.J., Johnson, G.L., Muehlberg, J. and Oppliger, G.L., 2002. Geologic Setting and Preliminary Analysis of the Desert Peak-Brady Geothermal Field Western Nevada. GRC Transactions, 26: 491-494.

Fauzi, A., Bahri, S. and Akuanbatin, H., 2000. Geothermal Development in Indonesia: An Overview of Industry Status and Future Growth, World Geothermal Congress. International Geothermal Association / IGA, Kyushu - Tohoku, Japan.

Fernandes, J., Tiampo, K.R., Rundle, J.B. and Jentzsch, G., 2005. On The Interpretation of Vertical Gravity Gradients Produced by Magmatic Intrusions. Journal of Geodynamics, 39: 475-492.

Foulger, G., 1982. Geothermal exploration and reservoir monitoring using earthquakes and the passive seismic method. Geothermics, 11(4): 259-268.

Fraser, S.J. and Green, A.A., 1987. A Software Defoliant for Geological Analysis of Band Ratios. Int. J. Remote Sensing, 8: 525-532.

Fridleifsson, I.B., 2003. Status of Geothermal Energy amongst the World's Energy Sources, IGA News, pp. 13-14.

Fry, N., 1979. Random Point Distributions and Strain Measurement in Rocks. Tectonophysics, 60: 89-105.

Gladwell, D.R., Lett, R.E. and Lawrence, P., 1983. Application of Reflectance Spectroscopy to Mineral Exploration. Economic Geology, 78: 699-710.

Götze, H.-J. and Krause, S., 2002. The Central Andean Gravity High, A Relic of An Old Subduction Complex? Journal of South American Earth Sciences, 14: 799-811.

Gulyás, E. and Hédervári, P., 1976. Concentration of seismic energy within the two active domains beneath individual volcanoes and groups of volcanoes of Java, Indonesia. Tectonophysics, 30(1-2): 129-140.

Gupta, R.P., 2003. Remote Sensing Geology. Springer, Berlin, 656 pp.

Hadi, J., Harrison, C., Keller, J. and Rejeki, S., 2000. Overview of Darajat Reservoir Characterisation: A Volcanic Hosted Reservoir, World Geothermal Congress. International Geothermal Association / IGA, Kyushu - Tohoku, Japan.

Hall, R., 1997. Cenozoic Plate Tectonic Reconstruction of SE Asia. In: R. Hall and R. Murphy (Editors), Petroleum Geology of Southeast Asia. Geol. Soc. London Spec. Pub., pp. 11-23.

Hall, R., 1998. The Plate Tectonics of Cenozoic SE Asia and the Distribution of Land and Sea. In: R. Hall and J.D. Holloway (Editors), Biogeography and Geological Evolution of SE Asia. Backhuys Publishers, pp. 99-131.

Hall, R., 2003. Cenozoic Tectonic of Indonesia: Problems and Models, Indonesian Petroleum Association, Short Course. SE Asia Research Group, Department of Geology, Royal Holloway, University of London, UK.

Hamilton, W., 1979. Tectonics of the Indonesian Region. USGS Professional Paper, 1078: 345 pp.

Hamilton, W., 1989. Convergent Plate Tectonics Viewed from The Indonesian Region. Journ. Indon. Ass. Geol., Special Volume No.60: 35-88.

Hanna, S. S. and Fry, N., 1979. A comparison of methods of strain determination in rocks from southwest Dyfed (Pembrokeshire) and adjacent areas. Journal of Structural Geology, v. 1, p. 155-162.

Hanus, V. and Vanek, J., 1989. Seismotectonics of Continental Wedges Overlying Circum-Pacific Subduction Zones. In: J. Aubouin and J. Bourgois (Editors), Tectonics of Circum-Pacific Continental Margins. Proceedings of The 28th International Geology Congress, pp. 229-243.

Healy, J., 1976. Geothermal Fields in Zones of Recent Volcanism, Second U.N. Symposium on the Development and Use of Geothermal Resources, San Francisco, pp. 415-422.

Hochstein, M.P., 1974. Geophysical exploration of geothermal areas in West Java and Bali, July to October, 1973, and November 1973 to January 1974. GENZL Report for G.O.I.

Hoffmann-Rothe, A., Ritter, O. and Haak, V., 2001. Magnetotelluric and Geomagnetic Modelling Reveals Zones of Very High Electrical Conductivity in the Upper Crust of Central Java. Physics of the Earth and Planetary Interiors, 124: 131-151.

Huttrer, G.W., 2001. The Status of World Geothermal Power Generation 1995-2000. Geothermics, 30: 1-27.

IDWR, 1987. Geothermal Investigations in Idaho: Evaluation of the Boise Geothermal System. Idaho Department of Water Resources (IDWR), Idaho (http://www.idwr.state.id.us/hydrologic/info/pubs/wib/wib30p16p1geothermal_boise_system.pdf).

IGA, 2001. Report of the IGA to The UN Commission on Sustainable Development, Session 9 (CSD-9), International Geothermal Association, New York, April.

INAGA, 2005. High temperature, developed geothermal fields. http://www.api.or.id, accessed 2005. (INAGA = Indonesian Geothermal Association).

ITC-ILWIS, 2001. ILWIS 3.0 Academic – User's Guide. ITC, Enschede, The Netherlands, 530 p.

Karig, D.E., Suparka, S., Moore, G.F. and Hehanusa, P.E., 1979. Structure and Cenozoic Evolution of the Sunda Arc in The Central Sumatra Region. In: J.S. Watkins, L. Montadert and P.W. Dicerson (Editors), Geological and Geophysical Investigation of Continental Margin. AAPG Memoir, pp. 223-237.

Katili, J.A., 1975. Volcanism and Plate Tectonics in the Indonesian Island Arcs. Tectonophysics, 26: 165-188.

Katili, J.A., 1989. Evolution of the Southeast Asian Arc Complex. Journ. Indon. Ass. Geol., Special Volume No.60: 113-143.

Kearey, P. and Vine, F.J., 1996. Global Tectonics. Blackwell Science Ltd.

Khesin, B.E., and Eppelbaum, L.V., 1994, Near-surface Thermal Prospecting: Review of processing and Interpretation. Geophysics, SEG, Vol.59 No.5, p.744-752.

Kusumoto, S., Fukuda, Y. and Takemura, K., 1999. A Distinction Technique between Volcanic and Tectonic Depression Structures Based on the Restoration Modeling Gravity Anomaly: A Case Study of the Hohi Volcanic Zone, Central Kyushu, Japan. Journal of Volcanology and Geothermal Research, 90: 183-189.

Lachenbruch, A.H., 1978. Heat Flow in the Basin and Range Province and Thermal Effects of Tectonic Extension. Pure and Applied Geophysics, 117: 34-50.

Lachenbruch, A.H. and Sass, J.H., 1977. Heat Flow in the United States and the Thermal Regime of the Crust. In: J.G. Heacock (Editor), The Earth's Crust. American Geophysical Union Monograph No. 20, Washington, pp. 626-675.

Lee, K. and Raines, G.L., 1984. Reflectance Spectra of Some Alteration Minerals - A Chart Compiled from Published Data 0.4-2.5 μm . US Geological Survey Open-File Report: 84-96.

Lucassen, F., Fowler, C.M.R. and Franz, G., 1996. Formation of Magmatic Crust at the Andean Continental Margin during Early Mesozoic: A Geological and Thermal Model of the North Chilean Coast Range. Tectonophysics, 262(1-4): 263-279.

Lugão, P.P.d., LaTerra, E.F., Kriegshäuser, B. and Fontes, S.L., 2002. Magnetotelluric Studies of the Caldas Novas Geothermal Reservoir, Brazil. Journal of Applied Geophysics, 49: 33-46.

Mahon, T., Harvey, C. and Crosby, D., 2000. The Chemistry of Geothermal Fluids in Indonesia and their Relationship to Water and Vapor Dominated Systems, World Geothermal Congress. International Geothermal Association / IGA, Kyushu - Tohoku, Japan.

Majer, E.L. and McEvilly, T.V., 1979. Seismological Investigations at the Geysers Geothermal Field. Geophysics, 44: 246-269.

Malengreau, B., Lénat, J.-F. and Froger, J.-L., 1999. Structure of Réunion Islan (Indian Ocean) Inferred from The Interpretation of Gravity Anomalies. Journal of Volcanology and Geothermal Research, 88: 131-146.

Mandl, G., 1988. Mechanics of Tectonic Faulting: Models and Basic Concepts. Developments in Structural Geology, 1. Elsevier.

Manzella, A., 2000. Geophysical Methods in Geothermal Exploration (lecture notes). Italian National Research Council. International Institute for Geothermal Research. Pisa, Italy.

Martodjojo, S., 1984. Evolusi Cekungan Bogor Jawa Barat. PhD Thesis, Institut Teknologi Bandung (ITB), Bandung, Indonesia, 396 pp.

Martodjojo, S., 1989. Stratigraphic and Tectonic Behaviour of A Back Arc Basin in West Java, Indonesia, Proc. Reg. Conf. Geol. Min. Hyd. Res. SE. Asia. IAGI, Jakarta, Indonesia, pp. 229-244.

Moore, J.N., 2002. Improving Exploration Models of Andesite-Hosted Geothermal Systems, In: Geothermal Technologies Program Geoscience and Supporting Technologies 2001 University Research Summaries. U.S. DOE Office of Wind and Geothermal Technologies.

Muffler, L.J.P., 1976. Tectonic and Hydrologic Control of the Nature and Distribution of Geothermal Resources, Second U.N. Symposium on the Development and Use of Geothermal Resources, San Francisco, pp. 499-507.

Muffler, P. and Cataldi, R., 1978. Methods for Regional Assessment of Geothermal Resources. Geothermics, 7(2-4): 53-89.

Nash, G.D. and Adams, M.C., 2001. Cost Effective Use of GIS for Tracer Test Data Mapping and Visualization. GRC Transactions, 25.

Nash, G.D. and Hernandez, M.W., 2001. Cost Effective Vegetation Anomaly Mapping for Geothermal Exploration, Geothermal Reservoir Engineering. Stanford University, Stanford, California.

Nash, G.D. and Wright, P.M., 1996. Remote Sensing and Geographic Information Systems (GIS) - Tools for Geothermal Exploration in the Great Basin, U. S. A, Sandia National Laboratories, Final Report, Contract #AB-6807, 74.

Nielson, D.L. and Nash, G.D., 1997. Structural Fabric of the Geysers. GRC Transactions, 21: 643-649.

Nishijima, J., Fujimitsu, Y., Ehara, S. and Motoyama, T., 2000. Reservoir Monitoring by Observation of Gravity Changes at Some Geothermal Fields in Kyushu, Japan, World Geothermal Congress. International Geothermal Association / IGA, Kyushu - Tohoku, Japan.

Nishimura, S., Nishida, J.I., Yokoyama, T. and Hehuwat, F., 1986. Neo-Tectonics of the Strait of Sunda, Indonesia. J. SE Asian Earth Sci., 1(2): 81-91.

Olsen, K.H. and Morgan, P., 1995. Progress in Understanding Continental Rifts. In: K.H. Olsen (Editor), Continental Rifts: Evolution, Structure, Tectonics. Elsevier, pp. 3-26.

Oskooi, B. et al., 2005. The deep geothermal structure of the Mid-Atlantic Ridge deduced from MT data in SW Iceland. Physics of the Earth and Planetary Interiors, 150(1-3): 183-195.

Pakiser, L.C., 1964. Gravity, volcanism, and crustal structure in the southern Cascade Range, California. Geol Soc Am Bull, 75(7): 611-620.

Parasnis, D.S., 1997. Principles of Applied Geophysics, 5th ed. Chapman & Hall.

Patmosukismo, S. and Yahya, i., 1974. The Basement Configuration of The North West Java Area, Third Annual Convention - Indonesian Petroleum Association. Indonesian Petroleum Association (IPA), pp. 129-151.

Pollack, H.N. and Chapman, D.S., 1977. The Flow of Heat from the Earth's Interior. Sci. Am., 237(2): 60-76.

Pollack, H.N., Hurter, S.J. and Johnson, J.R., 1993. Heat Flow from the Earth's Interior: Analysis of the Global Dataset. Rev. Geophys., 31: 267-280.

Prol-Ledesma, R.M., 2000. Evaluation of the Reconnaissance Results in Geothermal Exploration using GIS. Geothermics, 29: 83-103.

Purbo-Hadiwidjojo, M.M., 1970. A Tentative Map of the Prospective Geothermal Areas of Java and Bali, 1:1,000,000. Geological Survey of Indonesia, Bandung, Indonesia.

Rae, A.J., Cooke, D.R., Phillips, D. and Zaide-Delfin, M., 2004. The Nature of Magmatism at Palinpinon Geothermal Field, Negros Island, Philippines: Implications for Geothermal Activity and Regional Tectonics. Journal of Volcanology and Geothermal Research, 129(4): 321-342.

Ranalli, G. and Rybach, L., 2005. Heat Flow, Heat Transfer and Lithosphere Rheology in Geothermal Areas: Features and Examples. Journal of Volcanology and Geothermal Research, Article in Press, www.elsevier.com/locate/jvolgeores.

Richards, J.A., 1999. Remote Sensing Digital Image Analysis, an Introduction, 3rd Edn. Springer-Verlag, Berlin, 363 pp.

Robinson, P.T., Elders, W.A. and Muffler, L.J.P., 1976. Holocene Volcanism in the Salton Sea Geothermal Field, Imperial Valley, California. Geol. Soc. America Bull., 87: 347-360.

Rowley, J.C., 1982. Worldwide Geothermal Resources. In: L.M. Edwards, G.V. Chilingar, H.H.R. III and W.H. Fertl (Editors), Handbook of Geothermal Energy. Gulf Publishing Company, Houston, Texas, pp. 44-176.

Rubie, D.C. and Hilst, R.D.v.v., 2001. Processes and Consequences of Deep Subduction: Introduction (Editorial). Physics of the Earth and Planetary Interiors, 127: 1-7.

Rybach, L., 1976. Radioactive Heat Production: A Physical Properties Determined by the Chemistry of Rocks. In: R.G.J. Strens (Editor), The Physics and Chemistry of Minerals and Rocks. Wiley, London, pp. 309-318.

Rybach, L., 1981. Geothermal Systems, Conductive Heat Flow, Geothermal Anomalies. In: L. Rybach and L.J.P. Muffler (Editors), Geothermal Systems: Principles and Case Histories. John Wiley & Sons Ltd.

Rybach, L. and Muffler, L.J.P., 1981. Geothermal Systems: Principles and Case Histories. John Wiley & Sons, 359 pp.

Sabine, C., 1999. Remote Sensing for the Earth Sciences: Manual of Remote Sensing. Ch. 8. Remote Sensing Strategies for Mineral Exploration, 3. John Wiley & Sons, Inc., 375-429 pp.

Sabins, F.F., 1999. Remote sensing for mineral exploration. Ore Geology Reviews, vol. 14, no. 3-4, pp. 157-183.

Sano, S.-I., 1978. Gravity Anomalies Associated with Island Arc, Third Regional Conference on Geology and Mineral Resources of Southeast Asia, Bangkok, Thailand.

Setijadji, L.D., 2005. Geoinformation of Island Arc Magmatism and Associated Earth Resources: A Case Study of Java Island, Sunda Arc, Indonesia. PhD Thesis, Kyushu University, Fukuoka, Japan, 201 pp.

Sibson, R.H., 1987. Earthquake Rupturing as a Mineralising Agent in Hydrothermal Systems. Geology, 15: 701-704.

Simandjuntak, T.O. and Barber, A.J., 1996. Contrasting Tectonic Styles in the Neogene Orogenic Belts of Indonesia. In: R. Hall and D.J. Blundell (Editors), Tectonic Evolution of SE Asia. Geological Society of London Special Publication 106, pp. 185-201.

Simiyu, S.M. and Malin, P.E., 2000. A "Volcanoseismic" Approach to Geothermal Exploration and Reservoir monitoring: Olkaria, Kenya and Casa Diablo, USA, Proceedings World Geothermal Congress. International Geothermal Association / IGA, Kyushu - Tohoku, Japan.

Sleep, N.H. and Fujita, K., 1997. Principles of Geophysics. Blackwell Science, 586 pp.

Smith, R.L. and Shaw, H.R., 1973. Volcanic Rocks as Geologic Guides to Geothermal Exploration and Evaluation (abs.). EOS (Am. Geophys. Union Trans.), 54: 1213.

Smith, R.P., Wisian, K.W. and Blackwell, D.D., 2001. Geologic and Geophysical Evidence for Intra-basin and Footwall Faulting at Dixie Valley, Nevada. GRC Transactions, 25.

Soengkono, S., 2001. Interpretation of Magnetic Anomalies over the Waimangu Geothermal Area, Taupo Volcanic Zone, New Zealand. Geothermics, 30(4): 443-459.

Soeria-Atmadja, R., Pringgoprawiro, H. and Priadi, B., 1990. Tertiary Magmatic in Java: A Study on Geochemical and Mineralogical Evolution, In: Prosiding Persidangan Sains Bumi and Masyarakat, Universiti Kebangsaan Malaysia, 9-10 Julai 1990, Kuala Lumpur, pp. 164-180.

Soeria-Atmadja, R., Maury, R.C., Bellon, H., Pringgoprawiro, H., Polve, M. and Priadi, B., 1994. Tertiary Magmatic Belts in Java. J. SE Asian Earth Sci., 9(1/2): 13-27.

Spatz, D.M., 1997. Remote sensing characteristics of the sediment- and volcanic-hosted precious metal system: imagery selection for exploration and development. International Journal of Remote Sensing, vol. 18, no. 7, pp. 1413-1438.

Spector, A. and Grant, F.S., 1970. Statistical models for interpreting aeromagnetic data. Geophysics, 35(2): 293-302.

Špicák, A., Hanuš, V. and Vanek, J., 2005. Seismotectonic Pattern and the Source Region of Volcanism in the Central Part of Sunda Arc. Journal of Asian Earth Sciences, 25: 583-600.

Sudarman, S., Suroto, Pudyastuti, K. and Aspiyo, S., 2000. Geothermal Development Progress in Indonesia: Country Update 1995-2000, World Geothermal Congress. International Geothermal Association / IGA, Kyushu - Tohoku, Japan.

Sugihara, M., Okuma, S., Nakano, S., Furukawa, R., Komazawa, M. and Supper, R., 2002. Relationship between Geothermal Activity and Geothermal Anomalies on Vulcano Island, Italy, 24th NZ Geothermal Workshop, New Zealand.

Suryantini, Ashat, A., Achmad, D.R., Simanjutak, J., Hutasoit, L.M. and Hasjim, I., 2005a. Searching for an Opportunity in the Development of Direct Use Geothermal Resources; a Case Study in West Java Province - Indonesia, World Geothermal Congress. International Geothermal Association / IGA, Antalya, Turkey.

Suryantini, Setijadji, L.D., Wahyuningsih, R., Ehara, S., Imai, A. and Watanabe, K., 2005b. Geothermal Fields of Java Island, Indonesia: Their Descriptions, Geologic Environments, and Preliminary Area-Selection Exploration Strategy. Proceedings of the 3rd International Workshop on Earth Science and Technology, Fukuoka, p. 11-18.

Susilohadi, S., Gaedicke, C. and Ehrhardt, A., 2005. Neogene Structures and Sedimentation History along The Sunda Forearc Basins off Southwest Sumatra and Southwest Java. International Journal of Marine Geology, Geochemistry and Geophysics, 219: 133-154.

Tamanyu, S. and Wood, C.P., 2003. Characterization of Geothermal Systems in Volcano-tectonic Depressions: Japan and New Zealand. Bulletin of the Geological Survey of Japan, 54(3/4): 117-129

Tanaka, S., Hamaguchi, H., Ueki, S., Sato, M. and Nakamici, H., 2002. Migration of Seismic Activity during 1998 Volcanic Unrest at Iwate Volcano, Northeastern Japan, With Reference to P and S Wave Velocity Anomaly and Crustal Deformation. Journal of Volcanology and Geothermal Research, 113: 399-414.

Telford, W.M., Geldart, L.P. and Sheriff, R.E., 1990. Applied Geophysics. Cambridge University Press, 770 pp.

Tezuka, S., Todaka, N. and Shimizu, I., 2000. The Fault System and Geological Structure of the Oguni Geothermal Field, Central Kyushu in Japan, World Geothermal Congress. International Geothermal Association / IGA, Kyushu - Tohoku, Japan.

Thamrin, M., 1985. An Investigation of the Relationship between the Geology of Indonesian Sedimentary Basins and Heat Flow Density. Tectonophysics, 121(1): 45-47.

Tripp, A., Moore, J., Ussher, G. and McCulloch, J., 2002. Gravity Modeling of The Karaha-Talaga Bodas Geothermal System, Indonesia, 27th Workshop on Geothermal Reservoir Engineering, Stanford University, Stanford, California.

Utami, P., 2000. Characteristics of the Kamojang Geothermal Reservoir (West Java) as Revealed by its Hydrothermal Alteration Mineralogy, World Geothermal Congress. International Geothermal Association / IGA, Kyushu - Tohoku, Japan.

Vearncombe, J.R. and Vearncombe, S., 1999. The Spatial Distribution of Mineralization: Application of Fry Analysis. Economic Geology, 94: 475-486.

Vearncombe, J.R. and Vearncombe, S., 2002. Tectonic Controls on Kimberlite Location, Southern Africa. Journal of Structural Geology, 24: 1619-1625.

VSI, 2005. Geothermal Resources in Indonesia. Volcanological Survey of Indonesia (VSI) Geothermal Division, http://www.vsi.esdm.go.id/pbumi/index.html.

White, D.E., Muffler, L.J.P. and Truesdell, A.H., 1971. Vapor-Dominated Hydrothermal Systems Compared with Hot-Water Systems. Economic Geology, 66: 75-97.

Whitney, G., Abrams, M.J. and Goetz, A.F.H., 1983. Mineral Discrimination Using a Portable Ratio-Determining Radiometer. Economic Geology, 78: 688-698.

Widianto, E., Santoso, D., Taib, I.T. and Kadir, W.G.A., 2004. Basin Boundaries Determination in West Java using 2-D Gravity Modeling (English abstract is available), Makalah Ikatan Ahli Geologi Indonesia XXXIII.

Wilson, C.J.N., Houghton, B.F., McWilliams, M.O., Lanphere, M.A., Weaver, S.D. and Briggs, R.M., 1995. Volcanic and Structural Evolution of Taupo Volcanic Zone, New Zealand. Jour. Volc. Geotherm. Res, 68: 1-28.

Windley, B.R., 1995. The Evolving Continents, 3rd ed. Wiley.

Woldetinsae, G. and Götze, H.-J., 2005. Gravity Field and Isostatic State of Ethiopia and Adjacent Areas. Journal of African Earth Sciences, 41: 103-117.

Wood, C.P., 1995. Calderas and Geothermal Systems in The Taupo Volcanic Zone, New Zealand, Proceeding of World Geothermal Congress, Florence, Italy, pp. 1331-1336.

Wright, D.F. and Bonham-Carter, G.F., 1996, VHMS favourability mapping with GIS-based integration models, Chisel Lake – Anderson Lake area, in Bonham-Carter, G.F., Galley, A.G., and Hall, G.E.M., eds., EXTECH I: A Multidisciplinary Approach to Massive Sulphide Research in the Rusty Lake – Snow Lake Greenstone Belts, Manitoba, Geological Survey of Canada Bulletin 426: Geological Survey of Canada, Ottawa, p. 339-376, 387-401.

Wright, P.M., Ward, S.H., Ross, H.P. and West, R.C., 1985. State-of-The-Art Geophysical Exploration for Geothermal Resources. Geophysics, 50(12): 2666-2699.

Wyllie, P.J., 1971. The Dynamic Earth. Wiley, New York, 416 pp.

Yang, K., Browne, P.R.L., Huntington, J.F. and Walshe, J.L., 2001. Characterising the Hydrothermal Alteration of The Broadlands-Ohaaki Geothermal System, New Zealand, Using Short-Wave Infrared Spectroscopy. Journal of Volcanology and Geothermal Research, 106: 53-65.

Zen, M.T. and Radja, V.T., 1970. Result of the Preliminary Geological Investigation of Natural Steam Fields in Indonesia. Geothermics, 2(1): 130-135.

Zhao, D., 2001. Seismological Structure of Subduction Zones and its Implication. Physics of the Earth and Planetary Interiors, 127: 197-214.